KYAMBOGO UNIVERSITY

FACULTY OF ENGINEERING

DEPARTMENT OF CIVIL AND ENVIRONMENTAL ENGINEERING

EXPERIMENTAL AND NUMERICAL INVESTIGATIONS OF FIRE RESISTANCE OF A HYBRID SLAB

ASIIMWE RONALD WILFRED

19/U/GMES/18808/PD

DISSERTATION SUBMITTED TO KYAMBOGO UNIVERSITY GRADUATE SCHOOL IN PARTIAL FULFILMENT OF THE REQUIRMENTS FOR THE AWARD OF MASTER OF SCIENCE IN STRUCTURAL ENGINEERING DEGREE OF KYAMBOGO UNIVERSITY

September, 2025

DECLARATION.

Declaration by candidate:

This Dissertation/thesis is my original work and has not been presented for a degree in any other University

. …… ……..

Signature Date

ASIIMWE RONALD WILFRED

19/U/GMES/18808/PD

Declaration by Supervisor:

We confirm that the work in this Dissertation/thesis was done by the candidate under our supervision

…….. … ……

Signature Date

Dr Kyakula Micheal, Department of Civil and Environmental engineering, Faculty of Engineering, Kyambogo University, For and on behalf of Kyambogo University

…… ……. ……

Signature Date

Dr Eng Bulolo Sam, Department of Civil and Environmental engineering, Faculty of Engineering, Kyambogo University, For and on behalf of Kyambogo University

DEDICATION

I dedicate my dissertation work to my family, most especially to my wife and children, Mercy Namara Asiimwe, Israel Abiel Asiimwe and Aaron Eleazer Asiimwe who encouraged me not to give up on this research journey. My sisters Lena, and Irene, thank you for your unlimited support.

Furthermore, I dedicate this dissertation to my friends who have been there to encourage me find the results of the research since the outcomes of it shade some light in the Ugandan building sector. My church family thank you for praying for me.

I also dedicate this work to my clients that have entrusted with their projects where I have been able to generate resources to study this Master's degree, especially Wilson Gunura Mutungi.

ACKNOWLEDGEMENT

I appreciate my supervisors Dr Kyakula Micheal and Dr Eng Bulolo Sam for their dedicated support towards this research.

Furthermore, I appreciate my wife for her emotional and mental support.

In a special way, thank you my classmates for your unwavering encouragement not to give up on the course despite the lockdown and corona virus season.

Table of contents

List of tables

List of figures

ABSTRACT

In Uganda, there has been a growing use of hybrid slabs which include timber steel and concrete within floor systems. On the 26th of September 2022, the government of Uganda through the minister of works and transport issued a ban on building houses with hybrid slab floor systems until enough studies have been done to deem it safe as a construction method. Therefore, there was a need to conduct an experimental and numerical investigation on the performance of the hybrid slab when subjected to a fire. The experimental and numerical model parameters and specifications considered were obtained from the baseline study carried out on buildings, designers and contractors employing the use of hybrid floor systems in Uganda. A 4x3m slab model was built on a construction site in Katta, Wakiso district. The model was constructed with a 75mm concrete topping cast on expanded metal lathe fixed, on top of 100x100mm Eucalyptus grandis beams, spaced 600mm cc which were simply supported on I-beams top flanges. The I beam were supported by SHS 75x75x5mm columns at the ends. The I-beams were spaced 2000mm perpendicular to the 4m side. Burnt clay brick wall were constructed around the perimeter of the structure to keep the heat in. Three openings were constructed on the 4m side and two openings were constructed on the 3m side. Due to the unavailability of the large laboratory furnaces to carry out the experiment, a natural fire was considered as the fire scenario to be used for experimenting following Eurocode specifications. It was observed from the experimental setup that hybrid slab could with stand a natural fire for more than one hour with the ability to maintain its load carrying capacity. Numerical simulation was done using ABAQUS-CAE a Finite Element Model programme. Natural fire curve, ECPC, ASTME119 and ISO 834 fire curves were used for numerical simulation. The numerical natural fire curve observations were consistent with the experimental results. The hybrid slab therefore meets the east African code recommendations of one hour fire resistance without collapse based on natural fire tests and therefore can be used as a construction method.

The ability of the slab to withstand fire action will depend among other factors the composite action between the timber and concrete therefore an investigation of the degree of composition between the timber and concrete was be determined considering three-inch wire nails and expanded metal lathe as shear connectors. Four test samples were cast according to Eurocode 4 for each of the connectors. A Universal Testing Machine (UTM) was used to test the samples under monotonic loading, and linear variable displacement transducers (LVDTs) were used to measure slip. It was determined that both the nails and expanded metal lathe create partial composite action between the concrete and timber elements.

1.0 CHAPTER ONE: INTRODUCTION

1.1 BACKGROUND OF THE STUDY

Conventional steel structures floor system often comprises of steel sections, sheeting, concrete, and embedded shear connectors. Figure 1.1 shows a typical arrangement of such a floor system (NBRB, 2021).

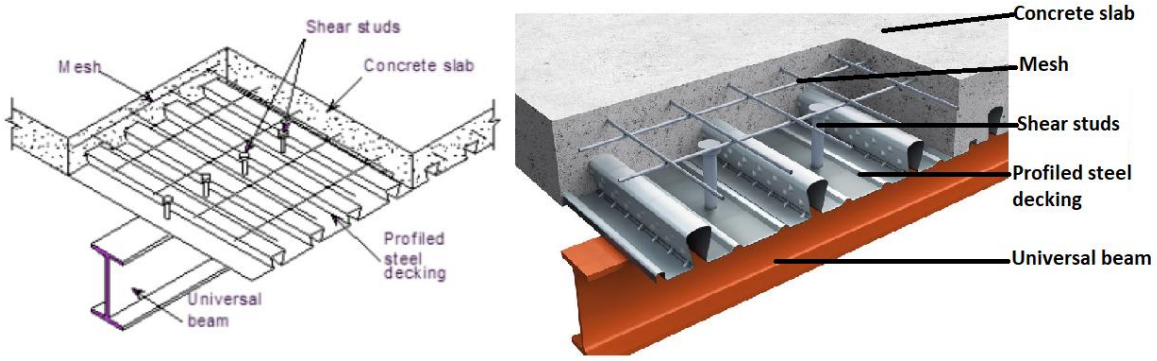

Figure 1.1: A typical steel concrete composite floor

Whereas the method illustrated in Figure 1.1 is generally recognized globally, in Uganda, there has been a growing use of timber within floor systems of steel structures. Figure 1.2 shows an example of a structural steel building in which timber is incorporated within the floor construction.

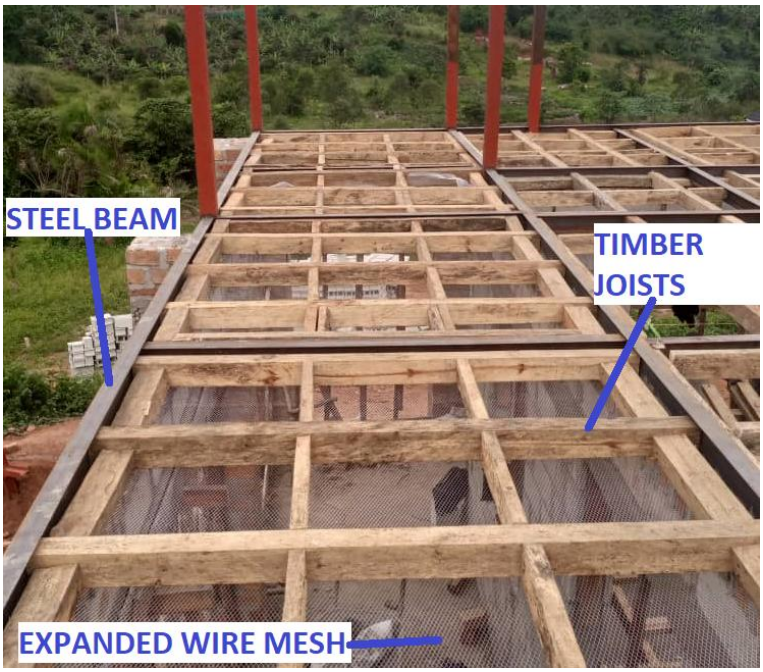

Figure 1.2: Steel frame incorporating timber in the floor.

This method consists of structural steel framing and timber joists horizontally laid on top or between the flanges of steel beams. The 100 x 100 mm timber joists are spaced at 600mm in the two orthogonal directions as shown in Figure 1.3 and 1.5. A pricking mortar coarse is applied on to an expanded metal lathe mesh that is attached to the bottom of the timber frame structure. A second layer of expanded Metal lathe (Mesh) is nailed onto of the timber framework on which a concrete toping reinforced with BRC Mesh is cast thus leaving a void between the concrete topping and the ceiling soffit as illustrated in Figure 1.4.

The timber frame is supported by steel beams in two different ways that is to say; on top of the top flange of the I-beam and at the bottom flange of the I beam as shown in Figure 1.3.

Figure 1.3: Support conditions for timber frame.

Figure 1.4: Casting the hybrid slab concrete topping.

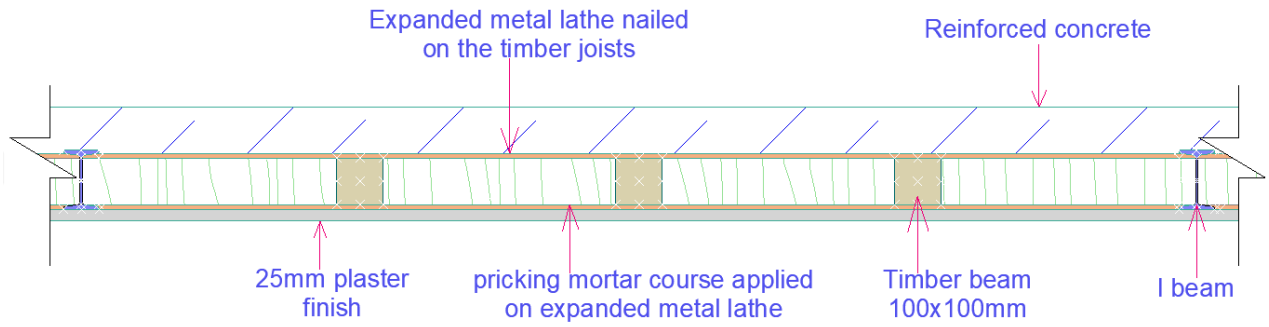

Figure 1.5: A two-dimensional view of the slab under study

Building inspectors in Uganda are now facing a challenge for not having governing guidelines for this kind of construction regarding design, durability, and performance of the structures during a fire hazard.

The challenge with this method of construction is that steel the primary supporting system loses strength during a fire and timber is a fire fuel.

Therefore, there was need to explore the structural performance of the hybrid slab when subjected to a fire hence filling a knowledge gap in fire rating for this kind of construction.

1.2 STATEMENT OF THE PROBLEM

The restriction on constructing houses with a hybrid floor system highlights the lack of clear, documented guidelines. It is unclear whether the expanded metal lathe, attached to timber and embedded in cast concrete, creates a composite action between the materials. No existing standards specify the fire rating for hybrid floors, complicating regulation efforts. As a result, it becomes essential to evaluate the structural safety of such floors under fire conditions. It is also important to determine if expanded metal lath and nails can act as shear connectors between concrete and timber.

Section 87 of the National Building Code in Uganda states that multi-storey buildings must have a one-hour fire resistance for their structural components. This requirement ensures safety during evacuation. Because of this, it is important to assess how the hybrid floor system behaves under fire conditions. The system combines timber and concrete, connected using expanded metal lath to act as a single unit. This connection must keep the structure stable even if one element loses capacity during a fire.

Research by Andreas (2010) shows that if shear connectors fail in a composite floor, the entire structure risks collapse. This can happen if the individual parts cannot support the load on their own. As a result, it is crucial to test whether expanded metal lath and nails can effectively serve as shear connectors between concrete and timber.

1.3 OBJECTIVES OF THE STUDY

1.3.1 The General Objective of the study

The primary objective was to determine fire rating of the hybrid slab made of steel, timber concrete jointed with expanded metal lathe insulated with Plaster mortar.

1.3.2 Specific Objectives of the Study

1. To determine the material specifications used in hybrid slab constructions in Uganda.
2. To determine the performance of a hybrid slab in a natural fire by comparing the numerical and experimental methods
3. To determine and compare the effect of expanded metal lathe and wire nails as shear connectors between timber and concrete.

1.4 RESEARCH QUESTIONS

Knowledge gaps that exist in the construction and design of hybrid timber concrete steel slabs.

- What are the specifications of the materials used in hybrid slabs in Uganda?
- Does plaster mortar offer insulation to the hybrid slab to increase its ability to withstand fire?
- How does expanded metal lathe perform as a shear connector in comparison to wire nails?

1.5 SIGNIFICANCE OF THE STUDY.

On the 26th of September 2022, the government of Uganda through the minister of works and transport issued a ban on building houses with hybrid slabs floor system (timber, concrete, and steel) until enough studies have been done to deem it safe as a construction method.

Furthermore, The National Building Review Board of Uganda mandated with monitoring building development on 23rd July 2021 held a consultative meeting on the viability of the hybrid building method that is currently being used to build storied structures in the country. For The Board to fulfill its mandate as mentioned above, it uses set guidelines in the national building codes to monitor the building process (NBRB, 2021). Therefore, there is need to fill some knowledge gap about the performance of this hybrid floor system in a fire.

1.6 JUSTIFICATION

The ban on building houses using the hybrid floor system shows that there is not well documented information to use in specifying codes of practice to follow when designing and constructing the hybrid floor system. In addition to the above, there is no standard that stipulates the fire rating for hybrid floors hence making the regulating of these buildings complex.

Therefore, the information that was generated in this study, will contribute to the body of knowledge about the Hybrid floor system performance in case of a fire.

1.7 SCOPE OF THE STUDY

1.7.1 Content scope

Material used in used in the study were limited the commonly used materials to build the hybrid slab in Uganda. The commonly used materials were determined from the baseline study. All materials used were locally sourced in Kampala Uganda.

The hybrid slab performance in a fire was determined using experimental and numerical methods. The experimental method was done using a natural fire and temperatures were measured using digital thermocouples. The deflection in the slab was determined using linear variable transducers. The numerical method was done using Abaqus CAE software. Temperatures recorded experimental and Eurocode parametric curve, ASTM E119, and ISO 834 fire curve temperatures were used in Abaqus software to study the performance of the hybrid slab. Experimental and Numerical results were compared. The slab layout that was studied is as shown in the Figures 1.5 above.

The effect of expanded metal lathe and wire nails as shear connectors between timber and concrete was done experimentally and numerically. The shear connector models were cast using C20/25 concrete, and timber used was eucalyptus grandis. Four specimens were made for samples using nails as shear connectors and similarly for expanded metal lathe. Two samples of the expanded metal lathe got spoilt during loading unto the universal testing machine. A non-linear numerical study of shear connectors was done in Ansys workbench software. The shear connectors materials were modelled as bilinear to determine to achieve non-linearity.

1.7.2 Geographical scope

The research study was conducted in Uganda. The slab model was built and tested in Katta, Wakiso district and the coordinates are as represented in the Table 1.1: Coordinates showing the location where the activities in this research were carried out from. Shear connectors test specimens were cast in Katta, Wakiso district and tested at college of engineering art and design (CEDAT) Laboratory in Makerere university. The structures/Sites visited in the baseline study were based in Wakiso district and Kampala districts, the coordinates are as shown in Table 1.1: Coordinates showing the location where the activities in this research were carried out from.

Table 1.1: Coordinates showing the location where the activities in this research were carried out from.

Activity	Location			
	UTM Easting/m	UTM Northing/m	UTM Zone	Altitude/m
Fire model slab constructed and tested	449115.60	52471.74	36N	1207
Shear connector models cast and cured	449115.60	52471.74	36N	1207
Shear connector models tested	451504.39	37174.77	36N	1234
Happy kids school building	449820.77	36890.12	36N	1196
Kyanja project	454745.61	43798.76	36N	1191
Kyanja Mussavu road project	454490.48	44242.78	36N	1173
Mall at kavule Makerere	452251.75	37834.73	36N	1175

UTM (Universal Transverse Mercator) coordinate system

1.7.3 Time scope

Baseline study was carried in a month. This included, two weeks desk study of design reports, structural drawing, conference reports from National building review board (NBRB).

The slab model took two weeks to build and 6 months to cure and stabilize with the environment in which it was built. Procuring the instrumental and items to use in burning procced required a month; this was due to the time required importing LVDTs from China. Assembling the instrumentation took a day. The fire was ignited and allowed to burn until all the fuel (firewood) was completely burnt out. The recording of the results started for ignition

to an hour into the cooling phase. The final observations were done a day after cooling of the specimen model.

The shear connector specimens' materials were assembled in one day and cast the following day. Allowed to be air cured for 28day and finally tested on the 29th day. The six cubes were prepared from the concrete to help determine concrete strength after 7 days and after 28days.

1.8 LIMITATION OF THE STUDY

The aim of the study was to determine the fire performance of a hybrid slab. A natural fire using wood was used instead of standard fire because there is no availability of laboratories in Uganda with furnaces where elements to a size of a slab can be tested.

There was no available diesel burner in the country to use for heating therefore wood was chosen as the fuel to be used for heating the slab.

1.9 CHAPTER SUMMARY

This research thesis is organized as follows: the research background, research objectives, significance of the study, scope, and limits discovered during the investigation are provided in the first chapter above. A review of the literature on steel-timber-concrete composite structural systems is presented in Chapter two (2). The approach used in the study is covered in Chapter three (3). The results and observations are discussed in Chapter four (4). The study's conclusions and recommendations are presented in Chapter five (5). Last but not least, the appendices, which contain any additional data mentioned in the proposal

2.0 CHAPTER TWO: LITERATURE REVIEW

2.1 INTRODUCTION

A review on timber concrete composite element, timber materials in Uganda and how timber concrete composite slabs perform in fire was presented in this chapter.

Furthermore, a review was done on the fire scenario of non-standard fire and Eurocode parametric curves of a natural fire.

A comparative review has been done of some of the studies that were conducted on timber / Wood concrete composite slabs performance in fire and research gaps were discussed.

2.2 THEORETICAL REVIEW

2.2.1 Materials

a. TIMBER

"Timber is a complex building material that does not have consistent, predictable, reproducible, and uniform properties as the properties vary with species, age, site, and environmental conditions" (Kliger, 2000).

The strength characteristics of 17 species of Ugandan ancestry were investigated by Zziwa et al. in 2010. Small clear specimen tests were carried out in shear, compression, and bending parallel to grain according to standard methods of the American Society for Testing and Materials.

Timber/ Wood species that Zziwa, et al., 2010 investigated were gathered through a survey of furniture workshops, building construction enterprises, wood yards in Kampala-Uganda and National Forestry Authority (NFA) department of wood utilization.

Zziwa, et al., 2010 concluded that: "The timber strength properties and the allowable bending stresses were comparable to those of strength classes C14 to C40 and TR 26 for softwoods and D30 to D70 for hardwoods. Hence eucalyptus grandis that was used in the study is classified as hard wood D30.

Table 2.1: Mean mechanical properties of timber species in Uganda (table adopted from (Zziwa, et al., 2010)

Species name						
Scientific name	Local/trade name	MOR, N mm^{-2}	MOE, N mm^{-2}	Compression parallel to grain, N mm^{-2}	Shear parallel to grain, N mm^{-2}	Basic density, kg m^{-3}
Albizia coriaria	Mugavu	45·8 (13·4)	5760 (1403)	35·11 (7·22)	9·82 (1·46)	567 (58)
Albizia zygia	White Nongo	54·5 (9·39)	8124 (1572)	38·62 (7·50)	7·20 (2·35)	480 (67)
Blighia unijugata	Nkuzanyana	48·5 (8·86)	9754 (1528)	35·43 (9·93)	11·79 (2·59)	536 (29)
Celtis mildbraedii	Lufugo	77·1 (11·18)	13 230 (1219)	41·55 (8·52)	13·02 (2·56)	569 (23)
Eucalyptus grandis	Kalitunsi	33·9 (14·36)	8207 (1567)	29·69 (7·94)	8·18 (2·98)	526 (34)
Lovoa brownii	Nkoba	46·2 (12·78)	9065 (1821)	36·36 (7·94)	12·06 (2·42)	514 (32)
Maesopsis eminii	Musizi	27·9 (7·83)	8569 (1110)	26·94 (7·04)	7·79 (1·19)	407 (17)
Uapaca guineensis	Namagulu	61·2 (10·59)	9320 (1835)	34·0 (7·90)	8·42 (1·13)	558 (43)
Pinus caribaea	Pine	26·9 (6·32)	7810 (1343)	26·33 (5·53)	9·67 (1·14)	383 (15)
Morus lactea	Mukooge	77·3 (11·49)	13 440 (1516)	58·45 (7·22)	9·445 (1·78)	595 (28)
Khaya anthotheca	Ugandan Mahogany	50·3 (9·04)	9388 (1733)	35·57 (7·33)	7·37 (1·123)	481 (9)
Markhamia lutea	Nsambya	43·9 (5·36)	7970 (1276)	31·74 (5·59)	7·534 (0·873)	427 (27)
Piptadeniastrum africanum	Mpewere	48·7 (7·54)	10 702 (715)	39·47 (6·06)	†	467 (26)
Funtumia elastica	Nkago	23·8 (6·55)	5612 (1044)	20·16 (4·797)	7·33 (2·444)	322 (23)
Aningeria altissima	Enkalati	38·1 (6·04)	6161 (1373)	28·07 (9·65)	8·5 (1·78)	402 (20)
Albizia gummifera	Red Nongo	43·7 (11·47)	9496 (1291)	40·11 (10·73)	8·27 (2·17)	410 (29)
Entandrophragma angolense	Mukusu	34·6 (5·9)	7482 (1093)	25·90 (5·70)	8·814 (1·231)	475 (42)

b. STEEL

Structural steel is a type of steel used to make construction components in a variety of shapes, most notably I-beams and UPN-channels. The Beams and Channels are made of high-grade steel, which makes them rigid in terms of cross-sectional areas and allows them to handle heavy weights without excessive sagging.

Steel (reinforcing bar and structural steel members) in Uganda is locally manufactured or imported. The companies that locally manufacture reinforcement bars and structural steel sections are; China Machine Building International Corporation, Steel and Tube Industries Uganda Limited, Tembo Steel Mills (Uganda) Limited, Mayuge Sugar Industries Ltd- Steel Division, Roofing Rolling Mills Limited, Pramukh Steel Limited, and MM Integrated Steel Mills (Uganda) Limited.

Steel and tube manufacture high grade steel that is Tested and approved to the following standards: ISO 657/13, US ISO 630-1, EN 10025-2 (Steel & Tube, 2023).

The Uganda National Bureau of Standards (UNBS), which is tasked with promoting fair trade and protecting the people and environment from unsafe and substandard products, specifies that hot-rolled steel sheets of high yield stress structural quality should comply with the US EAS 415: 2005 code (UNBS, 2022).

c. CONCRETE

Concrete is a composite material made of Cement, fine aggregate, and coarse aggregate. The mix ratios, cement type, water cement ratio and aggregate quality will determine the concrete grade that will be obtained. The concrete grade used in various structural members is always determined by the designer.

(i). Cement

Cement is a binder, that is used to hold together sand and gravel as a composite material. Therefore, it is used in concrete and mortar mixes. Water added to the mixture facilitates hydration of cement particles that bind aggregate together.

Cements in Uganda is manufactured by the three major companies namely; Tororo Cement Limited, Simba Cement Uganda Limited, and Hima Cement Limited. The companies listed above produce the following types of cement: -

i. White Cement
ii. Portland Slag Cement (PSC)
iii. Portland Pozzolana Cement (PPC)
iv. Ordinary Portland Cement (OPC), 53 Grade Cement
v. Ordinary Portland Cement (OPC) 43 Grade Cement

(ii). Aggregate

Fine aggregate in Uganda is obtained either from crushed rock or naturally occurring sand that is mined at river beds, lakes, swamps, and sand pits.

Coarse aggregate is obtained from stone quarries where it is crushed manually using hand tools or with mechanical crushers. Aggregate from the mechanized crushers is usually graded into sizes unlike hand crushed.

Mechanized crushers use rock blasting to break the rock away from the solid rock that can be feed in the crusher. From the crushing and sieving process, fine and coarse aggregate is obtained of various sizes that can used as a construction material.

2.2.2 DESIGN FIRE SCENARIO

Fire can be defined as; *"a chemical reaction of a combustible material with oxygen under the influence of heat. When the chemical reaction produces sufficient heat, it will trigger a chain reaction that continues if combustible materials and oxygen are available"* (Wilf Malcolm Institute of Educational Research, 2009).

Given the uniqueness of a fire scenario, it was inevitable that standardization of fire tests takes place due to the infinity possible time- temperature curves which are governed by fuel load quantity, fuel type, oxygen availability, ventilation, type of enclosure, size of structure.

The standardization resulted into generating nominal fire curves which show the relationship between the gas temperature and the time of the fire. When generating these curves an assumption was made which states that; "temperature is uniform in the whole compartment," when the fire enters the fully developed stage. The second assumption applies to most of the curves stating that, "temperatures of these curves grow without any cooling phase."

Types of fire curves

1. **Standard fire curve**

This is the oldest and first fire curve. It is shown in Figure 2.8 and 2.10. The curve depicts a fire within a single compartment of a building. It is a termed as a cellulosic curve, even though flammable materials in buildings might be of other forms other than cellulosic substance. Furthermore, the curve illustrates a fire during full development phase after the flash over point. Globally, national standards such as ISO 834, BS 476: part 20, EN 1363-1, AS 1530, and DIN 4102, specify the standard fire curve. The equation below describes the temperature development with time for a standard fire curve:

$$T = 20 + 345log(8t + 1)). \quad 2.1$$

2. **External fire exposure curve**

During a flame may emerge via openings in the exterior of a building. These flames might be long enough to heat the building's exterior as well as the floors above the fire compartment. The external fire curve is utilized in the design of buildings to provide safety against fire re-entering the building upper floors from a lower story. This curve takes into account the effect of air cooling the flames on the outside the building. A typical curve is displayed in Figure 2.8 (PROMAT, 2020).

3. **Slow heating curve**

There is usually a development phase to any real fire, during which the temperature within the compartment remains comparatively low and the fire is confined to the area where it started. This occurs before the flashover stage when all the flammable materials in the compartment will eventually start to contribute to the hence the period preceding flash-over. It takes long

due to lack of oxygen shortage causing the temperatures in the compartment to increases gradually over an extended duration (PROMAT, 2020).

4. Hydrocarbon curve (liquid pool fires)

When liquid fuel, like petrol or kerosene spills from an oil tanker and catches fire, temperatures rapidly rise to around 1,100°C. This is illustrated by the hydrocarbon (HC) fire curve in Figure 2.1. This is not common in buildings except those which serve as storage for highly flammable material. This fire curve is more relevant in industrial situations, for example; refineries and oil rigs. The following equation describes the temperature rise for the Hydrocarbon (HC) fire curve: (Chandrasekaran & Nagavinothini, 2020).

$$T = 20 + 1080(1 - 0.325e^{-0.167t} - 0.675e^{-2.5t}) \qquad 2.2$$

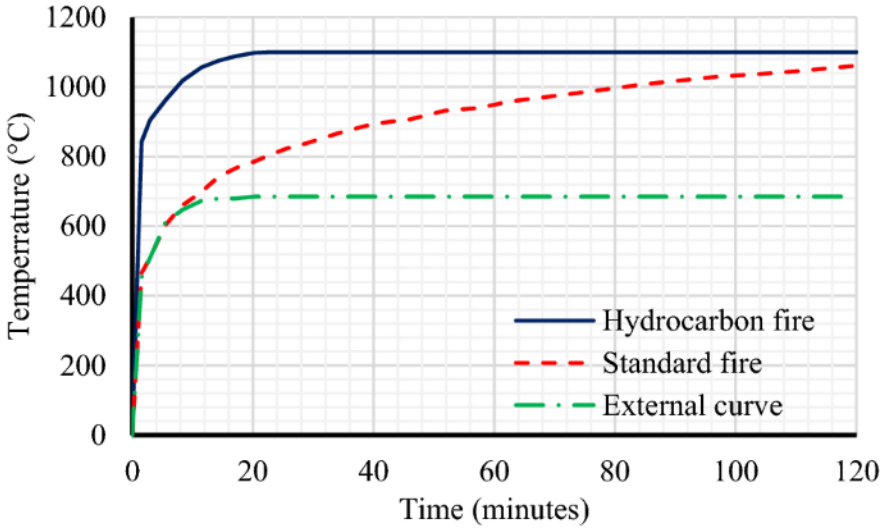

Figure 2.1: Temperature time curve for hydrocarbon, external and standard fire. Image adopted from (Chandrasekaran & Nagavinothini, 2020)

5. Tunnel fires

Tunnels are characterised with high amount of fuel in vehicles hence the fire develops quickly to high temperatures thou with limited oxygen due to ventilation conditions. Temperatures can rise higher than 1,000 ºC in less than five minutes.

The fire curve used for tunnels are:

- The RWS fire curve, created around the 1980s by the Dutch Ministry of Transportation as shown by Figure 2.2
- NFPA 502 internationally used standards.
- ASTM E3134 internationally used standards.
- HCM fire curve used in France.

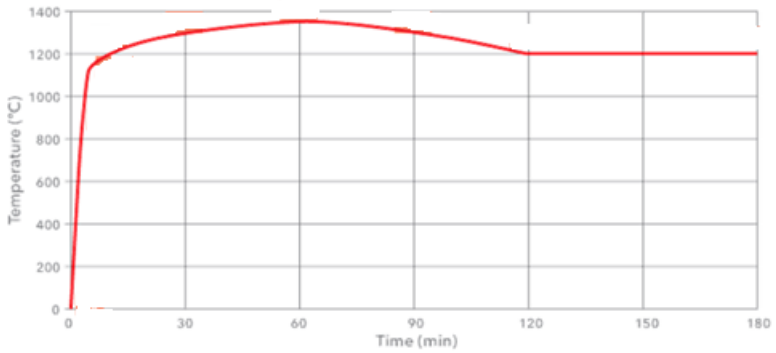

Figure 2.2: The Rijkswaterstaat (RWS) curve was created by the Netherlands' Ministry of Transportation. (adopted from (PROMAT, 2020)

6. Eurocode parametric fire curve (EPFC)

Since its introduction in Annex A of EN 1991-1-2:2002, the EPFC depicted in Figure 2.3(b) has served as a parametric estimate for one-zone compartment fires. This method uses analytical formulas to calculate a uniform "gas temperature" over time in a post-flashover fire compartment (Tom , 2011). The EPFC are computed taking into account the fuel load density, compartment geometry and building characteristics which have the following limits:

(i) The compartments should have an area less than 500 m^2 and height less than 4 m;

(ii) Openings must be in Vertical components of the building.

(iii) The Materials lining the compartment must have a thermal emissivity between 100 and 2200 $J/m^2s^{0.5}K$.

The temperature-time curves that arise are used to measure how much heat structural parts are exposed to throughout each of the typical stages of a natural fire.

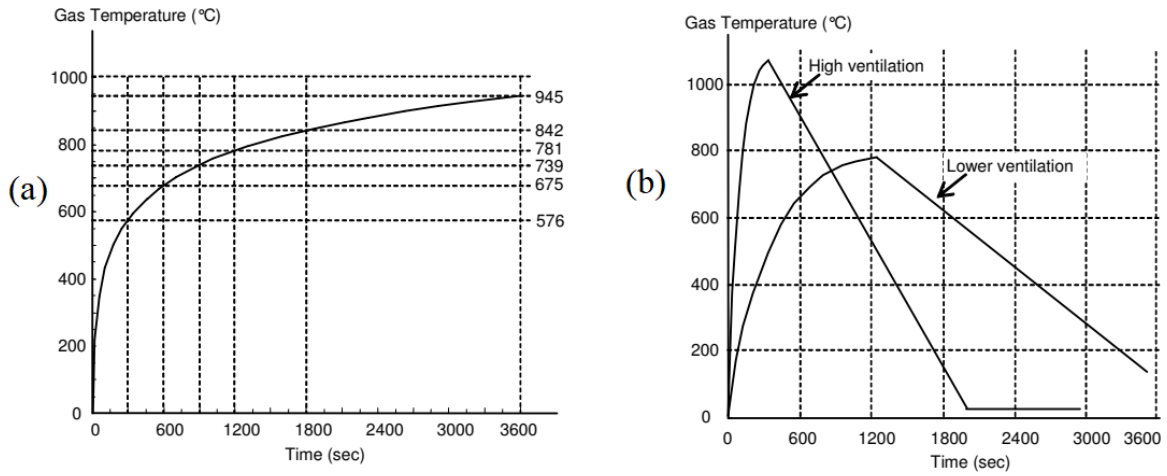

Figure 2.3: (a) ISO 834 Standard Fire curve, (b) Eurocode 1 Parametric fire curves, (figure adopted from (Burgess, 2015))

7. Natural fire curves

With the use of contemporary technological advances, it is possible to compute natural fire curves, that can describe the development of temperatures over time inside an enclosure putting into consideration its actual shape and geometric properties, the rate of heat discharge from combustible substances, the quantity of oxygen present and availability of active fire protection. These curves are not "standard" and solely apply to a particular situation that occurs for the entirety of the fire in a particular compartment.

Choosing between using a nominal fire curve or a "natural" fire model to assess the compartment time-temperature response is the main decision the designer must make at this point in order to protect the building from unwanted fire effects. For classification and comparison reasons, nominal fires are representative fire curves; nonetheless, they are unrelated to the physical features of the building in question. In contrast natural fire curves consider the physical characteristics unique to a given building during calculating. (Lennon, 2011).

The most dangerous scenario from a structural point of view is when there is a flashover inside the compartment and all combustible elements get engaged in a fire. It is during this stage of the fire that the most significant hazard to structural stability occurs. (Lennon, 2011).

This intricate process can be reduced to a three-phase behavior that is defined by the "flashover" transition point as depicted in Figure 2.11.

2.2.3 Natural fire phase description

The fire phase descriptions are as shown in the Figure 2.4

Growth phase (pre-flashover)

The fire stays contained in a small area as a hot layer forms beneath the ceiling as a result of the combustion products accumulating. Smouldering and flaming may be observed governed by the availability of oxygen for combustion. Limited oxygen will create a layer of carbon monoxide and other harmful gasses can frequently undermine tenability conditions, making this phase the most dangerous for life safety. Availability of oxygen and enough heat released from the combusting material will determine whether the fire will continue to grow and spread. (Tom , 2011).

Flashover

This marks the change from a contained to a fully grown fire. When continuous flames from flammable material reach the ceiling and the hot gas layer's temperature is between 550 and

600 degrees Celsius, flashover is likely to happen. After flashover, the oxygen concentration will drop and the rate of heat release will accelerate until it the maximum temperature value.

Fully developed phase (steady state)

At this point, all fuel that is accessible is burning. Either the amount and type of fuel or the availability of oxygen will determine the maximum amount of heat emission. It is during this stage that structural failure and damage is likely to occur.

Decay phase (cooling)

Once 70% of the fuel has been used, or after a prolonged burning period, the fire will eventually die and the temperature will drop. (Tom , 2011).

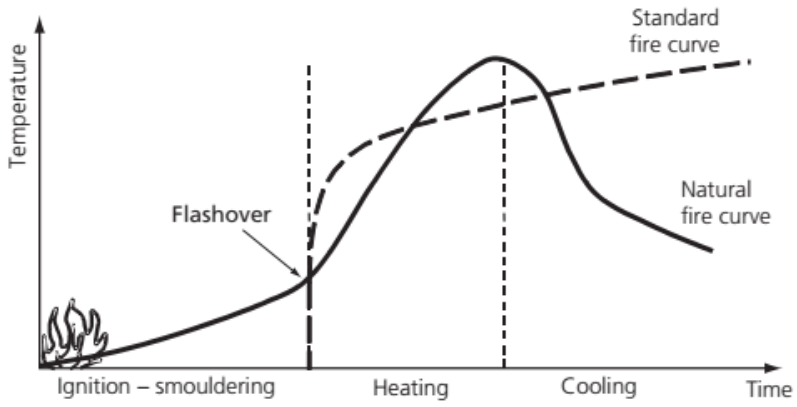

Figure 2.4: A typical natural fire curve showing the fire growth stages. (adopted from (Tom , 2011)

2.2.4 Timber concrete steel composite design

The degree of composition between wood and concrete, steel and concrete, steel and timber/ wood depend on the stiffness of their interfacial connection. “A typical composite material is a system of materials composing of two or more materials (mixed and bonded) on a macroscopic scale”, (NAGAVALLY, 2016). Hence the construction industry employs composite construction by joining two or more materials to form a structural element.

To design a composite floor the degree for composite action is governed by shear connectors. Fragiacomo & Lukaszewska, (2011) State that there are two bounds of composite action namely:

(a) An upper bound of fully composite action: Timber and concrete components that are rigidly connected with no interlayer slip, have cross-sections with a single neutral axis and identical flexural strains at the timber-concrete interface as illustrated in Figure 2.5(a).

(b) A lower bound of fully non-composite action, the two components (Timber and concrete) work independently, with no horizontal force transfer between the two layers. The layers have individual neutral axes hence flexural strain is discontinuous at the interface of the two materials as illustrated in Figure 2.5(c).

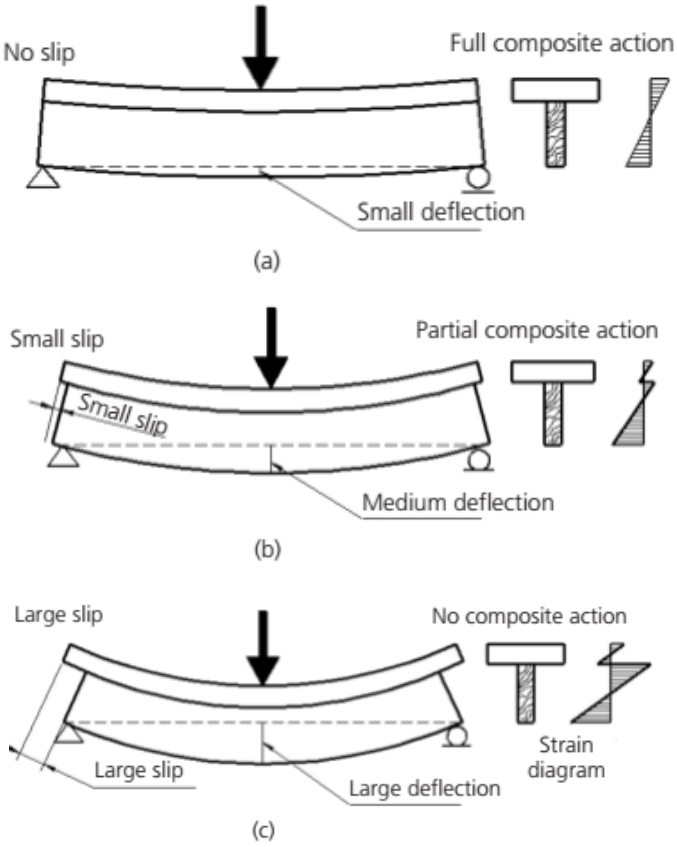

Figure 2.5 Strain diagrams for composite structures with (a) a rigid connection, (b) a deformable connection and (c) no connection between the timber beam and concrete slab

The terms complete and partial shear connection are used to describe shear connections based on their strength. A full shear connection implies that the shear connection has sufficient strength and that the final load is determined by the maximum moment of resistance. As a result, adding more shear connectors will not raise the ultimate load. When fewer shear connectors are used, the maximal moment of resistance cannot develop, hence the shear connection is referred to as partial. In the absence of shear connectors, the ultimate loads is dependant on the maximum moment the beam can support. As a result, beams with partial shear connections fail due to failure of the shear connectors.

Transferring internal shear stress from one material to another through a shear connection system is necessary to accomplish full or partial composite behavior within a timber, steel, and concrete floor system. The distribution of shear forces determines how shear connections are

structured. They are positioned closely near the supports, where the internal shear force is highest, and gradually spaced out towards the middle of the span, where the internal shear force reaches zero. (Yeoh & Chuan , 2010).

Shear connectors

Shear connectors resist shear forces at the connection between the elements in a composite structure. If the separate sub-elements of a composite floor are not able to withstand the load independently, a failure of the shear connectors could result in the floor collapsing. (Andreas , 2010).Higher shear forces in timber concrete composite require shear connectors that are stiffer and stronger. (Andreas , 2010).

The connectors should be ductile hence maximizing the composite action. To characterize a connection system as ductile or non-ductile, push put shear tests carried out on composite samples subjected to a direct shear force. The results are then used to determine the shear connector's stiffness and strength.

Push out tests are performed in line with EN 26891 (CEN, 1991), and load-displacement curves are drawn. Strength is characterized as the maximum load imposed before failure. Stiffness is defined by the slip modulus which is the secant gradient of the load-displacement graph at three distinct load values (40, 60, and 80% of the average peak load), as illustrated in Figure 2.6.

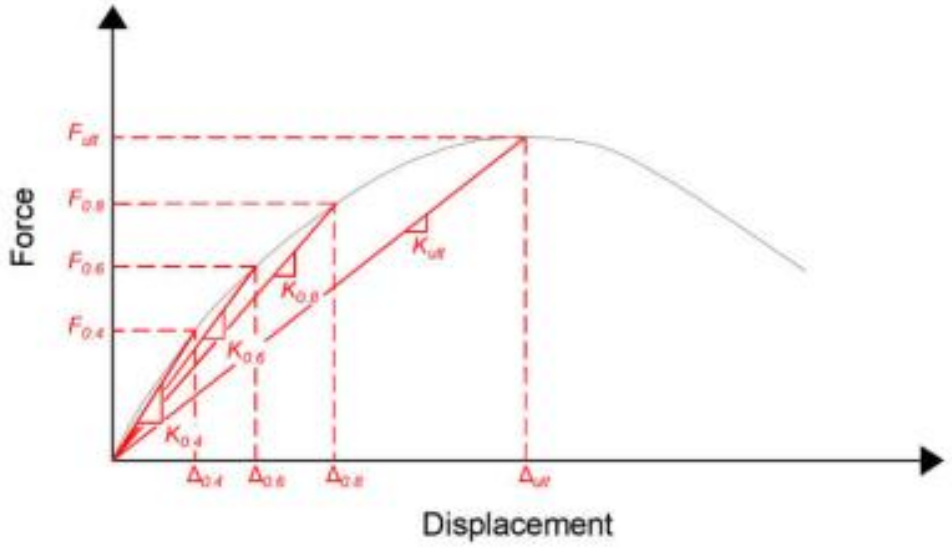

Figure 2.6: A sample load slip curve. (Figure adopted from (Hong, 2017))

The load-slip curves indicate whether shear connectors are ductile or nonductile as illustrated in Figure 2.6. When ductile shear connectors are as characterised by further slip as soon as the

ultimate load is reached. The connectors continue to deform further, and slip occurs at the composite member contact. Whereas for nonductile rigid shear connectors, once the peak load is attained failure of the beam occurs since the connectors lack deformation capacity.

As a result, the bending strength of a composite component with nonductile connectors cannot be estimated using rigid plastic analysis. Design codes either consider an overconservative elastic analysis or nonlinear analysis to be applied. Furthermore, it should be mentioned that there are some circumstances when the rigid plastic analysis is unable to determine the bending strength of beams with ductile shear connectors. (Kostic & Deretic-Stojanovic, 2018).

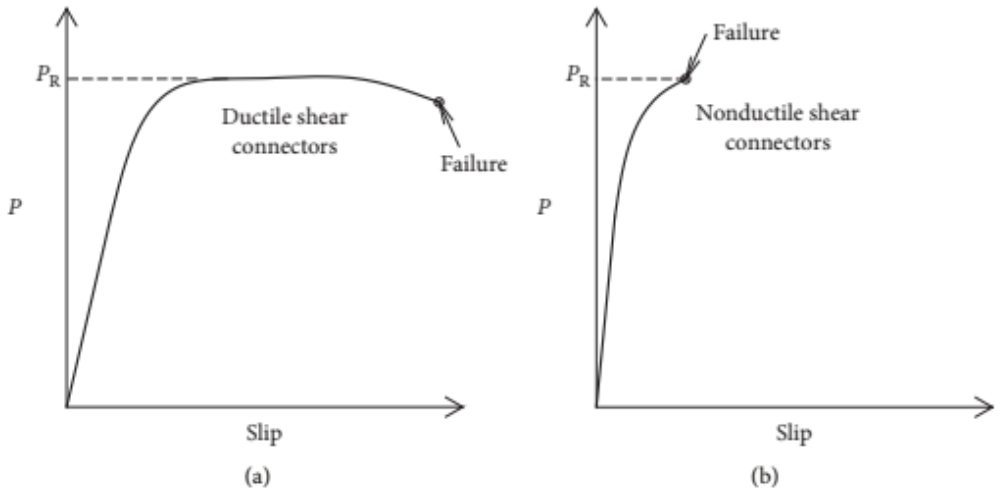

Figure 2.7: typical load-slip relations for (a) ductile and (b) non-ductile shear connectors. Adopted from (Kostic & Deretic-Stojanovic, 2018).

2.2.5 Design methods.

Several approaches have been developed and studied to design timber concrete composite bending members, which include: - The γ-method of transformed sections, only applies to fully composite sections when used with steel-concrete composites. For partially composite sections, like in the case of Timber Concrete Composite Systems with Semi-rigid Connectors, it is non-conservative. (Hong, 2017)

Frangi & Fontana 2003, proposed that, "the elastoplastic solution for cases in which the failure of the Timber concrete composite is attained after connector plasticization. This is common when the connectors are low strength, low stiffness, and high ductility. The failure load is evaluated by assuming a rigid-perfectly plastic connection."

Comprehensive formulas based on the γ-method are available in the European Standard for Timber Design, Eurocode 5, Part 1, Annex B (CEN, 2004), for the design of composite bending elements. Currently, the most common application of this clause is in the design of Timber Concrete Composite bending members. (Hong, 2017).

1. The Gamma (γ) method

According to EN 1995-1-1 (2002), the following conditions must be met in order to apply the γ -method; The design of timber constructions (Andreas , 2010);

1. For simply supported beam, the span is *l* whereas for continuous or cantilever beams, *l* is as follows:
    a. *l = 0,8*l* for continuous beams
    b. *l = 2*l* for cantilevered beams
2. The individual timber elements are either full length or have glued end joints.
3. The separate components fastened together using mechanical fasteners with a sliding modulus K.
4. Depending on the shear force, the spacing "s" between the fasteners either remains constant or changes uniformly, between s_{min} and s_{max} with $s_{max} \leq 4*s_{min}$
5. The load is applied in the z-direction, producing a shear force V=V(x) and a moment M=M(x) that varies sinusoidally or parabolically.

Equation 2.01 can be used to compute the effective beam bending stiffness if the above presumptions are met. (Andreas , 2010)

$$(EI)_{eff} = \sum_{i=1}(E_i I_i + \gamma_i E_i A_i a_i^2) \qquad 2.3$$

Where:

E_i – the i-th sub-element's mean elasticity modulus value

$I_i = \frac{b_i h_i^3}{12}$ - The i-th sub-element's second moment of inertia

$A_i = b_i h_i$ – the cross-sectional area

$\gamma_i = \frac{1}{1+\frac{\pi^2 E_i A_i s_i}{K_i l^2}}$ – parameter (for i=1 and i=3) for the composite action

$\gamma_2 = 1$

a_i – The separation distance between the neutral layer of the composite element and the centroid of the i-th sub-element

Equation 2.3 becomes Equation 2.4 for a timber-concrete composite T-beam, as shown in Figure 2.7.

$$(EI)_{eff} = E_1 I_1 + \gamma E_1 A_1 a_1^2 + E_2 I_2 + E_2 A_2 a_2^2 \quad 2.4$$

where γ and a are calculated using equations 2.5, 2.6, and 2.7, respectively, and index one represents the concrete component whereas index two relates to the timber component.

$$\gamma = \gamma_1 = \frac{1}{1+\frac{\pi^2 E_1 A_1 s}{kl^2}} \quad 2.5$$

$$a_2 = \frac{\gamma E_1 A_1 (h_1+h_2)}{2(\gamma E_1 A_1 + E_2 A_2)} \quad 2.6$$

$$a_1 = \frac{h_c+h_t}{2} - a_2 \quad 2$$

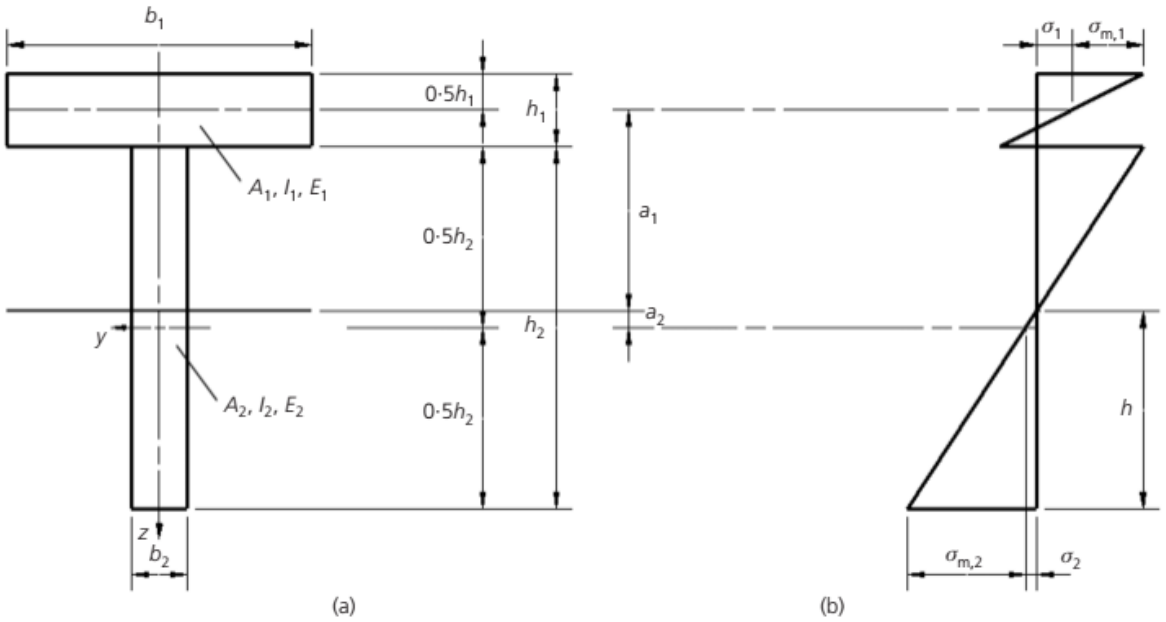

Figure 2.8 A timber concrete composite T- beam

2. Girhammar's simplified approach

The following presumptions must be met for the method to become applicable.

1. With a constant slip modulus K, the mechanical shear connectors are uniformly spaced and generate evenly distributed slip forces.
2. The fully composite section's centroid contains the x-axis. The symbols u and w, respectively, represent the displacements in the x- and z-directions.

Thus, the effective bending stiffness of a composite T-beam can be determined using equation 2.8. (Andreas , 2010)

$$EI_{eff} = \frac{\mu_\infty^2}{\mu^2}\left[1 + \frac{\frac{EI_\infty}{EI_0}-1}{1+\left(\mu/\pi\right)^2(\alpha L)^2}\right]^{-1} EI_\infty \quad 2.8$$

Where:

μ – partially composite beams buckling length coefficient

μ_∞ - fully composite beam Buckling length that corresponds to the standard Euler-buckling length coefficient

$\alpha L = \sqrt{\frac{Kr^2}{EI_0(1-EI_0/EI_\infty)}L}$ - The non-dimensional shear connector parameter.

$EI_O = E_1I_1 + E_2I_2$ - The bending stiffness of the corresponding non-dimensional section

$EI_\infty = EI_0 + \frac{EA_p r^2}{EA_o}$ – fully composite section bending stiffness where r = distance between sub-elements centroids

$EA_O = E_1I_1 + E_2I_2$ – sub-element axial stiffness sum

$EA_P = E_1I_1 + E_2I_2$ – sub-elements axial stiffness product.

Equation 2.8 can be simplified to Equation 2.9 because the buckling length coefficients given partially composite beams are essentially identical to Euler buckling length coefficients for the majority of boundary conditions. (Andreas , 2010):

$$EI_{eff} \approx \left[1 + \frac{\frac{EI_\infty}{EI_0} - 1}{1 + \left(\mu/\pi\right)^2 (\alpha L)^2}\right]^{-1} EI_\infty \qquad 2.9$$

Equations 2.10–2.14, once the effective bending stiffness has been determined, can be used to determine the internal actions.

$$N_{1,eff} = -\left(1 - \frac{EI_O}{EI_{eff}}\right)\frac{M}{r} \qquad 2.10$$

$$N_{2,eff} = -\left(1 - \frac{EI_O}{EI_{eff}}\right)\frac{M}{r} \qquad 2.11$$

$$M_{i,eff} = \pm\frac{E_i I_i}{EI_{eff}} M \qquad 2.12$$

$$V_{s,eff} = \left(1 - \frac{EI_0}{EI_{eff}}\right)\frac{V}{r} \qquad 2.13$$

$$V_{i,eff} = \frac{E_i I_i}{EI_{eff}} + V_{s,eff} r_i \qquad 2.14$$

$V_{s,eff}$ interlayer slip/shear force between the sub- elements,

$V_{i,eff}$ shear force operating on sub-element i's cross section, As shown in Figure 2.9. The load that is exerted on the shear connector can be simply calculated through multiplying the interlayer slip force by the fastener spacing (see Equation 2.15) whereas The interlayer slip is derived from Equation 2.16. (Andreas , 2010).

$$F_{s,eff} = V_{s,eff} s \qquad 2.15$$

$$\Delta u = V_{s,eff}/K \qquad 2.16$$

The deflection can be calculated by substituting the effective bending stiffness in conventional equations with the effective bending stiffness derived using equation 2.8. (Andreas , 2010)

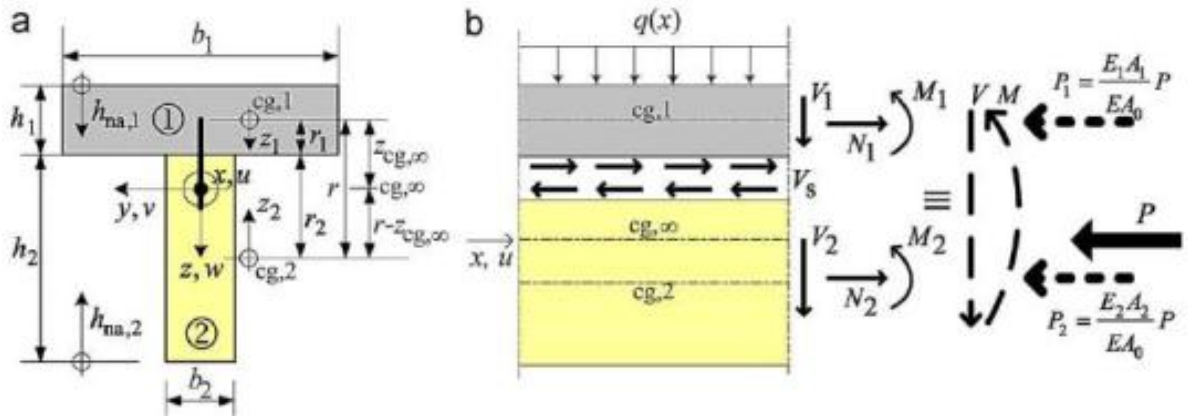

Figure 2.9 The Quantiti1es used in Girhammar's simplified method (Girhammar's, 2009)

2.3 EMPIRICAL REVIEW

2.3.1 Fire testing of composite slabs

Meena *et al*. in 2014 conducted a study on; "Experimental and Numerical Investigations of Fire Resistance of Novel Timber-Concrete-Composite Decks" shown in Figure 2.10. The study was aimed at establishing fire resistance rating of a Timber Concrete Composite floor system in relation to ISO 834-1 (ISO 1999) in addition to confirming the numerical model's validity as a basis for parameter optimizations and forecasting the fire resistance ratings of systems that have been modified.

Meena *et al*. in 2014 designed and tested a complete assembled floor system that comprised all structural and mechanical functions, e.g., floor heating and cooling, and sprinkler system.

Figure 2.10 The schematic illustration of the novel Timber Concrete Composite system (Meena, et al., 2014)

Meena *et al*. in 2014 conducted his experiments at the Swiss Federal Laboratories for Materials Science and Technology (EMPA) fire testing facility. He considered an ISO 834-1 (ISO 1999) condition fire condition for sixty minutes.

The slab element was exposed to fire only at the bottom surface that is to day where the concrete element of the slab was. Temperature was measured using thermocouples which were connected to a measuring device. Thermocouples were evenly distributed over the various slab elements.

Meena *et al*. in 2014 in his research was to also carry out a numerical analysis. The numerical analysis was carried out using ANSYS workbench software to simulate the fire effect on the slab. When numerical and experimental results were compared, they show resemblance.

(Meena, et al., 2014) concluded that: -

1. The slab system was assumed to have a fire rating of R60 (sixty minutes).
2. the reinforcement's minimum concrete cover of 25 mm is adequate for the slab to withstand fire flames for sixty minutes
3. water pipes installed in the slab as to serve as a firefighting mechanism were observed to have melted and water escaped through thermal cracks.
4. The beam slab groove connection of timber and concrete respectively was able to sustain the slab load for the entire time sixty minutes of the experiment concluding that the 50mm concrete cover on the groove was sufficient
5. To achieve system optimization the numerical model can be used since the results obtained through numerical analysis tallied with results obtained experimentally.

O'Neill, 2009 researched about, “The Fire Performance of Timber-Concrete Composite Floors” illustrated in Figure 2.11. O’Neil 2009 aims of the study were to: -

- Examine how timber concrete composite flooring behave in the event of a fire. This entails not only observing the floor's failure mechanism but also learning about the individual system components, such as the concrete's spalling and wood beams' charring patterns.
- To create a rudimentary spreadsheet analysis tool that can forecast the anticipated fire resistance of these kinds of flooring, taking into account any time-dependent variable properties that might emerge from the full-scale testing, such as a fluctuating rate of charring, a smaller section size, or a loss of the floor's composite action that might arise from extended exposure to the fire.

The aforementioned goals were achieved through full-scale furnace testing of two timber concrete composite floors. In addition, a secondary small-scale timber testing was conducted to ascertain the mechanical characteristics of the wood at high temperatures and whether any further connection problems could result from the heating of the wood.
it was from both types of testing that a spreadsheet was developed with the use of test data and visual observations.

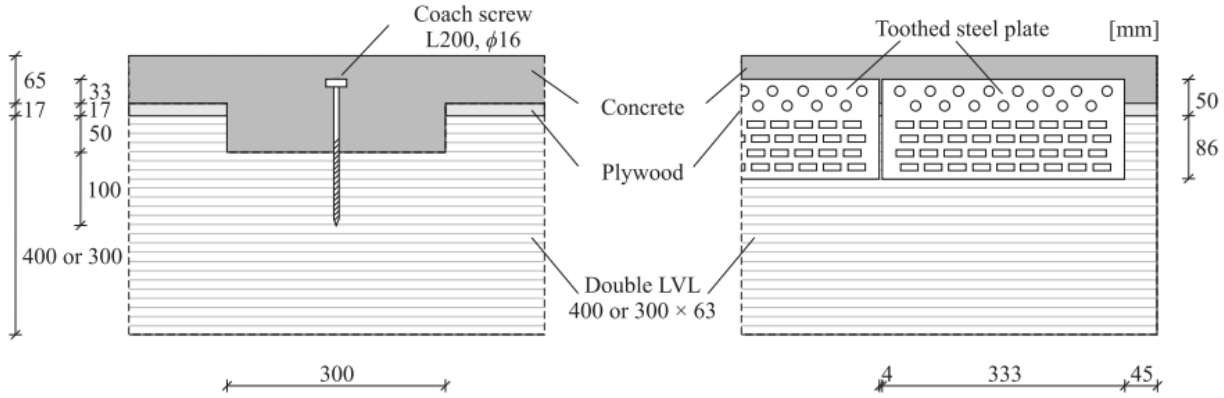

Figure 2.11 Section view of the two full scale slabs investigated by O'Neill 2009; "Notched connection with screws and toothed steel plate connection." (Adopted from O'Neill 2009).

O'Neill 2009, likewise as Meena *et al*. in 2014 developed a spreadsheet tool to aid in quick numerical check of the fire resistance duration of a floor under user-defined load circumstances and floor geometries.

(O'Neill, 2009) concluded that: -

a. The 15% of the timber section was not sufficient to sustain design load, hence timber charring governed the floor failure.
b. The composite beam floors showed a higher fire resistance compared to non-composite beams tested in the same furnace conditions.
c. The bottom of the concrete slab expanded because of the higher thermal exposure at the bottom than at the top but the composite connections was observed to serve as a restriction hogging of the entire specimen. This helped the floors resist the gravity loads placed on them and decreased their vertical deflections. Hence an extended floor fire resistance time.
d. The slab thickness and the concrete mix ration affected the slab insulation capability. Concrete mix was inversely proportion to the spalling (the lower the concrete mix quality the higher the spalling) and Thickness was also inversely proportion the

temperature measured at the top of the slab (Smaller slab thickness were equivalent to higher temperatures measured at the top of the slab).

e. Non-composite beams experienced higher charring rates and quicker failure since all sides of the beam were exposed to the fire after separation.
f. On comparing steel plate vs notched connection beams, steel plate connections showed a stiffer and less deflection than notched counter parts during the experimental investigation.

2.3.2 Shear connectors used between timber and concrete.

Timber concrete composite shear connection systems have been grouped by Ceccotti, (2002) in depending on the stiffness as shown in Figure 2.2: Groups A, B, and C connectors are arranged from low stiffness to high stiffness and give partially composite action. Group D connectors are the stiffest and can achieve full composite action (Aicher, et al., 2003).

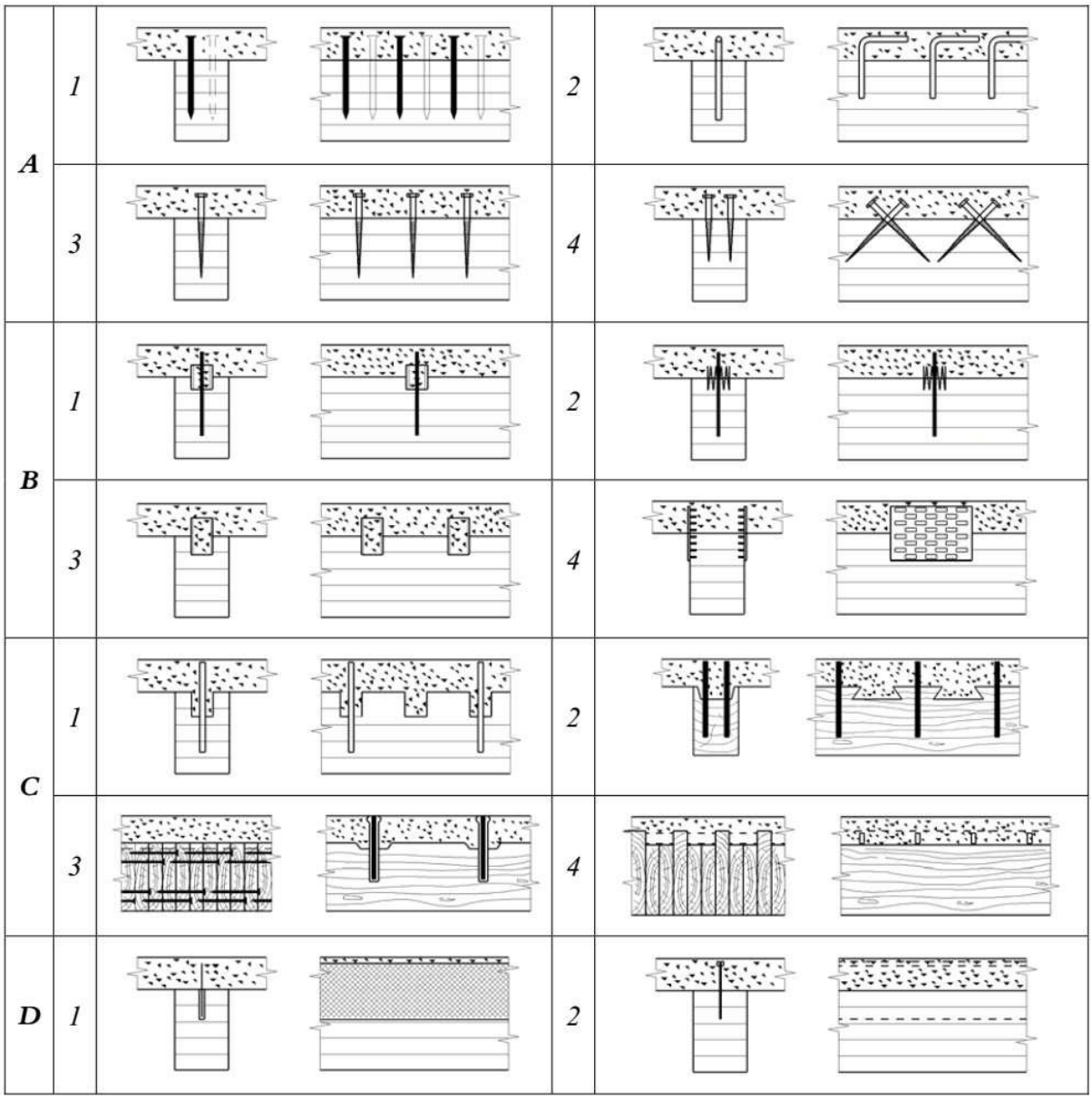

Figure 2.12: Timber concrete composite connections with: "nails (A1); glued reinforced concrete steel bars (A2); screws (A3); inclined screws (A4); split rings (B1); split rings and toothed plates (B2); steel tubes (B3); steel punched metal plates (B4); round indentations in timber, with fasteners preventing uplift (C1); square indentations, ditto (C2); cup indentations and prestressed steel bars (C3), nailed timber planks deck and steel shear plates slotted through the deeper planks (C4), steel lattice glued to timber (D1); and steel plate glued to timber (D2).". Adopted from (Ceccotti, 2002)

Different connection categories as describe in Figure 2.2 while exhibit unique load displacement relationship in a load displacement graph as illustrated in Figure 2.4.

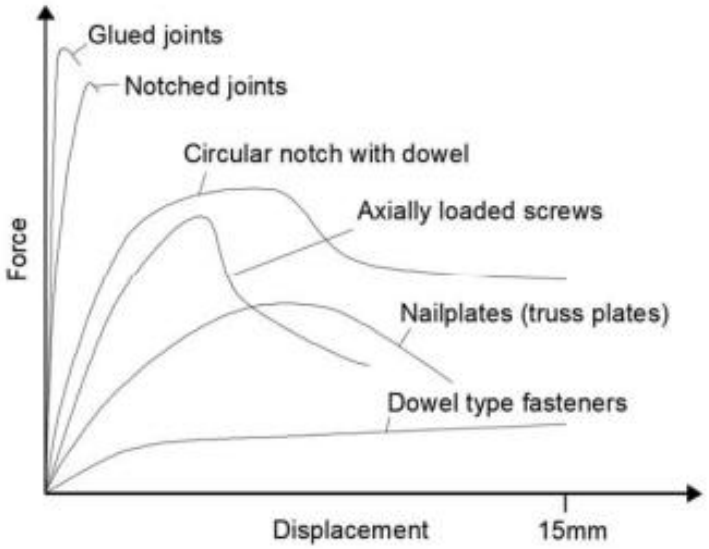

Figure 2.13: A graph comparing the Load slip curves of different shear connector categories (Adopted from (Dias, 2005))

2.4 SUMMARY OF LITERATURE AND RESEARCH GAPS

In relation to the above literature, the following gaps were identified and addressed: -

1. It was determined from research that exposed timber beams experience high charring rates and therefore this research focuses on finding out if plaster mortar mix can be used as an insulation to the slab structural elements.
2. Literature has established that notched dowel bars, nails, and screws serve as effective shear connectors for forming a timber-concrete composite structural element capable of withstanding loads as a unified entity. The hybrid slab being examined utilizes expanded metal lath positioned between timber and concrete, yet there is no indication of whether this configuration facilitates composite action, thereby highlighting a recognized research gap for further investigation.

2.5 CONCEPTUAL FRAME WORK

2.5.1 Introduction

The performance of hybrid floor systems under fire conditions is a critical concern in structural engineering, particularly as sustainable materials like timber are increasingly integrated with steel and concrete. This study investigates the fire resistance of hybrid slab (steel–timber–concrete slabs), using both experimental and numerical methods to understand how various structural and environmental factors interact.

The conceptual framework guiding this research is built upon the interplay between material properties, connection techniques, and environmental stressors, all of which influence the fire resistance of the composite slab system. The framework is designed to capture the complexity of these interactions by categorizing variables into independent, mediator, moderator, and dependent roles, within the context of laboratory investigations and field data sets.

2.5.2 Conceptual frame work presentation

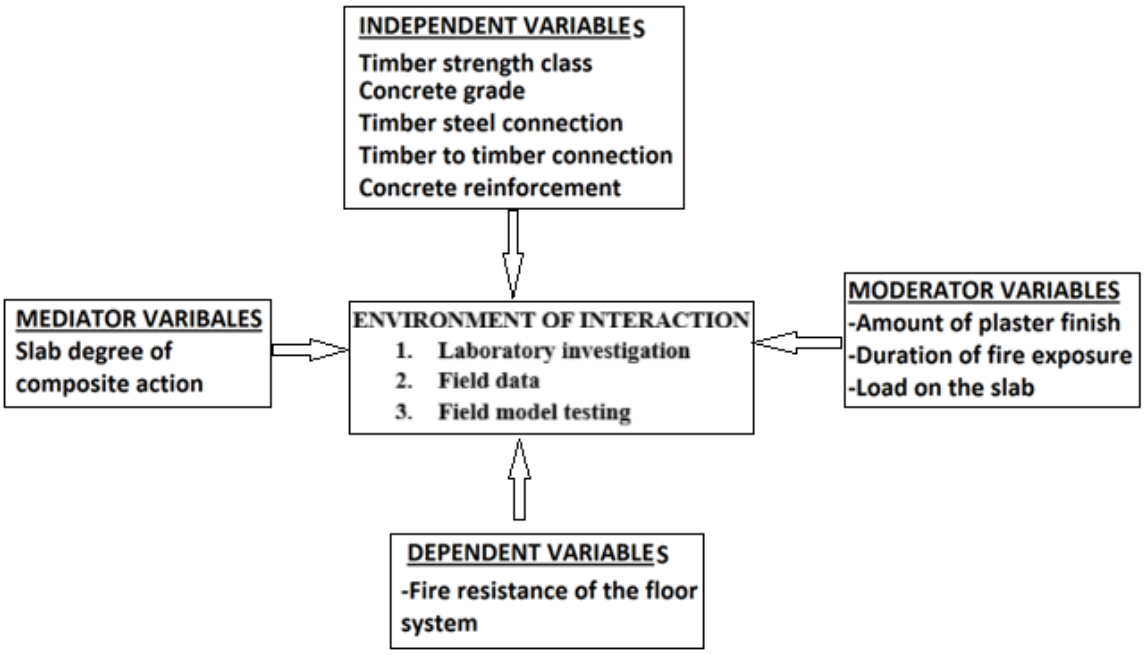

Figure 2.14: Conceptual frame work

2.5.3 Conceptual framework: discussion

1. **Independent Variables**

These are the primary design and material parameters hypothesized to influence fire resistance:

a. **Timber Strength Class**: Determines the charring rate and structural integrity under heat.
b. **Concrete Grade**: Affects thermal conductivity and spalling behaviour.
c. **Timber–Steel Connection Type**: Influences load transfer and thermal bridging.
d. **Timber–Concrete Reinforcement**: Enhances composite action and fire endurance.

These variables are manipulated or observed to assess their direct and indirect effects on the slab's fire performance.

2. **Mediator Variable**

Slab Degree of Composite Action: This variable mediates the relationship between material/construction choices and fire resistance. A higher degree of composite action typically improves load distribution and thermal stability, thereby enhancing fire resistance.

3. **Moderator Variables**

These variables are external conditions that may amplify or diminish the effects of the independent variables:

a. **Amount of Plaster Finish**: Acts as a passive fire protection layer, delaying heat penetration.
b. **Duration of Fire Exposure**: Determines the extent of thermal degradation.
c. **Load on the Slab**: Influences stress distribution and failure modes during fire.

These moderators are crucial for understanding performance under realistic fire scenarios.

4. **Dependent Variable**

Fire Resistance of the Floor System: Measured in terms of time to failure, temperature thresholds, and structural integrity during fire exposure. This is the ultimate outcome the study seeks to predict and improve.

5. **Environment of Interaction**

a. **Laboratory Investigations**: Provide controlled conditions to isolate and test specific variables.
b. **Field Data Sets and test**: Offer real-world validation and variability, enriching the robustness of the findings.

3.0 CHAPTER THREE: METHODOLOGY

3.1 INTRODUCTION

In this chapter methods and experimental setup used were defined. It includes the baseline study methodology, the experimental investigation of the a hybrid steel timber concrete slab methodology, the numerical simulation methodology for both fire resistance of the hybrid steel timber concrete slab and push out analysis set up last but not least the experiment methodology of the push out test.

3.2 BASELINE STUDY METHODOLOGY

A baseline study was carried out about the hybrid steel timber concrete slabs constructed in Uganda. This was to help establish the parameters to be consider in building the experimental model.

3.2.1 Procedure used to carry out a baseline study.

1. **Defining the baseline study objectives**

Before carrying out the baseline study, objectives were defined to as to ascertain the scope of the study and the objectives were as follows: -

(a) The average thickness of the concrete topping cast used in these hybrid slabs.
(b) The concrete class designed for the hybrid slabs.
(c) The reinforcement used in the concrete.
(d) The existence of shear connections.
(e) The dimensions of timber employed.
(f) The type of timber used.

2. **Identifying the information Sources:**

Since this is a new construction method in Uganda, the best information sources identified were; - the contractors, the designers, and the National building review board (NBRB) report about the hybrid slabs.

3. **Gathering Data:**

Data was gathered by interviewing the contractors, designers, and reading the National building review board report (NBRB, 2021)

4. **Reviewing and analyzing the data**

The data gathered was categorized to obtain valuable information about the baseline study objectives. Grouping the data aided to draw conclusions.

5. Drawing Conclusions

Basing on the analysis, conclusions that addressing the goals and aims of the baseline study were drawn. Through these findings,' valued knowledge was to be obtained from which to base on to build the experimental and numerical model for testing.

3.3 EXPERIMENTAL PROCEDURE FOR HYBRID (STEEL TIMBER CONCRETE) SLAB FIRE TESTING

Experimental work procedure to investigate the fire resistance of the hybrid steel timber concrete slab was done according to the following procedure: -

Set of the specimen

- A 4x3m slab was constructed as specified in section 4.5 of BS 476-20: 1987. The model setup constructed was illustrated in Figure 3.1 and Figure 3.2 (a, b, c, and d)

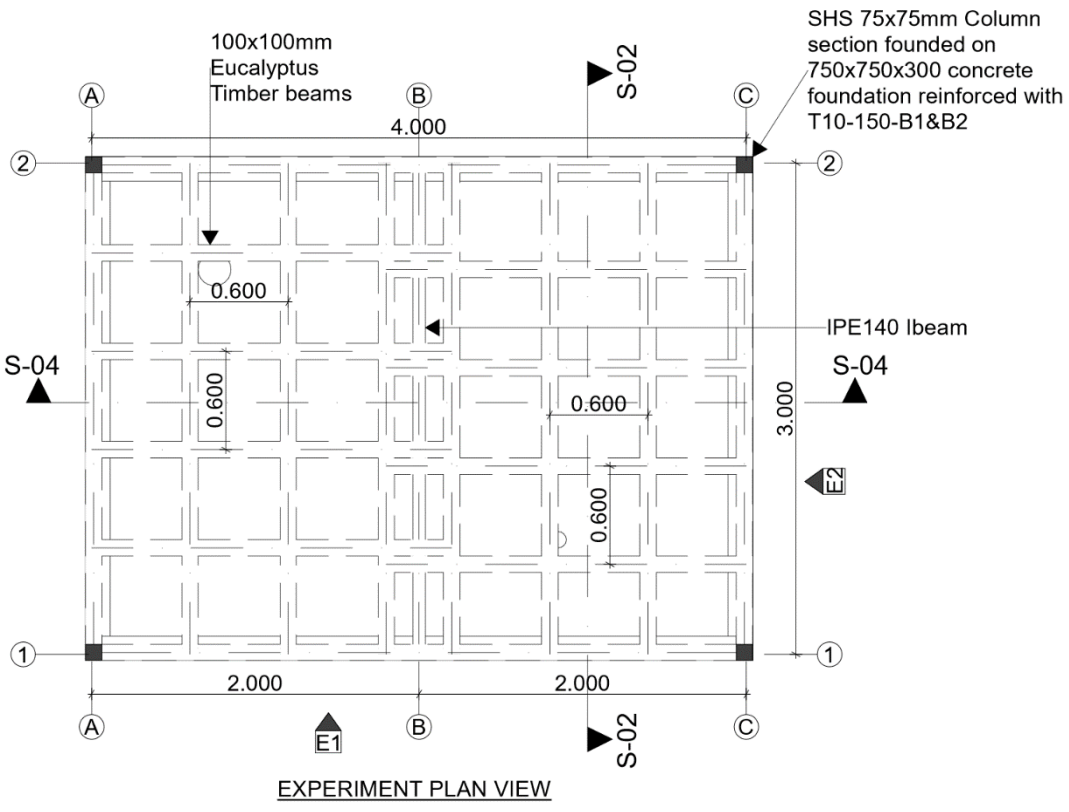

Figure 3.1: Hybrid (steel timber concrete) Slab model floor plan view

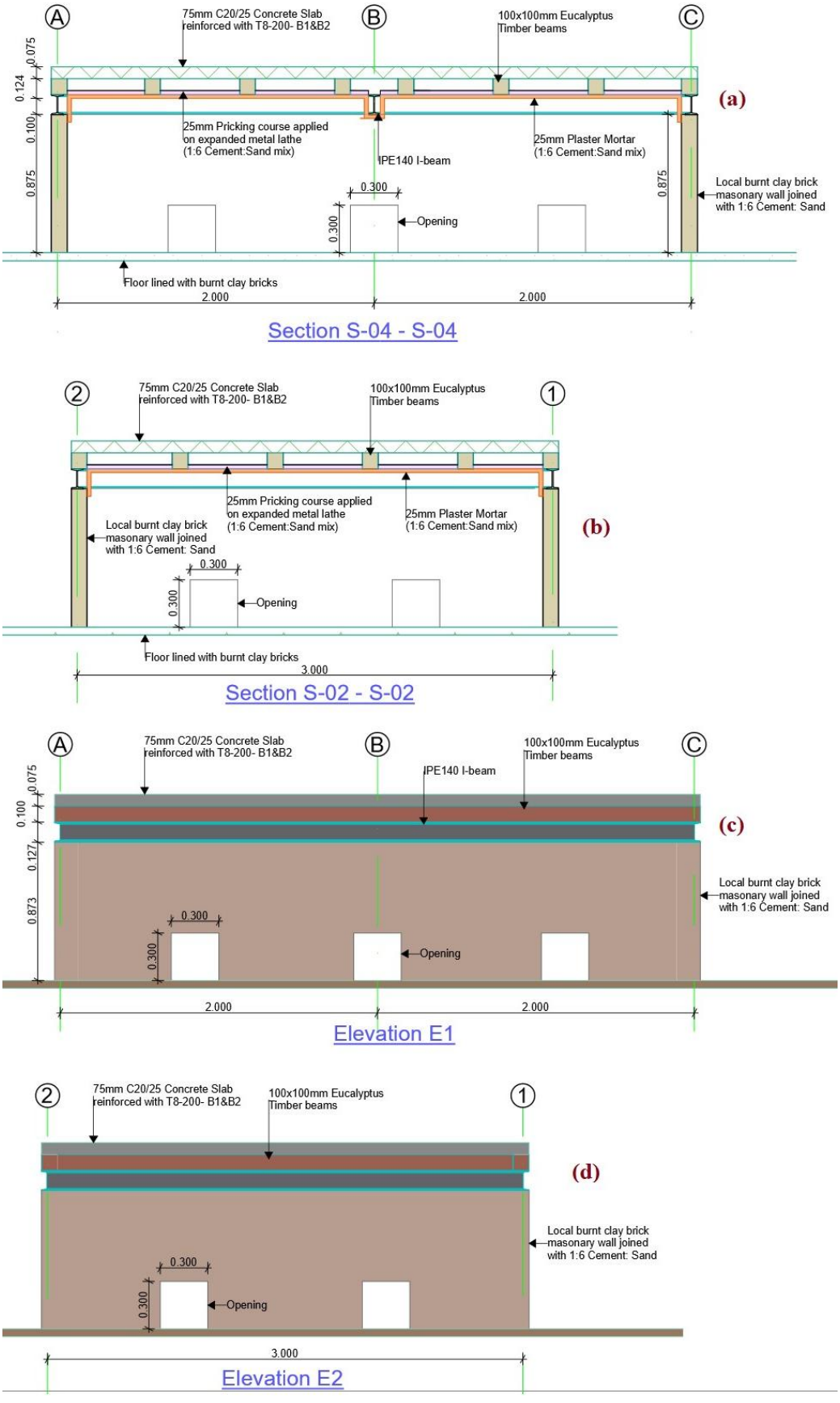

Figure 3.2: Hybrid (steel timber concrete) slab model setup, (a) Section s-04 - s-04, (b) Section S-02 - S-02, (c) Elevation E1, (d) Elevation E2

- The model parameter and material selection were guided by the baseline study. According to the baseline study material specification commonly used in commercial structures were selected for study. Therefore, a 75mm concrete topping was cast on top of the 26-gauge expanded metal lathe that was fixed on 100 x100 mm Eucalyptus grandis timber sections. The timber was simply supported on top of the I-beam top flange. The I-beam selection was from the structural design considering a variable load of 3kNm^2, permanent load of 2.5kNm^2, and weight of the slab element. IPE 140 was considered as the center beam from calculation. The model set up is as show in the Figures 3.1, 3.2, 3.4 - 3.11.
- Local burnt clay masonry brick wall was constructed around the perimeter of the of the slab with 300x300mm opening, three on the 4m sides and two on the 3m sides. The aim of the clay burnt masonry wall around the perimeter was to keep the heat in.
- According section 4.4 of BS 476-20: 1987 one slab specimen was used for the study.

Test Procedure

1. Initial temperature was measured and recorded using a thermocouple thermometer 15 minutes before heating.
2. The test load was applied 15minutes before heating. The load was applied according to clause A.4.2 of BS 476-20: 1987. 5.5kNm^2 total of the permanent and variable load was simulated using local burnt clay bricks. A single brick had an average weight of 4.5kg. the slab was loaded with 1500 pieces of bricks distributed uniformly on the entire slab as shown in Figure 3.4.
3. Datum temperature values were recorded before heating.
4. Fire was ignited after all the above was finished. Fire wood was used as the fire fuel according to EN 1991-1-2.
5. Temperature recording was done at intervals of 1minute and 5 minutes.
6. The slab deflection was measured using linear variable displacement transducers set up above the slab.
7. Failure of the Insulation capacity of an element was considered to occur when the temperature of the un-exposed surface of an element exceeded 180^0 C above the initial temperature of the unexposed surface. Spalling and cracking of plaster was also considered as a measure of insulation failure.

The Figures 3.4 & 3.5 below show the experimental setup of the slab model that was tested

Instrumentation

1. The thermocouples as shown in figure 3.4(b) and 3.5 (c) were placed in the following elements and spaces.
    a. Concrete in four layers at 15mm, 30mm, 45mm and 60mm.
    b. I-Beam on the bottom flange, web flange and top flange
    c. In the heating compartment four thermocouples
    d. Plaster in three layers at the bottom of the plaster, top of the plaster bottom of pricking course and top of the pricking course.
2. The linear variable transducers were placed in five locations at A, B, C, D and E as shown in figure 3.3 and 3.4a

Figure 3.3 shows the location of the linear variable transducers on the slab to detect deflection

(a)

(b)

Figure 3.4: (a) LVDT setup and loading (b) Thermocouples and digital display.

(a)

(b)

(c)

(d)

(e)

(f)

Figure 3.5: (a) Building the model, (b) Cast Concrete cubes, (c) Model setup with thermocouples, (d) shows Pricking course before plastering, (e) Complete model. , and (f) Artist impression of the experimental set up

3.4 NUMERICAL MODELLING PROCEDURE OF HYBRID STEEL TIMBER CONCRETE SLABS IN A FIRE USING ABAQUS.

Modelling of Timber, Steel Concrete floors in ABAQUS

3.4.1 Introduction of the ABAQUS software

This is a finite element computer software that simulates most of the engineering problems and all fields of engineering. (Chiara , et al., 2018).

The Abaqus analysis is done in three different stages and these are: -

1. Preprocessing / Modeling
2. Simulation/ Analysis
3. Postprocessing/ Results

3.4.2 Modeling

Abaqus-cae software was started and a new model was created in the database as “2D”, “Deformable”, “Shell”, “Planar” and approximate size = 2.

Parts created included, Timber, IPE140 I-beam, Plaster mortar, Pricking coarse mortar and concrete.

Materials were defined with following properties in SI units, Thermal conductivity, density, Heat specific capacity and emissivity. Materials created included; concrete C20/25, timber hardwood D30, steel S235, and plaster mortar 1:6 Cement: Sand.

The materials created were assigned to the relevant part created in the model.

The parts were assembled to create a model which was named as a Heat transfer model. The parts were meshed individually as Standard, Linear order and Heat Transfer family.

Steps to analysis the model were created i.e. Initial step and “Heat Transfer step.” In the initial step, the model was set to ambient temperature and the heat transfer step was set as a transient heat transfer.” In the heat transfer step time-period and rate of increase of temperature was defined.

The load or the boundary condition were defined after the step. Fire gas temperature was modelled as convectional currents applied on the plaster bottom surface.

3.4.3 Analysis/ Simulation

In the analysis step, a job was created in which processing requirements and output options were assigned.

A data check was done to correct any modelling errors and warnings. Warning and errors were corrected before submitting the job.

The Job was submitted for solving. While solving the problem In the Monitor window a check for errors or warnings was done. The cause of errors was investigated before re-solving.

3.4.4 Results/ Postprocessing

After the job analysis was completed, the output being displayed was changed by clicking results in the menu bar.

"NT11 Nodal temperature at nodes" was selected to display the contour of the temperatures

To study the temperature distribution in the elements "Plot Contours on Deformed Shape" icon was selected. The graph of the temperature against time was plotted for the selected nodes in the model.

To probe the temperature values at nodes, the probe option was changed to "nodes", "Nodes ID" and "NT11"

3.4.5 Assumptions regarding material properties and heat transfer mechanisms:

1. Material Properties Assumptions:

a. Material Homogeneity:

Materials were assumed to be homogeneous uniform properties throughout. For example, timber was assumed to have isotropic or orthotropic elastic properties based on species, age, and moisture content, constant Young's modulus, shear modulus, and Poisson's ratio and no degradation over time.

b. Thermal Properties and Temperature Dependence:

i. Thermal Conductivity (k) and Specific Heat Capacity were defined as temperature dependant for steel, concrete and plaster as prented in table 2.

ii. Density (ρ): was input as a temperature dependant for steel concrete and plaster as presented in table 2.

2. Heat Transfer Assumptions:

a. Modes of Heat Transfer: ABAQUS accounts primarily for:

i. Conduction through solids (governed by Fourier's law).

ii. Convection the fire was modelled as a heat transfer via film conditions using heat transfer coefficients (h).

iii. Radiation, of heat from the bodies was considered by specifying the material emissivity (ε), master and slave surfaces.

b. Boundary Conditions:

i. Fire was Simulated as a convective heat transfer as a surface film

ii. The plaster was specified as the insulating part of assembly

iii. The initial temperature (27 ^{0}C) for the all bodies and unexposed surfaces was obtained from experimental temperature measurements

Contact Conductance:

Objects in contact with each other were modelled as ties hence heat transfer by programme specified conduction. The contact modelling is as illustrated in Figure 3.6

How contact was modelled

1. Defined Contact Surfaces: In the Interaction module, surface sets for each material interface were created. These surfaces were acting as the master and slave in the contact pair.
2. Create Interaction Property: in the Interaction an Interaction Property was created. Thermal Contact chosen and thermal conductance defined (W/m²·K), which is the inverse of thermal contact resistance
3. Create Contact Interaction by Selecting Surface-to-Surface Contact and choosing the surfaces to assign the thermal contact property ensuring the interaction is active during the transient heat transfer step.

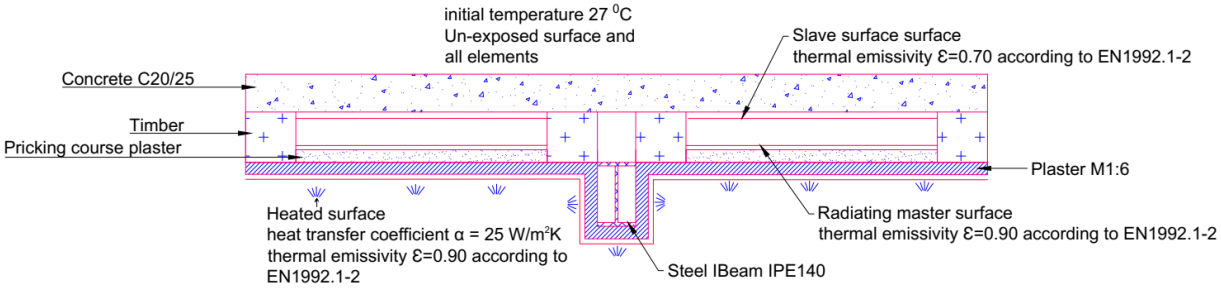

Figure 3.6: boundary conditions for the numerical model in ABAQUS CAE

Mesh model

The parts were meshed individually to a mesh size of 1mm . Concrete was meshed as linear quadrilateral elements of type DC2D4. Steel IBEAM was meshed as linear quadrilateral elements of type DC2D4 and linear triangular elements of type DC2D3. Plaster was meshed as linear quadrilateral elements of type DC2D4 and linear triangular elements of type DC2D3. Pricking course was meshed as linear quadrilateral elements of type DC2D4 and Timber was

meshed as linear quadrilateral elements of type DC2D4. The example of the meshed elements is as illustrated in Figure 3.7and Figure 3.8

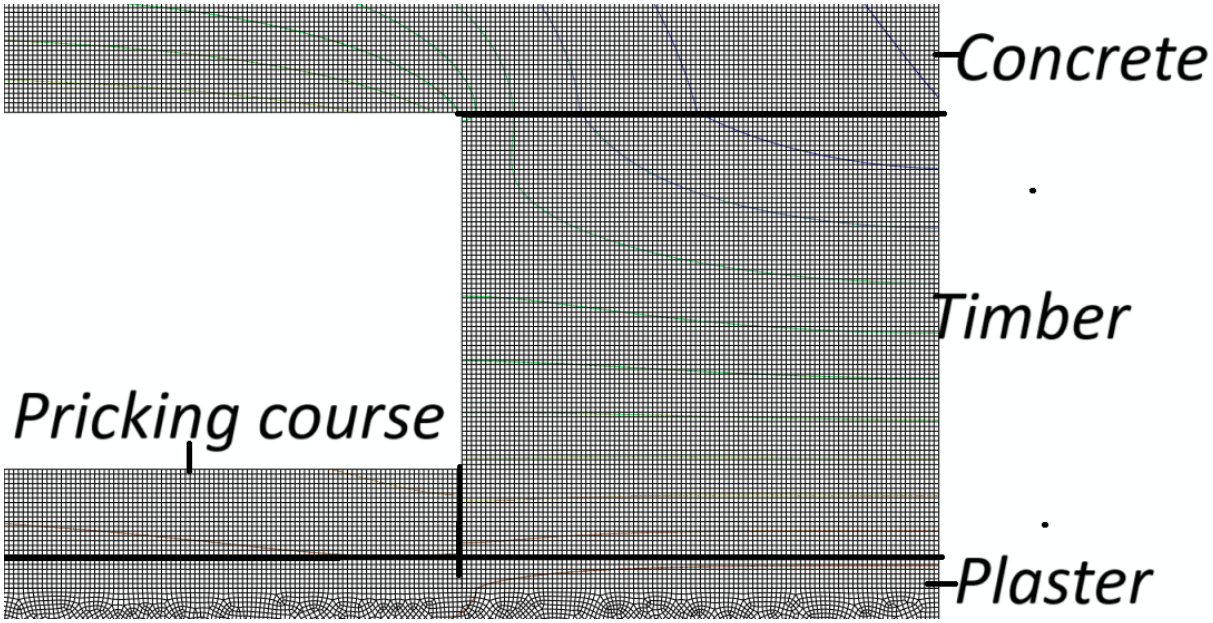

Figure 3.7 mesh example for plaster, concrete, timber and pricking course

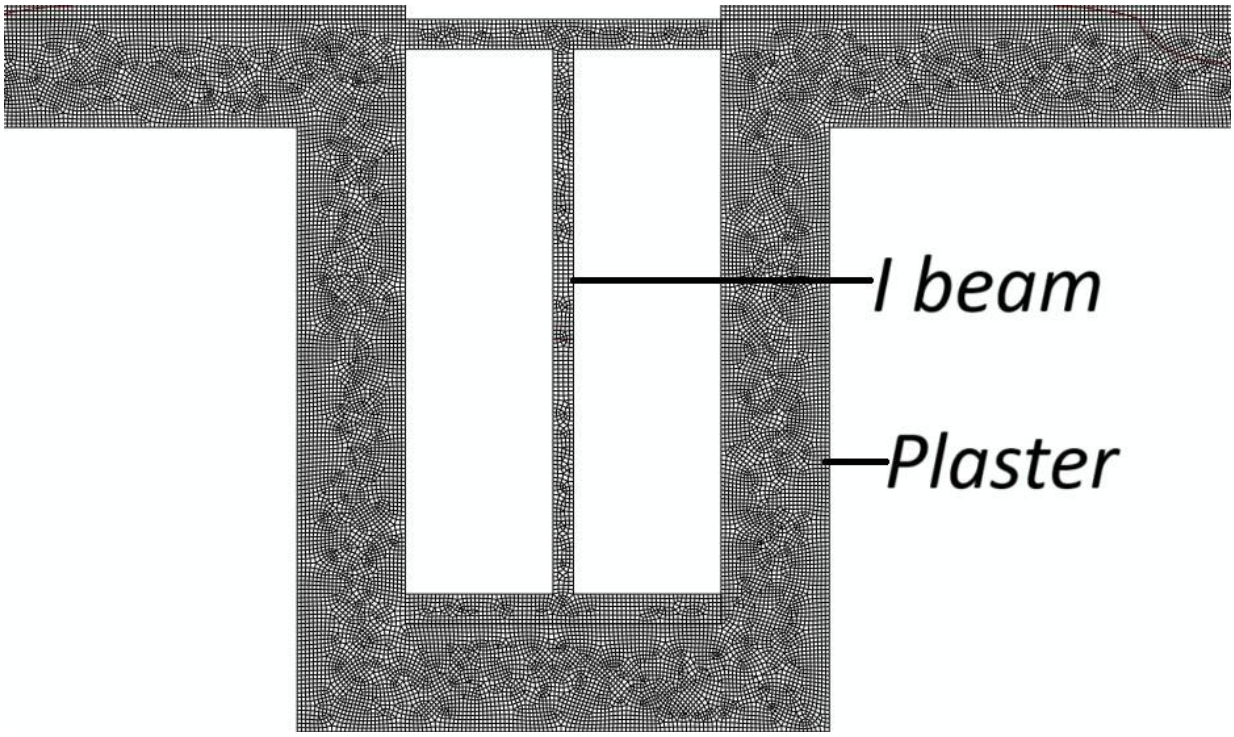

Figure 3.8 steel I-beam and plaster mesh sample

3.5 EXPERIMENTAL TESTS ON SHEAR CONNECTORS

The performance of hybrid steel timber concrete construction will depend upon the shear connection between timber and concrete. A push out test experiment was done according to DD ENV 1994-1-1; "Design of composite steel and concrete structures- General rules and rules for building, London: British Standards Institution."

3.5.1 Preparation of specimens

a. Formwork for the specimen was fabricated out of timber ready to receive concrete.
b. Timber was greased to prevent the timber element from bonding with concrete elements.
c. Reinforcement made of H10 bars was fixed in the formwork model.
d. Concrete slabs were cast in the horizontal position and air cured
e. Four concrete cubes were casted for testing compressive strength of the concrete used.
f. Test were carried out on material including yield and tensile strength, maximum elongation on the shear connector materials used in this research.

The setup of the specimen was as shown in the Figures 3.9, 3.10 and 3.11 below.

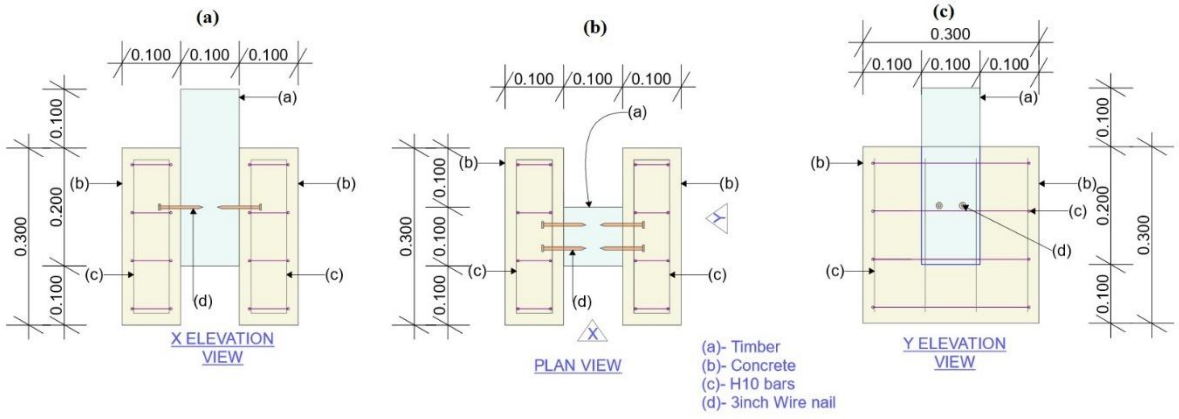

Figure 3.9: Shear connector experiment set up for the nails (a) Elevation X, (b) Plan view and (c) Elevation Y

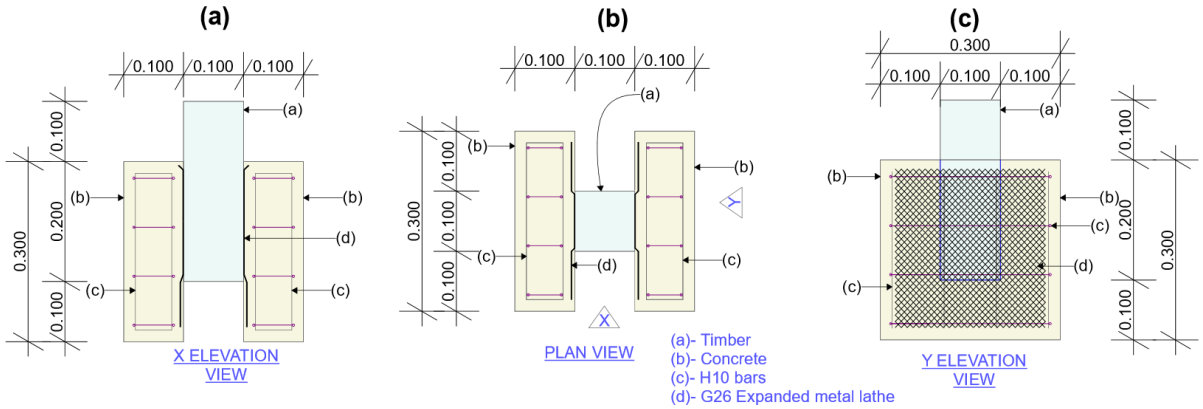

Figure 3.10: Shear connector experiment set up for the expanded metal lathe (a) Elevation X, (b) Plan view and (c) Elevation Y

Figure 3.11: A physical pushout test specimen ready for testing.

3.5.2 Testing procedure

1. The load was applied monotonically until fai1ure using a UTM “universal” testing machine.
2. The slip until failure occurring at the interface of concrete and timber sections was measured throughout loading process using linear variable displacement transducers.

3. A graph showing the relationship between Load and slip was plotted for all the four push out specimens.
4. The cracking patterns during loading was carefully observed to see the failure mechanism.

The experiment set up was as show in the Figure 3.12.

Figure 3.12 The setup of the push out test experiment before testing

3.6 NUMERICAL MODELLING METHODOLOGY OF PUSH OUT EXPERIMENT IN ANSYS WORKBENCH.

3.6.1 Introduction of the ANSYS software

ANSYS workbench just like ABAQUS is a software used to solve static structural, dynamic structural, thermal, mechanical, electromagnetic, fluid dynamics, acoustics, and other problems in physics and engineering using finite element (Chiara , et al., 2018)

3.6.2 Modelling simulation procedure.

ANSYS workbench 2021 software was installed on the PC and loaded into the system.

The model was simulated by defining engineering data, geometry, model setup, and analyzed to generate results that were validated and verified.

Engineering data

In this step Mechanical properties of the materials were defined. These include: density, Tensile yield and compressive yield strength, elasticity modulus plus Poisson's ratio. These were based on material tests carried as shown in section 4.3 and relevant Eurocode standards for wire nails, concrete, expanded metal lathe and timber.

Bilinear plasticity was considered in order to simplify the plasticity model by specifying the yield strength and tangent modulus to describe the plastic behavior.

Geometry

The model was prepared in design modeler a computer-aided design (CAD) system in ANSYS. The timber, concrete, wire nails and expanded metal lathe (mesh) were modelled as solid bodies as shown in Figure 3.13 and Figure 3.14.

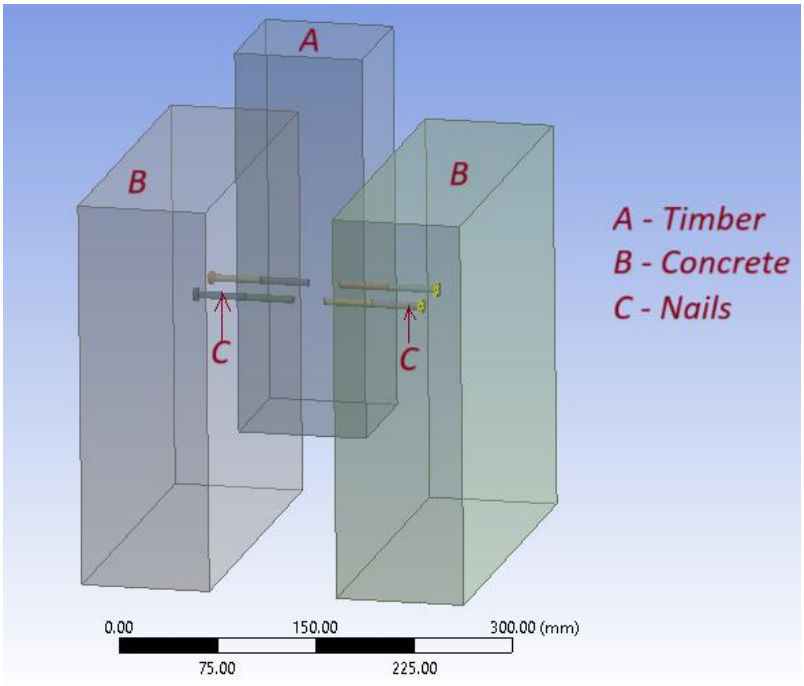

Figure 3.13: The Nails shear connectors push out test model setup in ANSYS

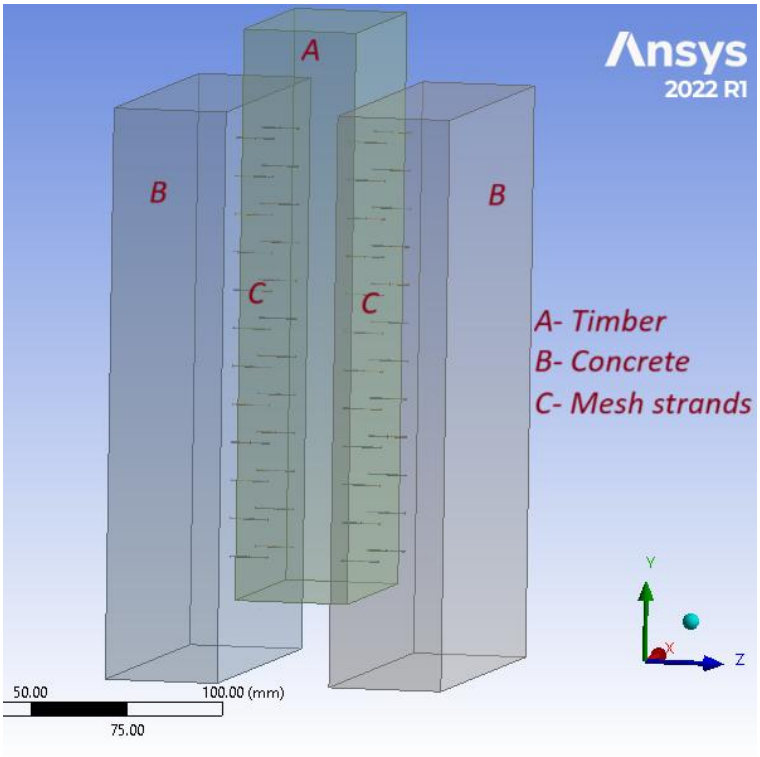

Figure 3.14: The Expanded metal lathe (Mesh) shear connectors push out test model setup in ANSYS

Model

During this phrase the materials that were defined in engineering data were assigned to the geometry model consisting of a series of solid bodies.

` **Model Setup**

During this stage the following parameters were defined;

Load were defined in incremental steps as 2kN for mesh model and 10kN for nails model.

A fixed support at the bottom face of the concrete part was taken as the boundary condition of the simulation.

The Analysis Settings were set so that the programme solver is initiated. The analysis had 7 steps for nails model and 10 steps for expanded metal lathe model. Each step was assigned one second time interval.

Model Solution

The solution data that is governed by the input conditions was accessed before analysis. A nonlinear static structural analysis was specified as the type of analysis. To perform a nonlinear analysis the bilinear material properties were specified in the engineering data to account for the plastic deformation of the nails and mesh and large deformation were allowed

Model Results

The analysis results status was accessed after the static structural analysis was done. Results were viewed as total or directional deformation (this represented displacement along an axis) plus strains, and stresses experienced at various nodes or whole elements.

Results verification and validation

Verification of the numerical model was checked following proposed numerical procedures whether is solved correctly.

Validation was be done by comparing numerical results against calculation and experimental investigation results.

The load vs deformation (slip) was presented on the graph for each load increments.

Furthermore, the numerical load vs slip graph was compared against experimental load vs slip graph with that obtained experimental.

4.0 CHAPTER FOUR: RESULTS AND DISCUSSION

4.1 INTRODUCTION

Results and discussions obtained from the baseline study, performance of hybrid slab subjected to fire are presented. Furthermore, the experimental and numerical test of the nails and expanded metal lathe as shear connectors are presented.

4.2 BASELINE STUDY

During the baseline study, interviews with two site engineers, two directors of construction companies were carried out. These engineer/ directors have carried out construction on more than twenty-five structures using the hybrid Steel timber concrete slab floor system.

The researcher visited three commercial building that were constructed using the hybrid floor method.

Furthermore, the NBRB (National building review board) report (NBRB, 2021) about timber steel concrete structures was reviewed.

4.2.1 Baseline study results

Baseline study results summary is presented in Table 4.1: Baseline study results summary and details of the results are in Appendix C.

Table 4.1: Baseline study results summary

Type of project	**Number of structures**	**Concrete class**	**Concrete thickness/ mm**	**Reinforcement**	**Timber dimensions**	**Timber type**
Residential	100	C20/25	75-100	H8 H12 BRCA142	100x75 100x100	Pine Eucalyptus
Commercial	10	C20/25	75-100	H8 H10 BRCA142	100x100 100x120	Pine Eucalyptus

4.2.2 Discussion of baseline Study results

From the Baseline study the following was determined: -

a) There were more residential structures projects than commercial projects on a ratio of 4:1 Residential: Commercial.
b) Ninety percent (90%) of residential projects were done using 100 x100mm eucalyptus poles and Ten percent (10%) using pine.

Whereas for commercial structures 100% eucalyptus were used.

c) The concrete class used for both commercial and residential was C20/25.
d) Concrete thickness on commercial projects was 60%-75mm, 30%- 100mm and 10% - 120mm whereas Residential projects 90% were 75mm.
e) Residential Concrete topping was reinforced using 50% BRCA142, 40% - H8 and 10% - H12. Whereas commercial Concrete topping was reinforced using 80% - H8 and 20% - H10.

According to NBRB investigation since 2020 it was determined that 52% of the fire incidents occur in commercial buildings, 35% in schools and 13% in residential Buildings (National Building Review Board, 2020). It was from this baseline study that a model was constructed based on commercial buildings using hybrid steel timber concrete floor system.

4.3 MATERIAL PROPERTIES

4.3.1 Timber

The timber used in the project was sawn from Eucalyptus grandis to dimensions of 100x100x2000mm.

Timber compressive strength

Timber pieces were obtained from a timber yard in Matuuga, Wakiso district, Timber pieces were sampled and compressive strength, bending strength, and Density tests were carried out. The following results were obtained: -Compressive strength 26.9Mpa, Bending strength 106.4Mpa, Density 532kg/m^3. The results obtained were compared with those obtained by (Zziwa, et al., 2010) and (EUROCODE 5, 2004) in Figure 4.1: Comparison of bending and compressive strength results obtained from laboratory tests with what was obtained by Zziwa, et al., 2010 and EUROCODE 5, 2004.

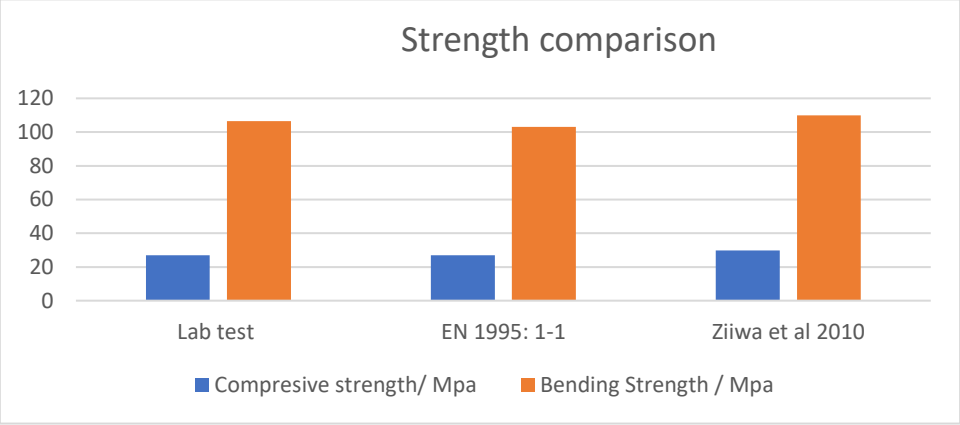

Figure 4.1: Comparison of bending and compressive strength results obtained from laboratory tests with what was obtained by Zziwa, et al., 2010 and EUROCODE 5, 2004.

4.3.2 Concrete Properties

Concrete cubes were cast during the casting of hybrid steel timber concrete slab model and the same concrete batch was used to cast the shear connector test samples. The cubes were cured for 28 days and taken for testing at Makerere University civil engineering department laboratory. The average concrete strength of 26.8N/mm^2, and the average density is 2415.3 kg/m^3 results that were obtained are as shown in Table 4.4 below.

4.3.3 Steel Properties

Table 4.2: Characteristic strength of various steel used in the hybrid slab

STEEL SECTION	Yield strength (Mpa)	Tensile strength (Mpa)	Elongation (%)	Tangent modulus (Mpa)	Grade
Wire nail	382.73	494.22	23.21	20000	
Expanded Metal lathe (Mesh)	38.81	43.13	35.00	2100	
Ribbed Rebar 8mm	614.81	775.81	16.67		
I Beam (IPE 140)	210	340	24.00		210

4.3.4 Material test results discussion

Eucalyptus grandis timber used in this study was found to be in range with other test carried out by (Zziwa, et al., 2010) and (EUROCODE 5, 2004) on D30 timber.

Concrete compressive strength results of 26.8N/mm^2 show that the strength class of C20/25 specified was achieved. The density of unreinforced concrete in Eurocode is specified as 2400kg/m^3 hence when compared with laboratory results it was determined is was within range by 2415.3 kg/m^3.

4.4 HYBRID SLAB PERFORMANCE IN A FIRE RESISTANCE RESULTS AND DISCUSSION

The slab was subjected to a natural fire using wood as fuel. The experiment lasted 280 minutes. The fire exhibited a three-phase fire behavior that is to say; ignition – smoldering, flash over point leading to heating phase and lastly cooling phase as show in the Figure 4.2.

A Eurocode parametric curve was plotted on the same graph as shown in Figure 4.2 the temperature values of the parametric curve we started at 80th minute when the flashover point was estimated to begin. The Eurocode parametric curve equation was calculated and presented in Appendix A. The experimental maximum average temperature recorded was 734ºC equivalent to the maximum temperature obtain from Eurocode parametric curve of 728 ºC.

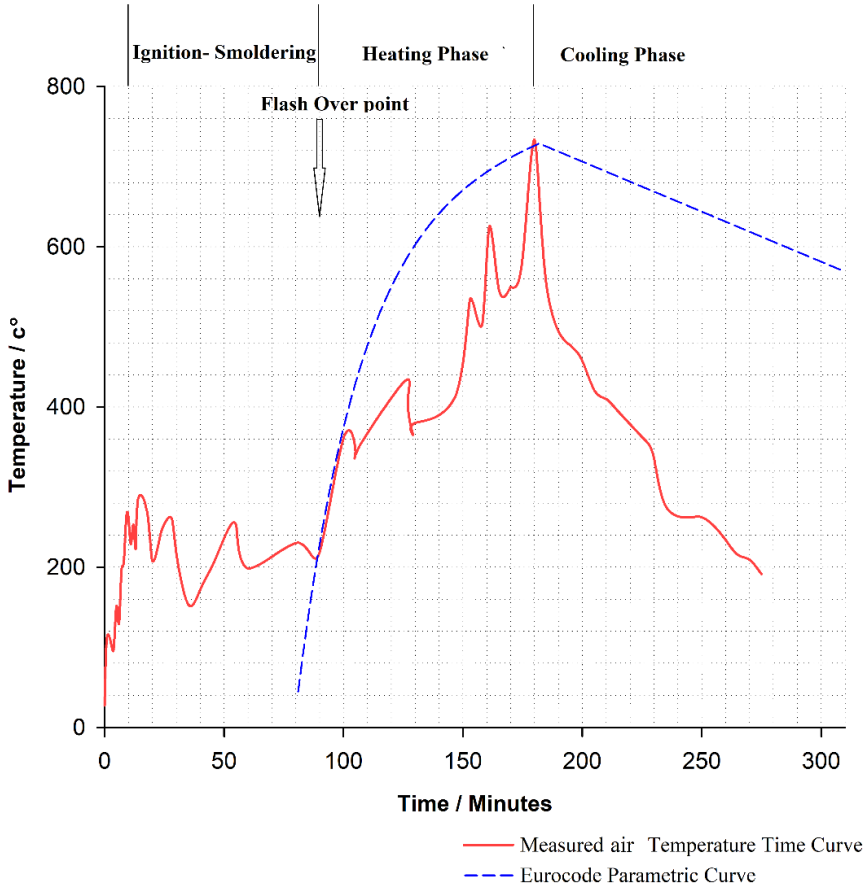

Figure 4.2: Average air temperature time graph measured in the fire compartment and air temperature time Eurocode parametric curve.

The sharp temperature increase in the heating phase caused spalling of plaster hence the integrity of plaster compromised as observed in the temperature time graph of plaster and pricking course in Figure 4.3 .

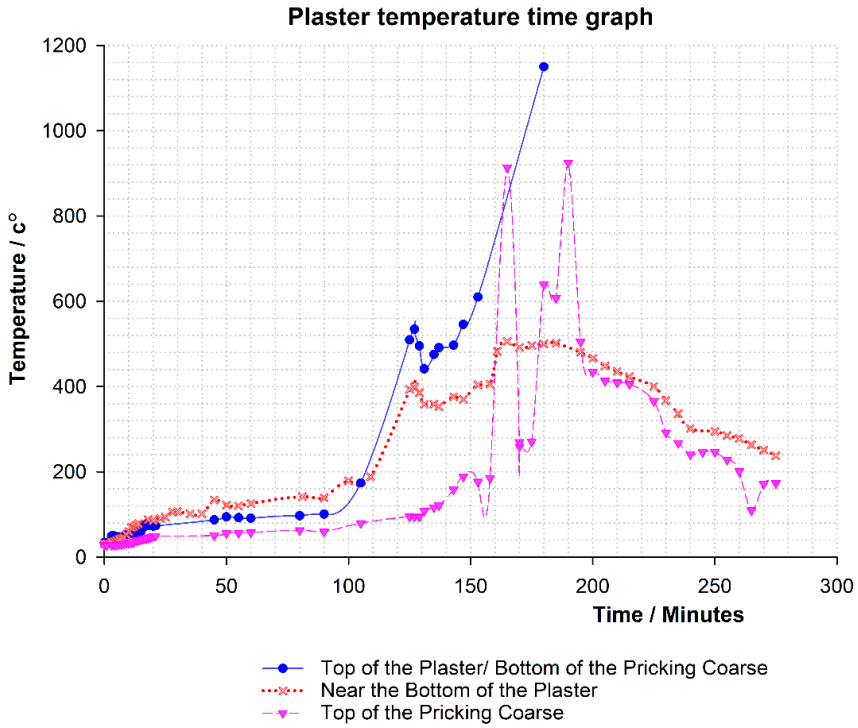

Figure 4.3: Temperature time graph for plaster and pricking coarse layers

When the integrity of the plaster was compromised in the heating phase, a sharp rise in temperature of Steel and concrete was observed as shown in the temperature time graphs Figure 4.4 and Figure 4.5 respectively.

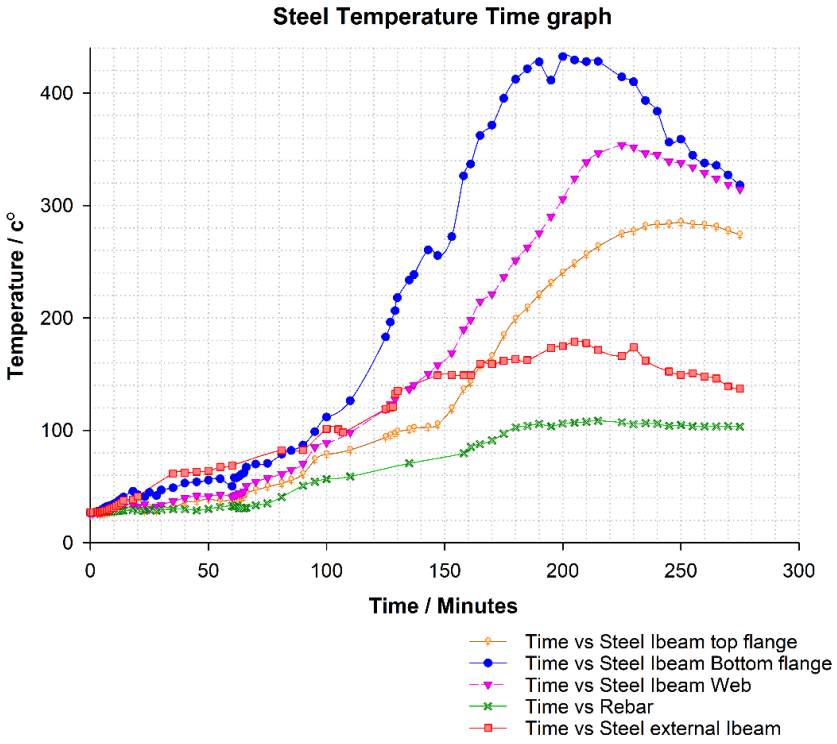

Figure 4.4: The temperature time graph for Steel members

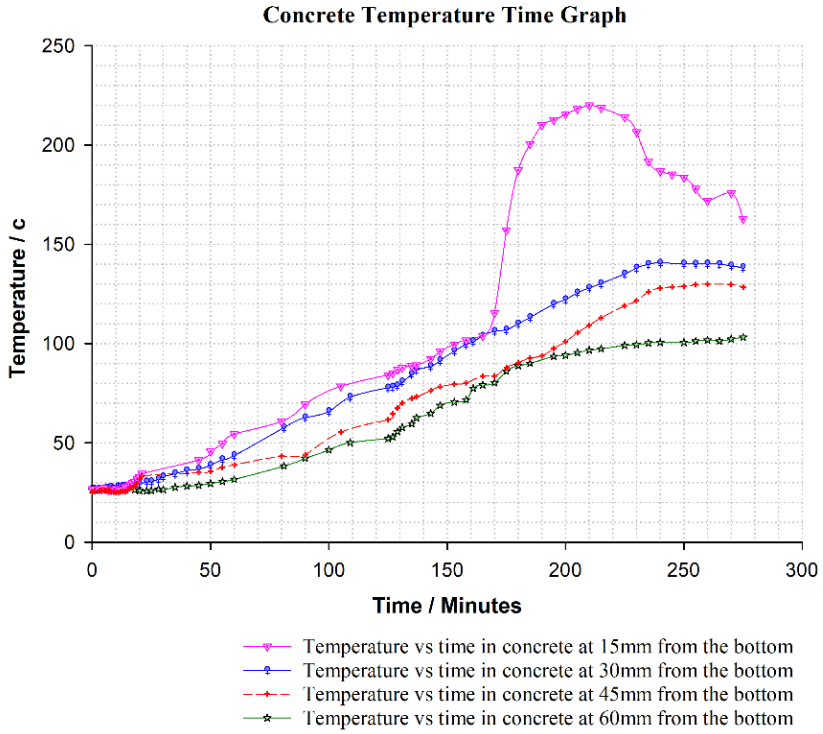

Figure 4.5: The average temperature time graph at different concrete depth

Plaster collapse was also observed in the heating phase as shown in Figure 4.6. This occurred at the 180th minute of the experiment.

The collapse of plaster and pricking course caused the beginning of the cooling phase with a sharp drop than expected from the Eurocode standard temperature curve as shown in the graph Figure 4.2. This was because the burning wood was covered by the plaster and pricking course rubble.

Furthermore, collapse of plaster showed a sharp rise of temperature at the bottom of concrete that was exposed to abrupt higher gas temperature as shown in the concrete temperature time graph in Figure 4.5.

Sharp abnormal high temperature rises observed in the plaster and pricking course as shown in temperature time graph Figure 4.3 were due to spalling and plaster collapse where by the thermocouples were measuring the gas/ air temperatures.

Timber ignition occurred in the 130th minute. This was observed by smoke coming out of the joint between concrete and timber. Burning timber was also observed in Figure 4.7.

Burning of timber weakened the bond of nails in timber that were holding the metal lathe hence collapse of the pricking coarse and plaster that was supported by the metal lathe.

Figure 4.6: Plaster collapse in the heating phase

Figure 4.7: Burning timber after ignition

Concrete was observed to curl at the edges. This was due to temperature rise at the bottom of concrete casing expansion. This was as observed in Figure 4.8 where hogging of the concrete edges can be seen.

Figure 4.8: Curling at the corner edges of concrete due to expansion caused by temperature rise at the bottom of concrete

After the fuel burnt out and the compartment cooled down and the following was observed:

- Timber charring of the entire timber in the slab as shown in Figure 4.11, and 4.12.

  char layer, $d_{char} = \beta_0 \times t$

  where:

  β_0 is the wood burning rate = 0.5mm/min from table 3.1 EN1995-1-2.

  t = 10 minutes (range of time from ignition to 60minutes fire resistant rating)

  Char layer at R60 $d_{char} = \beta_0 \times t = 0.5 \times 10 = 5mm$

  Char layer at R (heating phase end) $d_{char} = \beta_0 \times t = 0.5 \times 50 = 25mm$
- Spalling of plaster as shown in Figure 4.9.
- Slight deflection of the center I-beam as shown in Figure 4.10.
- The concrete returning to normal with no curling as illustrated in Figure 4.13.

Figure 4.9: Plaster spalling

Figure 4.10: Deflection in the central I-Beam

Figure 4.11: Charring of timber secondary beams

Figure 4.12: Charing of timber even where the plaster had not fallen

Figure 4.13: The concrete returning to normal with no observed curling

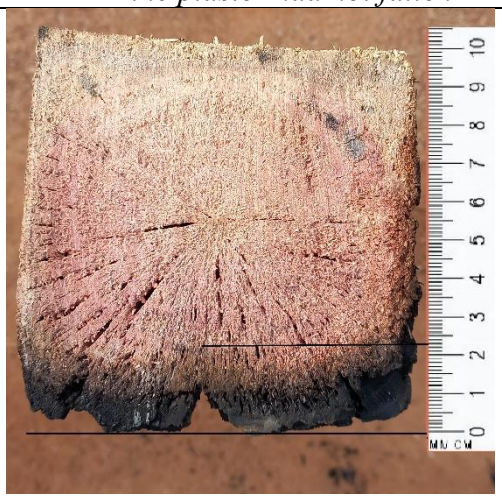

Figure 4.14: The timber char and pyrosis layers

4.4.1 Load bearing ability of the slab

The slab was subjected to a total load of 5.5kN/m^2. On placing the load, the initial deflection of 4 mm was recorded at the center.

The center of the slab experienced a positive maximum deflection of 22mm and the corners of the slab experienced and negative deflection maximum of 10mm as shown in Figure 4.15(a) and 4.15(b).

The maximum deflection at the center is above the limiting values of timber l/250 to l/350 in (EUROCODE 5, 2004) table 7.2 and steel limiting values of $\Delta_{max} = L/\alpha$ (Steel Construction Institute , 2003) section 16.3.3. Hence the slab failed in deflection beyond the allowable limit as specified by Eurocode 5 and Eurocode 3.

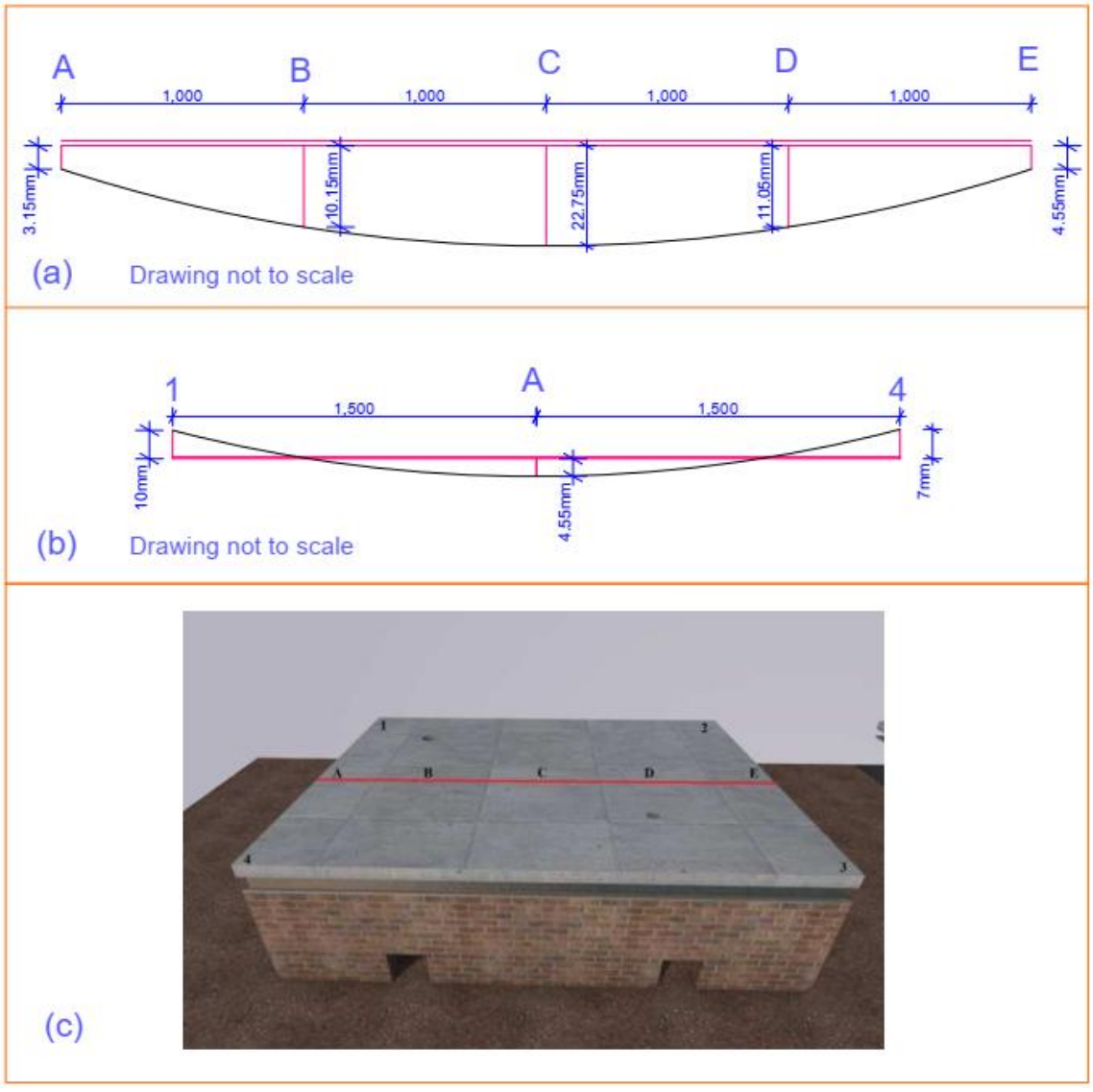

Figure 4.15 (a) the deflection of the slab parallel to the long side of the slab, (b) deflection along the short edge of the slab (c) an artistic impression showing the points of deflection.

4.4.2 Hybrid slab experimental fire investigation discussion

The air furnace temperature showed a four-phase fire growth as expected of a natural fire that is to say; Ignition – Smoldering, Flashover, Heating, and cooling phase.
According to Tom , 2011 the Heating stage is where expected structural damage and failure happens. Even in this experimental setup, it was in the heating phase that spalling, Collapse of plaster and pricking coarse, timber ignition, and concrete curling was observed.

Insulation failure occurred when temperature of the unexposed surface exceeded 180^0C at the 105^{th} minute of testing and 25minutes after the flashover point. After insulation failure the timber was ignited and evidence of smoke coming out of the concrete timber joint was observed. This weakened the nails that were joining the metal lathe onto the timber hence plaster collapse at the 180^{th} minute. The thickness of the char was *5mm* specified from ignition to R60 fire resistant rating = 10minutes.
Whereas the thickness of the char layer from ignition to end of Heating phase was calculated as 25mm which was the approximate measurement the length the 2-inch nail was driven into the timber to hold the expanded metal lathe. This is why the plaster collapsed at the end of the heating phase. The section that was left of the beam was capable of supporting the total weight subjected on the slab which is design load and self-weight.

Temperature rise in the Concrete and steel was also observed as evidence of insulation failure. The maximum temperature rise in steel I-beam obtained experimentally was 434^0 C in the bottom flange. At 434^o C the steel retains Ninety percent (90%) of the yielding strength hence it was able to support the load applied (EUROCODE 3, 2005). Whereas 575ºC obtained numerically steel retains only Fifty percent (50%) of the yielding strength.
Since the slab was not in considered composite with lack of document shear connector, the elements were deemed to act alone to support the load and their own weight. Therefore, the deflection was considered on the individual elements. Hence the middle I-Beam IPE140 was considered to have failed since it experienced a deflection higher than the limiting value specified in Eurocode 3. Timber secondary beams also were deemed to fail in deflection since it experienced a deflection of 22mm which was higher than the Eurocode 5 limiting value.
The maximum average reinforcement temperature measured was 100^0C. At this temperature the reinforcing bars can retain 100% of the yield strength according to (EUROCODE 3, 2005). Therefore, the reinforced concrete was able to sustain the load and self-weight

4.5 HYBRID SLAB PERFORMANCE IN A FIRE NUMERICAL RESULTS AND DISCUSSION

4.5.1 Introduction

The second objective of study compares the temperature gradient obtained in the experimental model in steel plaster concrete elements with the analytical model. And further determines the temperature gradient of the elements based on Eurocode parametric curve (CEN, 2004), ASTM E119 (American Society for Testing and Materials, 2020) and ISO 834 (International Organization for Standardization, 1999). The model was simulated in Abaqus-CAE as 2D element as illustrated in Figure 4.16: The 2D Abaqus model.. Temperature readings were taken at node as shown in Figure 4.17

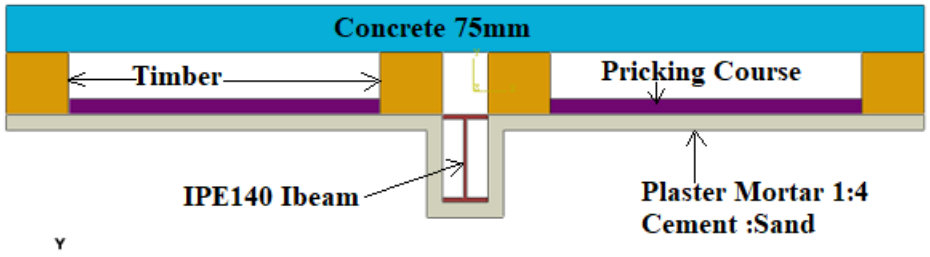

Figure 4.16: The 2D Abaqus model.

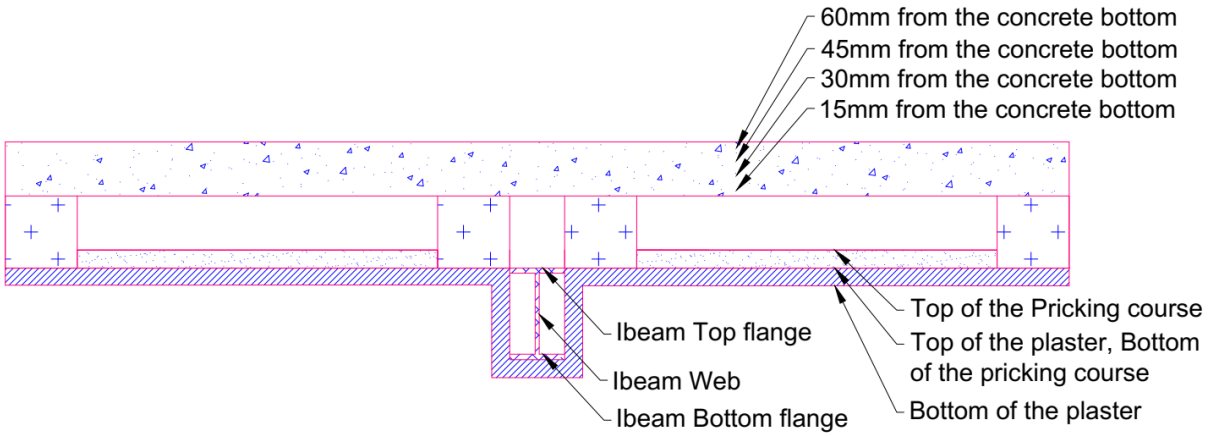

Figure 4.17: placement of thermocouples as per experimental setup the same where nodal numerical temperatures were picked.

4.5.2 Thermal Material Properties

To simulate the behavior of the hybrid steel timber concrete slab acted upon by a natural fire in ABAQUS software the relevant material properties were: - Thermal conductivity, Specific heat, and Density. Meena, *et al.*, 2014 defines Thermal conductivity λ as, “an intrinsic material

property (independent of material size, shape or orientation), which describes the material's ability to conduct heat." (Meena, et al., 2014).

The above-mentioned properties for the timber, steel and concrete materials were specified as in table 4.7 below indicating the literature sources from which the properties were obtained. All properties used for modelling were considered at ambient temperatures.

Table 4.3: The properties used in the transient thermal analysis to determine the temperature at different times and locations

STEEL (Wang, et al., 2018)									
t, ^{0}C	20	100	300	450	550	600	720	800	1450
k,W/(mK)	53.3	51.1	46.1	41.05	37.5	35.6	30.64	26.00	29.45
c, J/kg K	450	499.2	565.5	630.5	705.5	773.3	1080.4	931.0	437.9
E, mpa	200000	200000	200000	150000	110000	88000	20000	20000	20000
υ	0.2786	0.3095	0.331	0.338	0.3575	0.3738	0.3738	0.4238	0.4738
CONCRETE (Wang, et al., 2018)									
t, ^{0}C	20	100	200	300	400	500	600	700	800
k,W/(mK)	1.36	1.35	1.34	1.32	1.22	1.10	0.97	0.85	0.72
c, J/kg K	840	963	1022	1075	1122	1164	1200	1231	1256
E, mpa	30000	27000		21000		15000		10000	
υ	0.15	0.15		0.17		0.2		0.2	
PLASTER (Shafigha, et al., 2020) (Iman , et al., 2020)									
t, ^{0}C	20	100	300	500					
k,W/(mK)	1.99	1.99	2.2	2.7					
c, J/kg K	870	900	950	1000					
E, mpa	4000	3600	2800	2000					
υ	0.15	0.15	0.17	0.2					
TIMBER (Zziwa, et al., 2010) (Nora , et al., 2022) (EUROCODE 5, 2004)									
k,W/(mK)	0.2								
c, J/kg K	1800								
Temperature t, ^{0}C, Thermal conductivity, k, Specific heat capacity, c, Young's modulus, E Poisson's ratio, υ									

4.5.3 Numerical results modelled with natural fire temperatures

The model was subjected to experimental temperature values as obtained in Figure 4.2. The following was observed. Figure 4.18 illustrates the temperature gradient at the maximum temperature during numerical simulation.

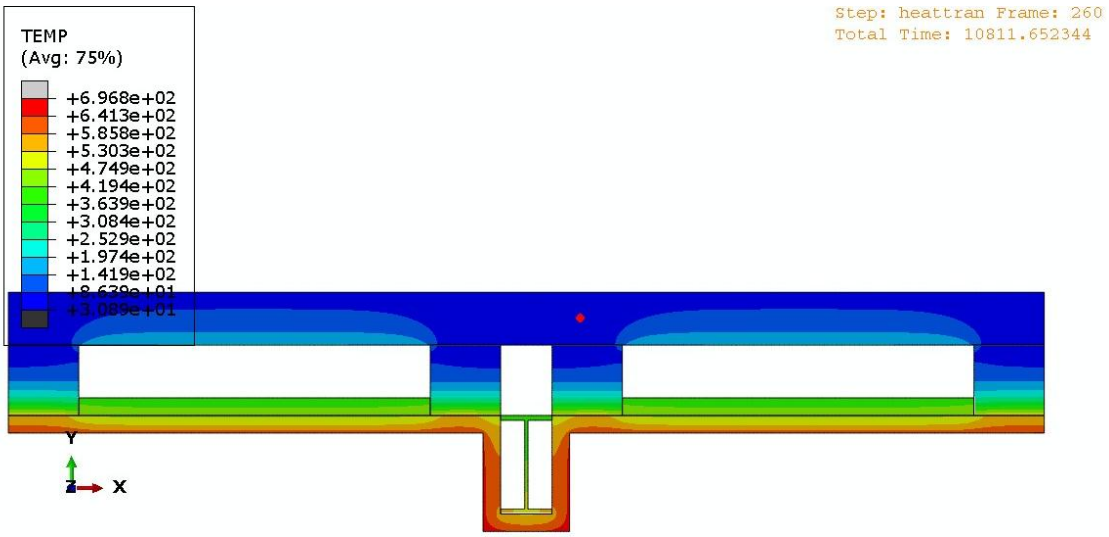

Figure 4.18: temperature gradient at maximum temperature when model is subjected to natural fire temperatures.

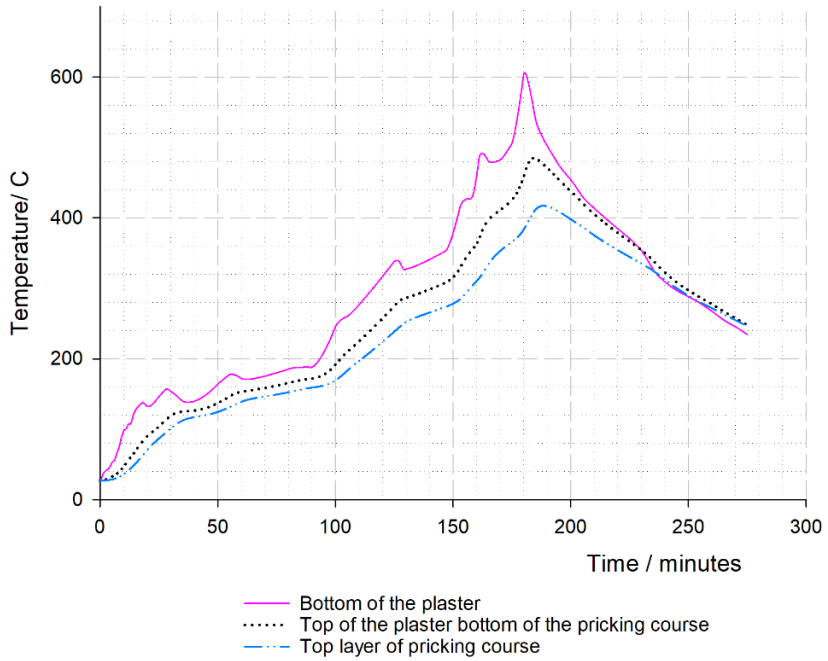

Figure 4.19: Numerical temperature time graph of the plaster and pricking course when subject to natural fire temperatures

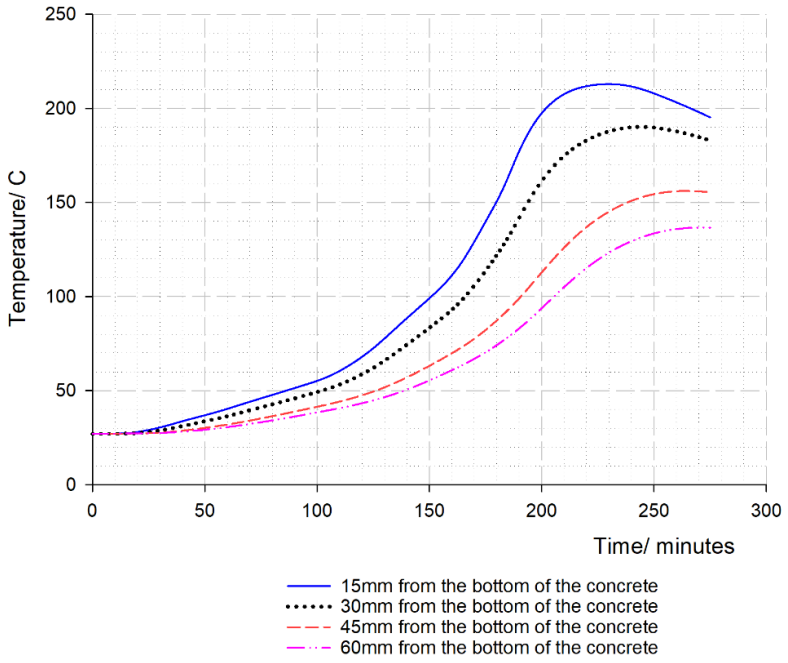

Figure 4.20: Numerical temperature time graph of the concrete when subject to natural fire temperatures

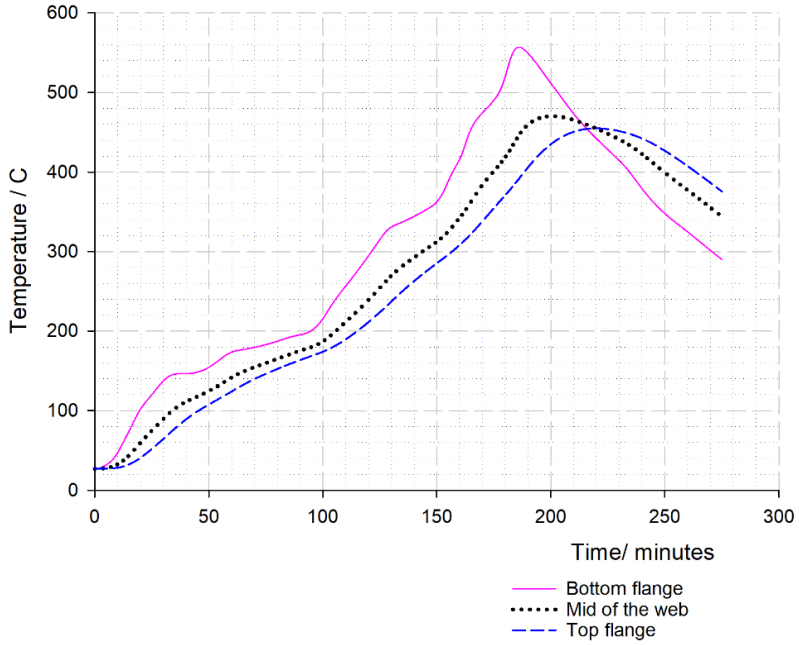

Figure 4.21: Numerical temperature time graph of the steel I-Beam when subject to natural fire temperatures

4.5.4 Discussion of results due to numerical investigation when modelled with natural fire temperatures

It was observed that plaster insulation failure occurred at the 100th minute where the unexposed surface exceeded 180^{o}C above the initial temperature as shown in the numerical graph in Figure 4.19 and validated by the experimental graph in Figure 4.3.

Maximum temperature observed in the numerical at the top of the plaster and bottom of the pricking course was equivalent and was observed to be in the same range in Figure 4.19 i.e 480 ^{o}C numerical and 500 ^{o}C experimental.

The numerical maximum temperature value of steel I-beam was 560 ^{o}C in Figure 4.21 which cause the steel to lose more that 50% of its strength as validated by (EUROCODE 3, 2005). It was also observed that sharp temperature rise occurred after the 100th minute when the plaster was is observed to fail in insulation.

This also applies to concrete that a sharp rise is temperature begins after insulation plaster insulation failure. Furthermore, equivalent maximum values of temperature are observed in the numerical and experimental results 210 ^{o}C and 220 ^{o}C respectively at the 210th minute. As shown in Figure 4.20 and Figure 4.5 respectively

When numerical model is used to study the slab performance it shows that the temperature equivalent values with concrete and plaster and less conservative with steel. This may be due to non-homogenous material, fire gas temperature distribution in the compartment, and non-perfect contact between the steel and plaster.

4.5.5 Numerical results modelled with ECPC, ASTM E119, and ISO 834 fire curve temperatures.

The slab section was also investigated of its performance when subjected to ECPC (Tom , 2011) ASTM E119 (American Society for Testing and Materials, 2020) and ISO 834 (International Organization for Standardization, 1999) fire curves.

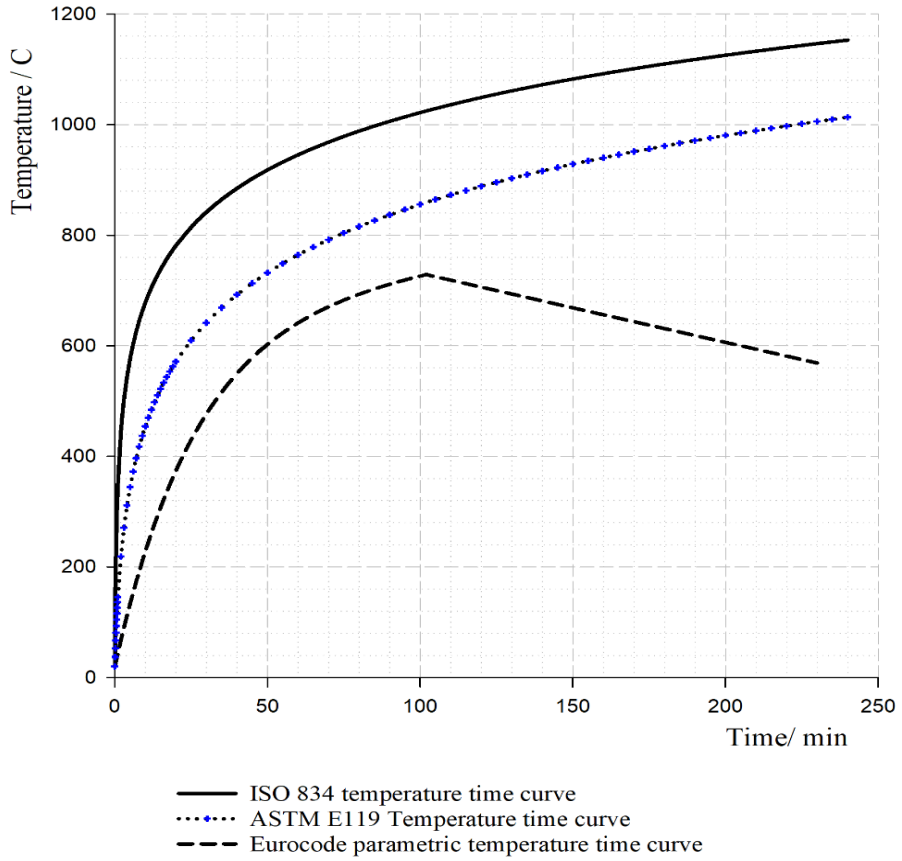

Figure 4.22: temperature time graphs for Eurocode parametric curve (ECPC), ISO834 and ASTM E119

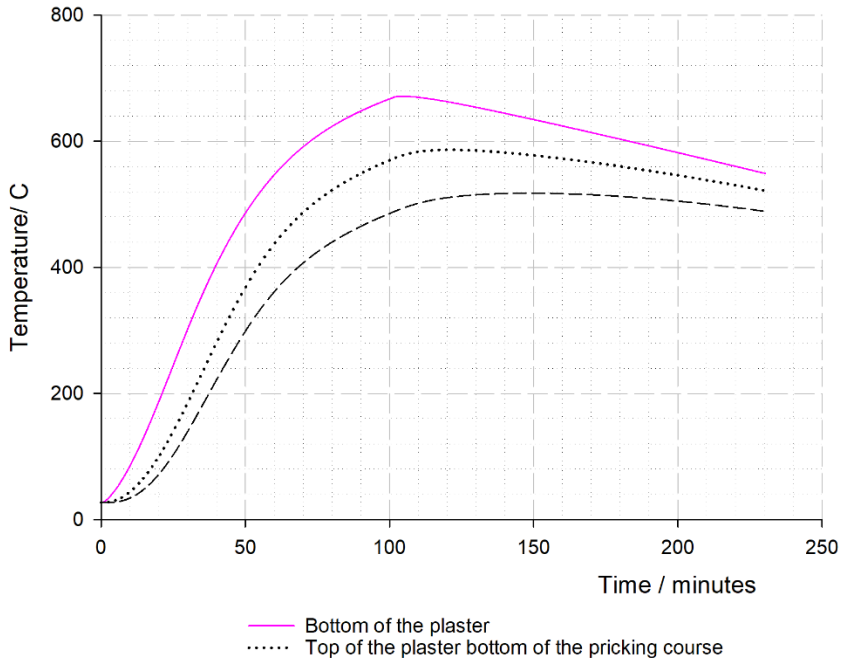

Figure 4.23: Numerical Plaster temperature time graph according to ECPC

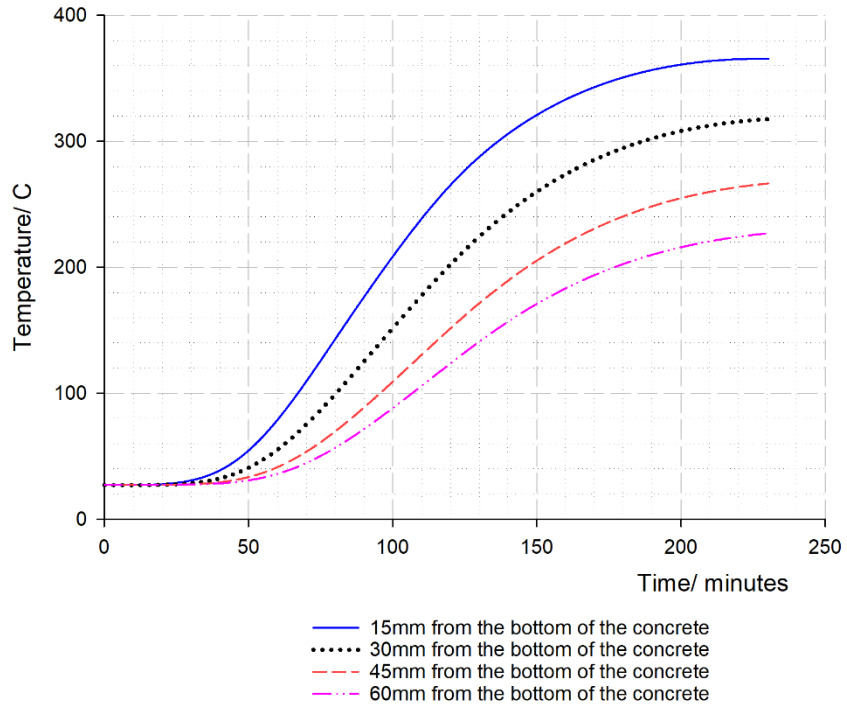

Figure 4.24: Numerical Concrete temperature time graph according to ECPC

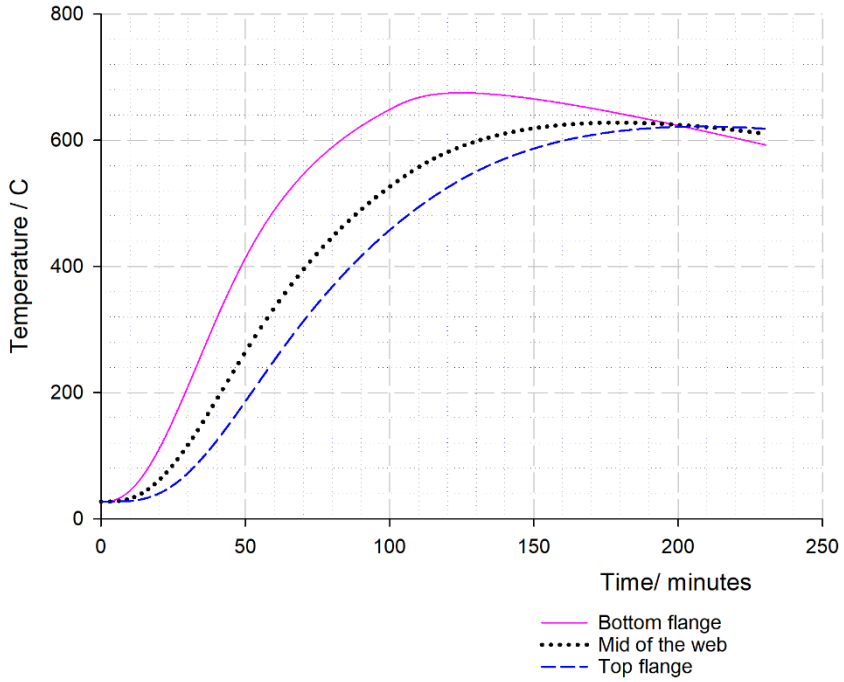

Figure 4.25: Numerical steel temperature time graph according to ECPC

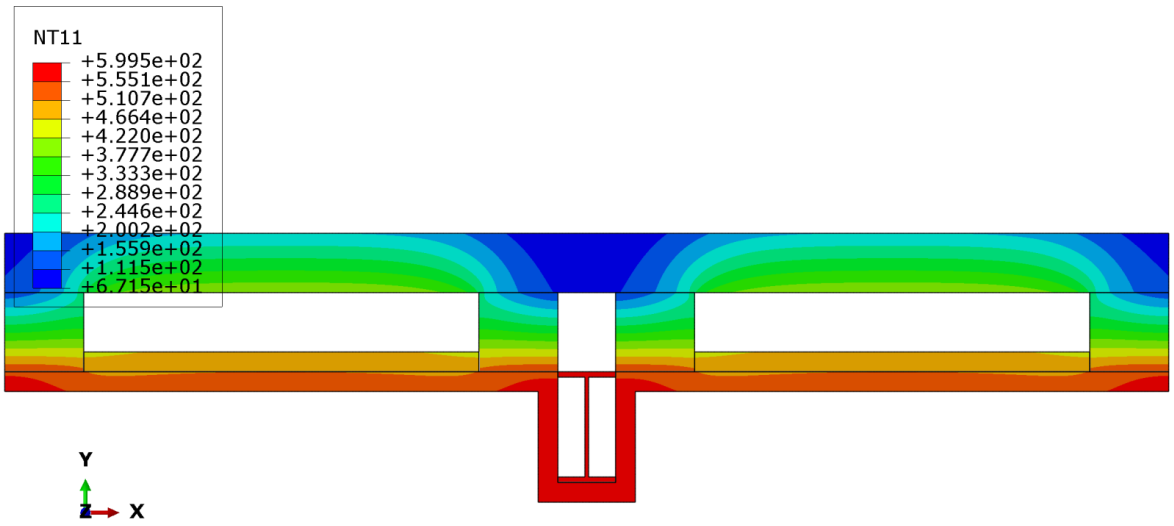

Figure 4.26: Temperature gradient according to the ECPC

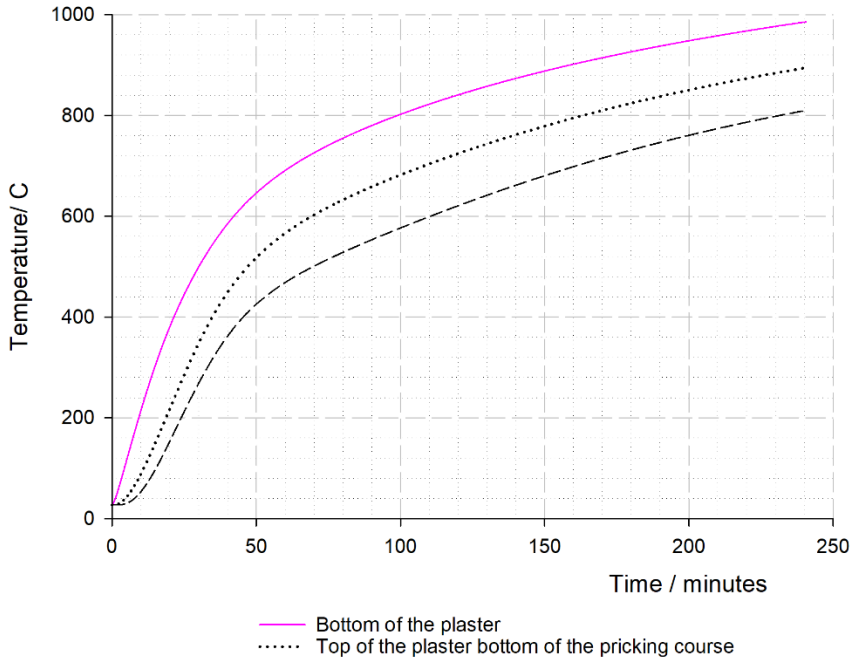

Figure 4.27: Numerical Plaster temperature time graph according to ASTM E119

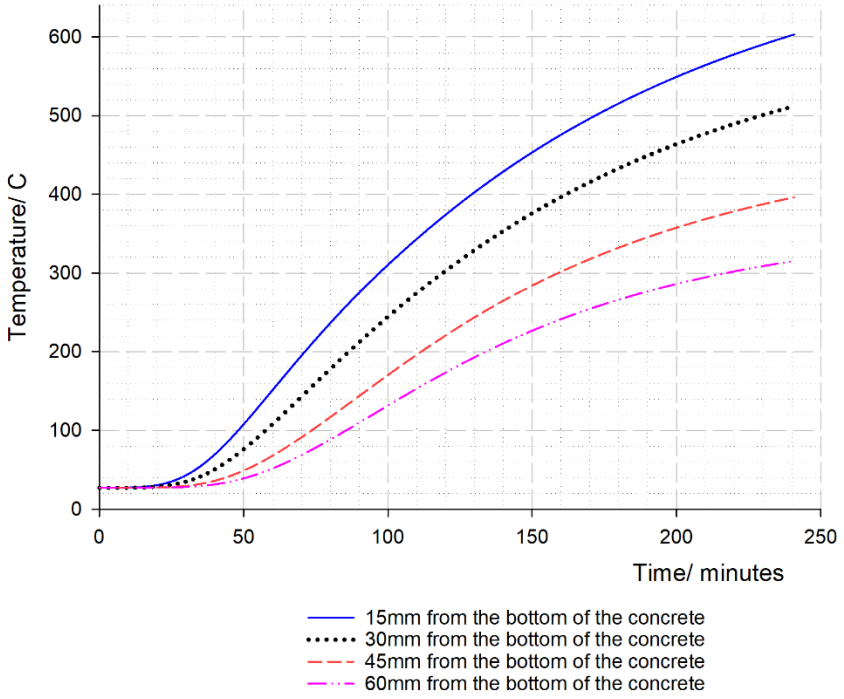

Figure 4.28: Numerical concrete temperature time graph according to ASTM E119

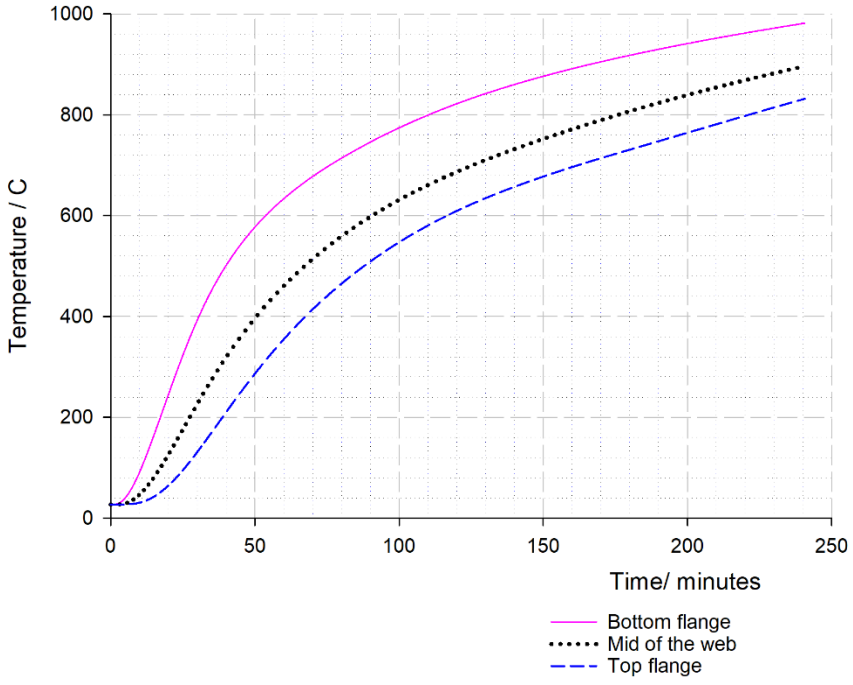

Figure 4.29: Numerical steel temperature time graph according to ASTM E119

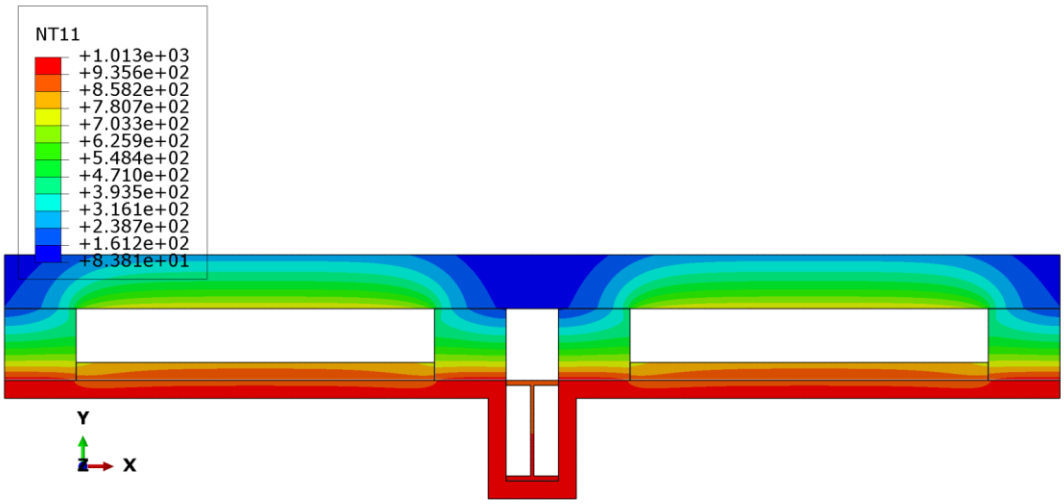

Figure 4.30: Numerical temperature gradient according to ASTME119

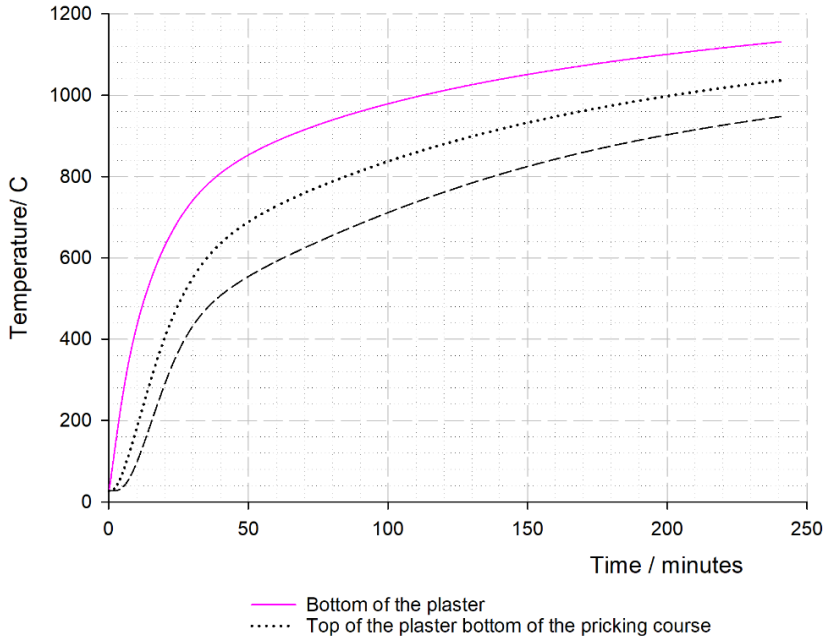

Figure 4.31: Numerical Plaster temperature time graph according to ISO 834

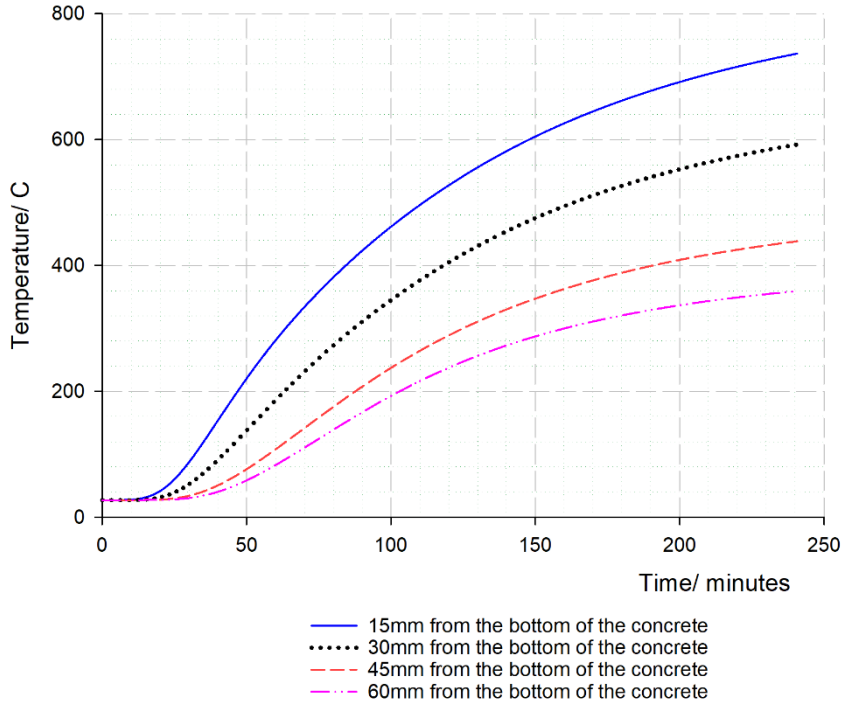

Figure 4.32: Numerical concrete temperature time graph according to ISO 834

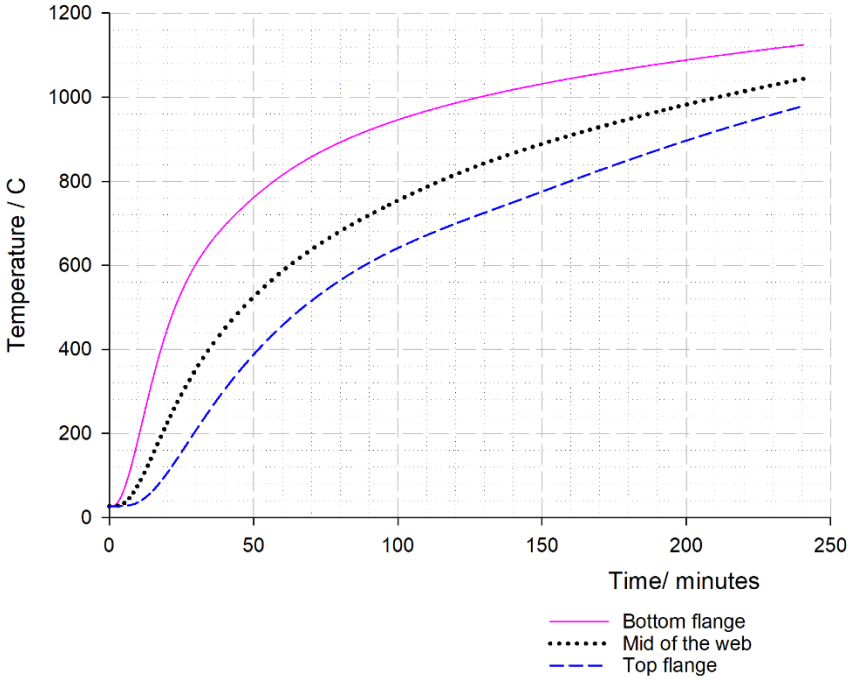

Figure 4.33: Numerical steel temperature time graph according to ISO 834

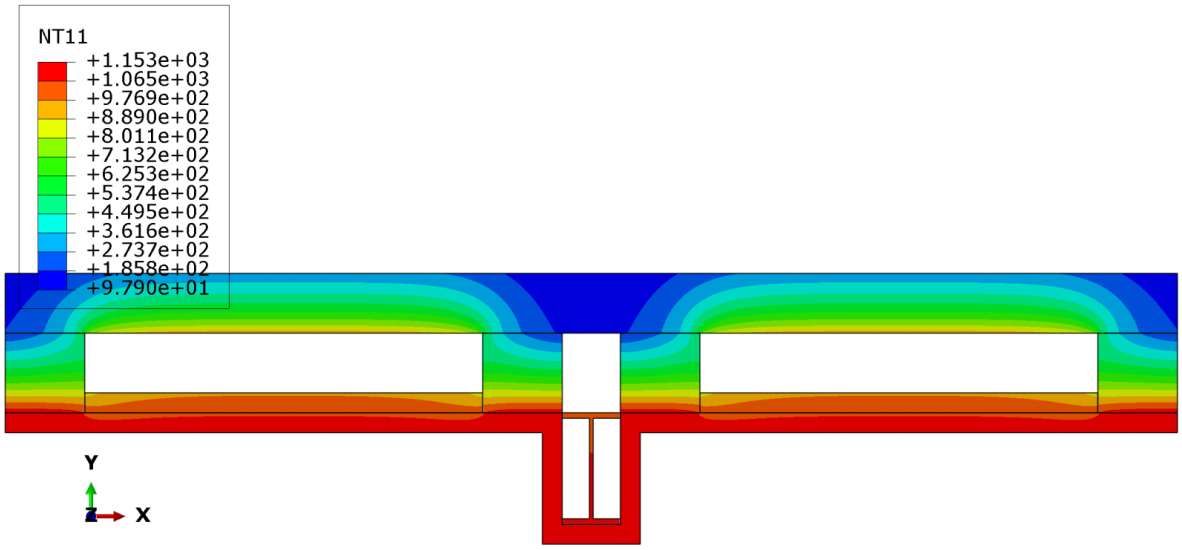

Figure 4.34: Numerical temperature gradient due to ISO 834

4.5.6 Discussion of results due to numerical investigation when modelled with ECPC, ASTM E119 and ISO 834 fire curve temperatures

As observed in the Figure 4.23, Figure 4.24, Figure 4.25, Figure 4.26, according to ECPC Figure 4.27, Figure 4.28, Figure 4.29, Figure 4.30, according to ASTME119 and Figure 4.31, Figure 4.32, Figure 4.33, Figure 4.34 according to ISO 834 higher temperatures that cause material degradation in steel and plaster occur within less than an occur. ISO834 is the most critical of the three fire curves. Plaster insulation failure occurs within ten minutes. Steel loses more than 90% of its strength by the end of one hour.

Since the slab is not in composition the failure of one element leads to global failure of the whole slab element. It can be deduced that the slab when tested against ASTM E119 and ISO 834 it cannot with stand fire for more than an hour.

4.6 SHEAR CONNECTOR EXPERIMENTAL RESULTS AND DISCUSSION

4.6.1 Introduction

The performance of the shear connector under load was determined by plotting a load slip curve as was illustrated in Figure 2.6. Load at different points is determined; that is to say, Ultimate load, 80% of the ultimate load and 40% of the ultimate. The stiffness (K_i) of the connector is measured by considering the slip modulus (secant slopes) at the 80% and 40% load levels.

$K_{0.4}$, Stiffness at $F_{0.4}$ is taken as the serviceability limit state stiffness K_{ser}.

$K_{0.8}$, Stiffness at $F_{0.8}$ is taken as the ultimate limit state stiffness K_{ult}.

4.6.2 Nails Samples

Four Push out specimens with 4inch nails as connectors between timber and concrete were subjected to monotonic loading. Load and corresponding slip were determined and plotted as seen in graph *Figure 4.35*. From the graph the ultimate load, load at 80% and load at 40% plus their corresponding slip was obtained and presented in Tables.4.8 and 4.9. Furthermore, in the same tables the slope which is equal to the stiffness at the respective loads was determined.

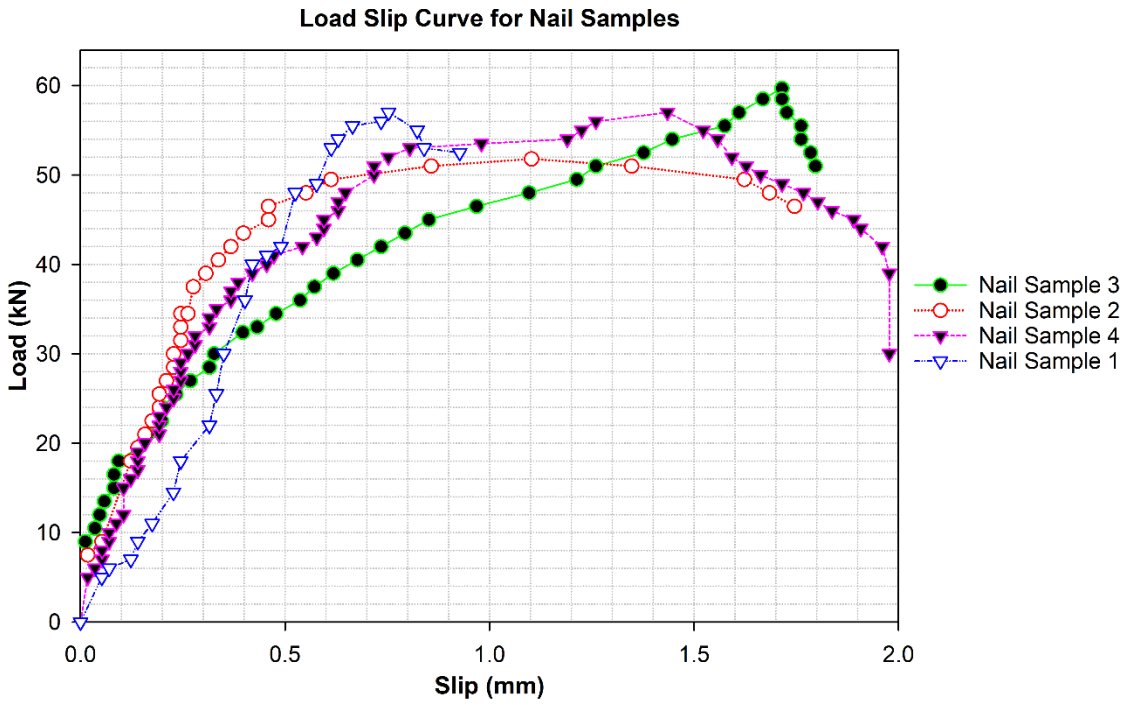

Figure 4.35: Load - Slip curves for wire nail connectors embedded in C25 concrete under monotonic loading

Table 4.4: Ultimate characteristic strength and slip values of the nail samples

Specimen	**F_{ult} (kN)**	**Slip at maximum load (mm)**	**Maximum Slip (mm)**	**Failure Type**
Nail sample 1	57.3	0.76	0.76	Nail pull out in timber
Nail sample 2	51.8	1.10	1.75	Nail pull out in timber
Nail sample 3	59.8	1.70	1.70	Nail pull out in timber
Nail sample 4	57.4	1.44	1.44	Nail pull out in timber

Table 4.5: Characteristic strength, slip and stiffness values for nail samples

Specimen	**Force $F_{0.8}$ (kN).**	**Slip at $F_{0.8}$ (mm)**	**Stiffness $k_{0.8}$**	**Stiffness $k_{0.8}$ per nail**	**Average Stiffness $K_{0.8}$**
Nail sample 1	45.84	0.50	91.68	22.92	20.69
Nail sample 2	41.44	0.35	118.40	29.60	
Nail sample 3	47.84	1.02	46.90	11.73	
Nail sample 4	45.92	0.62	74.06	18.52	
	$F_{0.4}$	**slip at $F_{0.4}$ (mm)**	**$k_{0.4}$**	**$k_{0.4}$ per nail**	**$k_{0.4}$ average**
Nail sample 1	22.92	0.33	69.45	17.36	26.73
Nail sample 2	20.72	0.16	129.50	32.38	
Nail sample 3	23.92	0.21	113.90	28.48	
Nail sample 4	22.96	0.20	114.80	28.70	

Failure of the nails samples was observed at the connection of the nail with timber as illustrated in Figure 4.36 and Figure 4.38. There was Plastic deformations of the nails as shown in Figure 4.36 and Figure 4.37. Withdraw of nails in the timber element was also observed. Concrete in all nail samples showed no sign of failure.

Figure 4.36: shows Plastic deformation of the nails and concrete showed no sign of failure

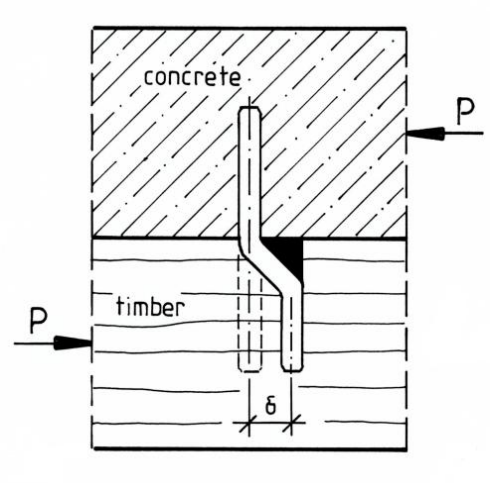

Figure 4.37: Timber concrete dowel connection failure. (Adopted from (Aicher, et al., 2003)) this is the failure observed in Figure 4.20 and 4.22

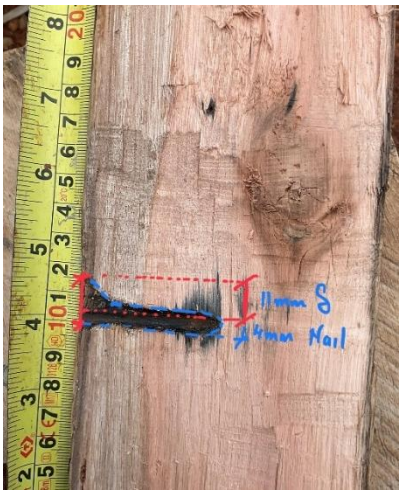

Figure 4.38 Timber concrete dowel connection timber failure

4.6.3 Nails Connectors discussion

The slip modulus obtained experimentally was $K_{ult,0.8}$ = 20.69kN/mm and K_{ser} = 26.73kN/mm. Aicher, et al., 2003 stated that, "*comparing the deformation shapes of the nail in the timber-concrete and the timber-timber connection situation, it is obvious that K_{ser} in the timber-concrete application should be very roughly 2times higher than slip modulus Eurocode 5 specifies for nails in predrilled and not predrilled holes."* (Aicher, et al., 2003)

The Average Experimental slip modulus of 26.73kN/mm was found to be three (3) times higher than the average slip modulus of $8.25\ kN/mm$ obtained by calculation. Calculation is attached in the Appendix A

Plastic failure was observed in the nails where by two plastic hinges were formed. The timber member was deformed and no observable deformation was noticeable in the concrete.

The graph shape obtained in Figure 4.19 shows that the nails are a ductility shear connector.

4.6.4 Expanded Metal lathe (Mesh) Samples

Four Expanded Metal lathe (Mesh) samples were prepared for testing but only two were tested because the other two failed while removing the concrete formwork hence showing weakness of the Expanded Metal lathe (Mesh). The remaining two samples were subjected to Monotonic loading. Slip was observed and measured by a linear variable displacement transducer. The results were plotted on a graph as shown in Figure 4.39. From the Figure it can be observed that the Expanded Metal lathe (Mesh) exhibit ductility.

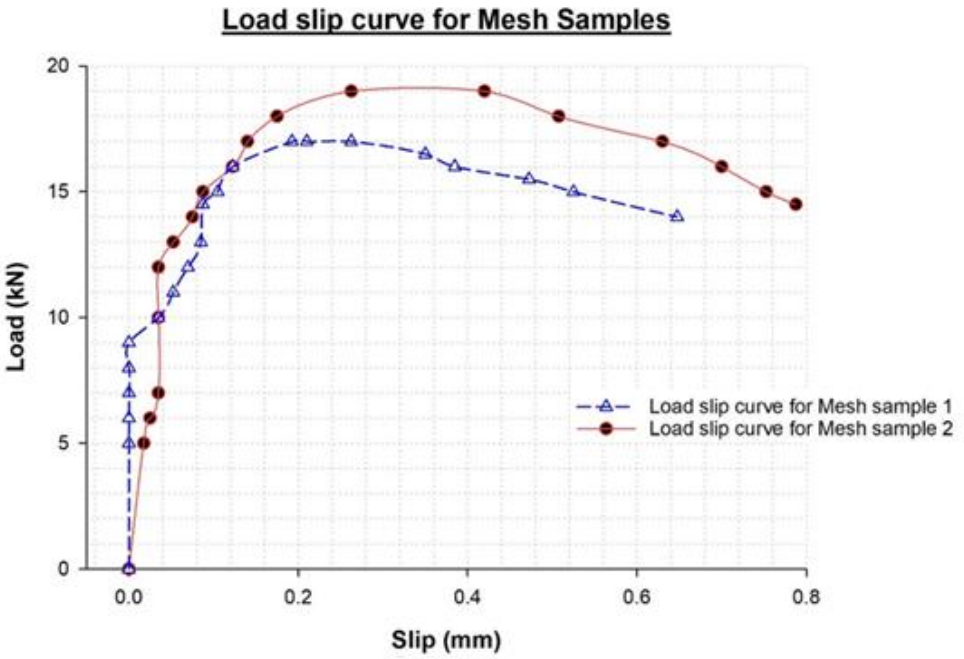

Figure 4.39: Load - Slip curves for metal lathe Expanded Metal lathe (Mesh) embedded in C25 concrete connected to timber under monotonic loading

From the graph Figure 4.39, the ultimate load, load at 80%, and Load at 40% was obtained plus their corresponding slips. Secant slopes were calculated representing stiffness at this load level. The results were presented in Table 4.10 and 4.11.

Table 4.6:Ultimate characteristic strength and slip values of the Expanded Metal lathe (Mesh) samples

Specimen	**F_{ult} (kN)**	**Slip at F_{ult} (mm)**	**Maximum Slip (mm)**	**Failure Type**
Mesh sample 01	17.1	0.25	0.65	Mesh rapture
Mesh sample 02	19.1	0.35	0.78	Mesh rapture

Table 4.7 shows characteristic strength, slip and stiffness values for Expanded Metal lathe (Mesh) samples

Specimen	**$F_{0.8}$ (kN)**	**Slip at $F_{0.8}$ (mm)**	**$k_{0.8}$**	**$k_{0.8}$ one Mesh**	**$K_{0.8}$ average**
Mesh sample 01	13.68	0.09	152.00	76.00	
Mesh sample 02	15.28	0.10	152.80	76.40	76.20
Specimen	**$F_{0.4}$ (kN)**	**Slip at $F_{0.4}$ (mm)**	**$k_{0.4}$**	**$k_{0.4}$ one Mesh**	**$k_{0.4}$ average**
Mesh sample 01	6.84				
Mesh sample 02	7.64	0.04	191.00	95.50	95.5

Failure of the Expanded Metal lathe (Mesh) samples was by rapture of the Expanded Metal lathe (Mesh) its self without any observable failure in concrete or timber. This was captured in *Figure 4.40* and Figure 4.41

Figure 4.40: Raptured Expanded Metal lathe (Mesh) sticking out of the concrete block

Figure 4.41: Timber that was attached to one of the Expanded Metal lathe (Mesh) samples. the bent nails were used to connect the Expanded Metal lathe (Mesh) to the timber

4.6.5 Expanded Metal lathe (Mesh) as a shear connector Discussion

The slip modulus obtained experimentally was $K_{ult,0.8}$ = 76.2kN/mm and K_{ser} = 95.5kN/mm. When compared with the nails slip modulus, the Expanded Metal lathe (Mesh) had a higher slip modulus than two nails.

The failure mode was rapture of the Expanded Metal lathe (Mesh). No deformation was observed in the timber nor concrete hence a less stiff or weak shear connector than the elements its connecting.

From the graph shape in Figure 4.39 it can be deduced that the shear connector is ductility.

4.7 SHEAR CONNECTORS NUMERICAL RESULTS AND DISCUSSION

4.7.1 Nail Shear Connectors Numerical Results

A model of representing a realist pushout setup was modelled in ANSYS workbench as seen in Figure 3.13. The boundary condition was fixed support at the concrete blocks bottom face which restrained the block against horizontal and vertical translation.

A vertical Load was applied in seven steps of 10kN incremental load starting from 0kN to 55kN on the timber part model. The model was analyzed and results generated.

The results of deformation in the Y axis obtained were tabulated and plotted on the graph as shown in Table 4.12 and Figure 4.42 respectively

Table 4.8: Nail model Numerical results obtained in from the pushout test simulation in ANSYS

No	1	2	3	4	5	6	7
Force/ kN	0	10	20	30	40	50	55
Slip/ mm	0	0.18569	0.23038	0.30862	0.38305	0.7200	1.344

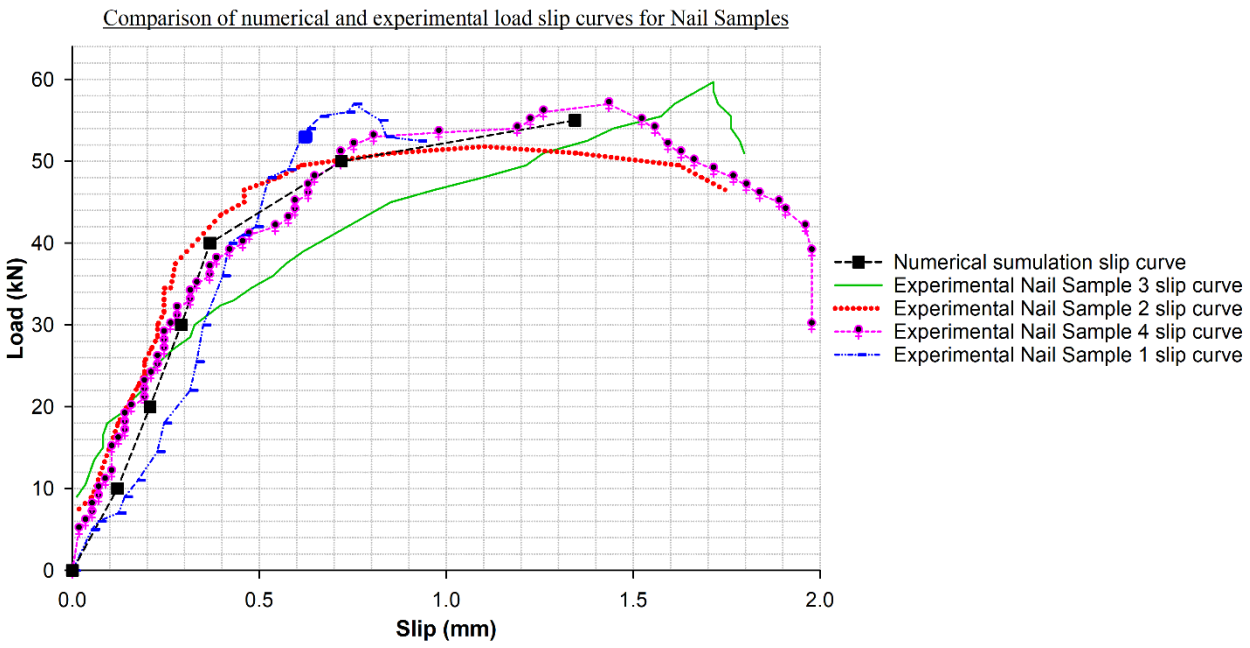

Figure 4.42: Comparison of numerical and experimental load slip curve for nail sample model.

Numerical results showed a linear relation between force and slip in Figure 4.42 up to 40kN and a non-linear relation beyond 40kN. However, when numerical and experimental results were compared against each other in Figure 4.42 the following was deduced: -

a. Both numerical and experimental show a similar slip values with both elastic and plastic deformation regions. The elastic region was between 0 and 40kN and above 40kN the plastic deformation began.
b. 40kN was determined as the yield point.

Further observations that showed similar Numerical simulation results as the experimental test, was the failure mode observed. It was observed from the numerical simulation that failure occurred in timber part model and not in the concrete part mode as shown in Figure 4.43.

In addition to the above, the nails formed two plastic hinges the side that was embedded in the timber part model illustrated in Figure 4.44.

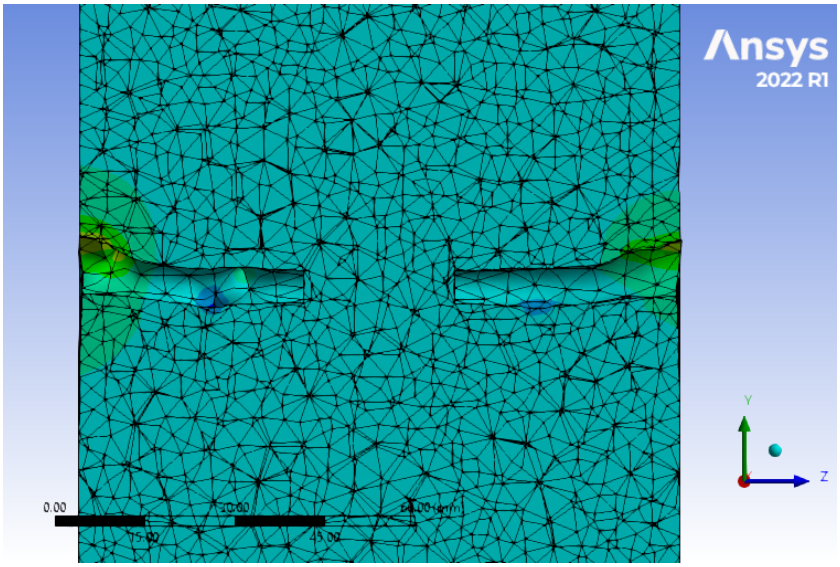

Figure 4.43:Deformation at the timber nail contact in the ANSYS model like the Experimental deformation shown in Figure 4.22.

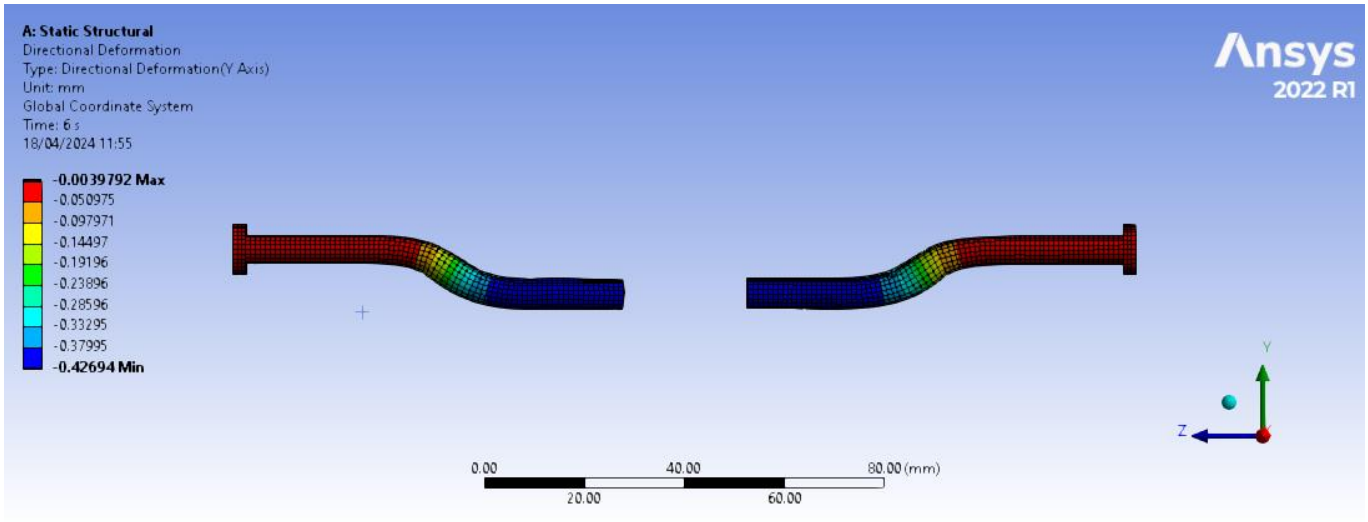

Figure 4.44: Nail deformation as obtained from simulation Nails push out test model in ANSYS

4.7.2 Expanded Metal lathe (Mesh) Shear connector Numerical results

A Numerical model representing a realist pushout setup was modelled in ANSYS workbench as seen in Figure 3.14. The bottom faces of the concrete blocks were specified as the boundary condition of fixed supports restraining the blocks against horizontal and vertical translations. A vertical Load was applied in eleven steps of 2kN incremental load starting from 0kN to 19kN on the timber part model. The model was analyzed and results were generated.

The results of deformation in the Y axis obtained were tabulated and plotted on the graph as shown in Table 4.13 and Figure 4.45 respectively.

Table 4.9: Tabulated results of slip obtained from numerical simulation of Expanded metal lathe (mesh) model in ANSYS.

No	1	2	3	4	5	6	7	8	9	10
Force/kN	2	4	6	8	10	12	14	16	18	19
Slip/ mm $\times 10^{-4}$	132	233	329	429	528	628	726	1020	1802	3450

The load and slip showed a non-linear relationship with an initial linear elastic region and a subsequent plastic region. The mesh exhibited both elastic and plastic deformation. The results obtained from the experimental setup were compared against those obtained numerical in Figure 4.45.

Both experimental and numerical results showed similar slip values with two regions of elastic and plastic deformation.

Hence the load numerical model can be used to study the force slip relationship.

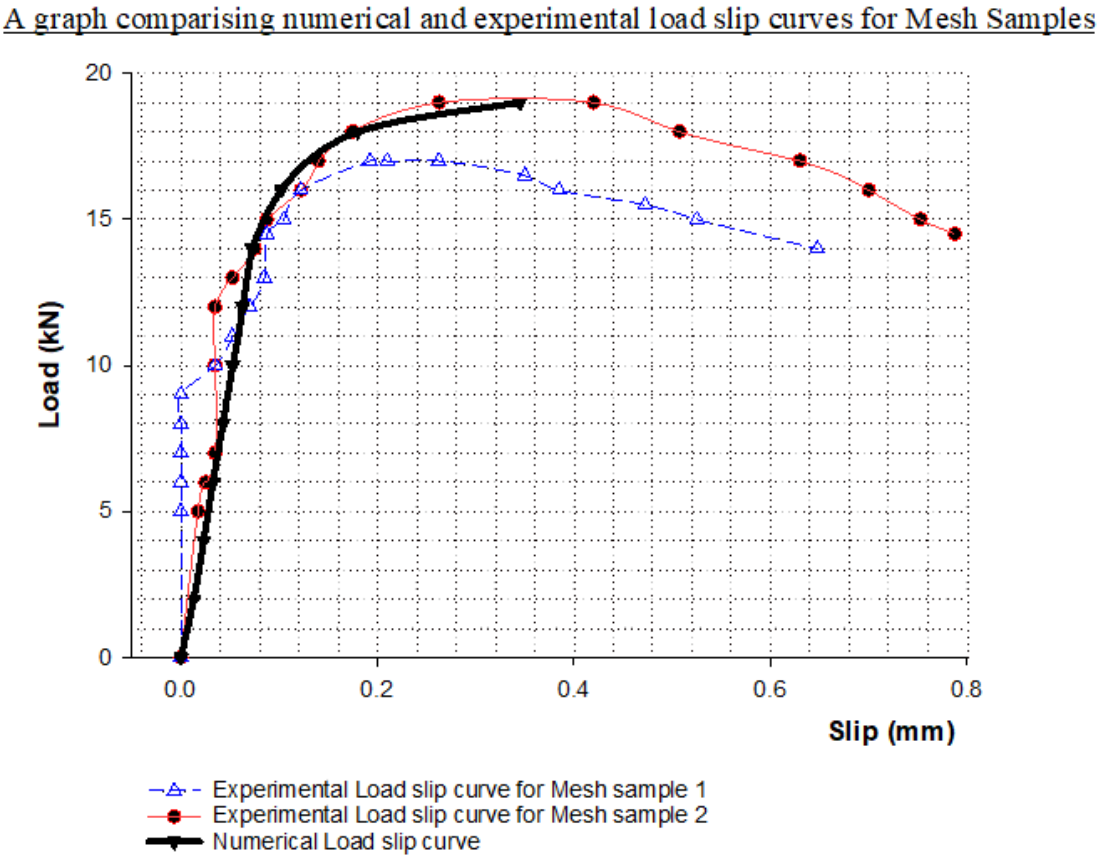

Figure 4.45: A graph comparing numerical and experimental load slip curves for mesh push out models

Similarly, failure in the expanded metal lathe (mesh) push out analytical model was observed in the mesh only. The mesh model part showed necking deformation (reduction in size) were timber concrete interface. This was depicted in Figure 4.46, Figure 4.47, and Figure 4.48.

No deformation was observed in the timber and concrete model parts as shown in Figure 4.47. This showed that a push out numerical model simulated in ANSYS can be used to predict the failure mode.

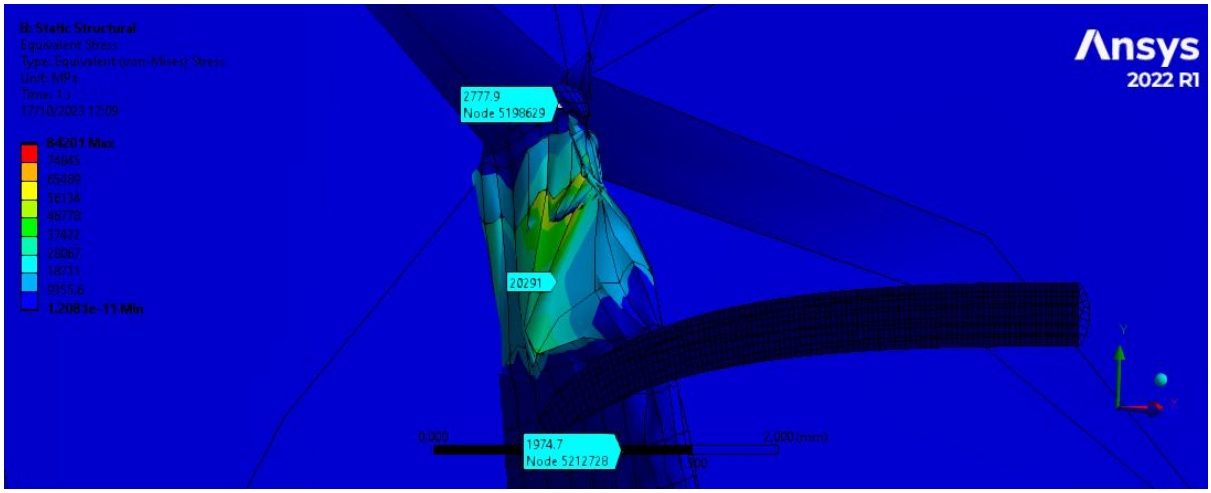

Figure 4.46 Necking of expanded metal lathe leading to rupture as observed in the experimental model

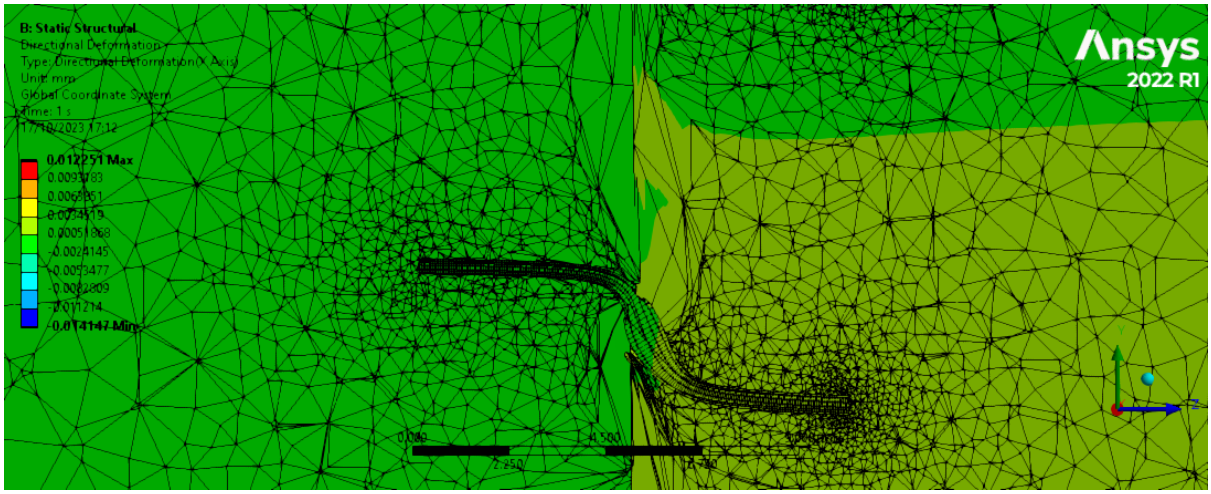

Figure 4.47 Timber, concrete interface with metal lathe showing now deformation whereas Expanded Metal lathe (Mesh) wire shows deformation.

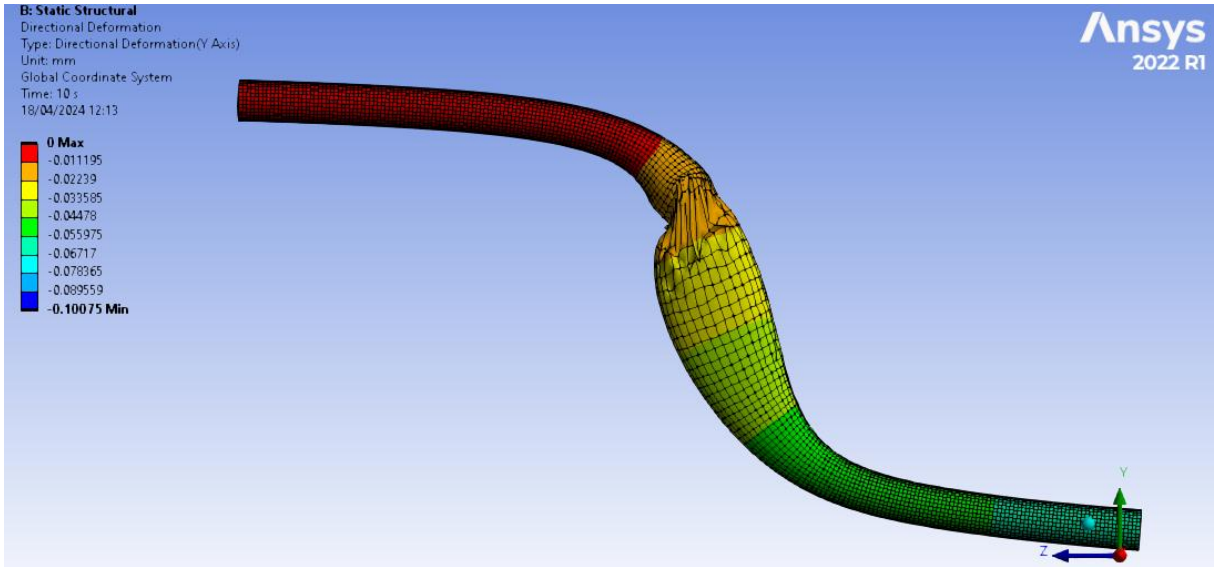

Figure 4.48: Necking in the mesh part model representing signs of rapture.

4.7.3 Numerical shear connector discussion

The push out numerical models simulated in ANSYS show a linear relation between Force and slip, an incremental in force will cause an equal increment in slip even when the ultimate force obtained experimental is reached.

Numerical and Experimental results showed equivalent slip values and slip curves with both elastic and plastic deformations. Therefore both numerical and experimental load slip curves showed a non linear graph after the yield point was reached.

Both numerical and the experimental model agreed on the deformation of the nails, Expanded Metal lathe (Mesh), and timber: -

- In the nails sample models, deformation was occurred only in the timber and two plastic hinges were formed in nails which was observable in both numerical and experimental investigations
- In the Expanded Metal lathe (Mesh) sample models, the Expanded Metal lathe (Mesh) was rapture as observed in both numerical and experimental investigations.

5.0 RECOMMENDATION AND CONCLUSION

5.1 CONCLUSIONS

It was concluded from the baseline study that commercial buildings are more prone to fire hazards in Uganda therefore the parameter used on commercial buildings were considered for the research model. The specifications selected were 100 x100 mm eucalyptus grandis timber, steel I-beam, welded joints for joining the steel sections, 75mm thick concrete topping, pricking coarse at the bottom of the timber, and H8-200mm reinforcing bars.

According to the Experimental and Numerical fire performance of the hybrid slab the following conclusions were drawn in this Thesis:

1. This study has presented a comprehensive investigation into the fire resistance of a hybrid Steel-Timber-Concrete (STC) slab system through both experimental testing and numerical simulation. The experimental program, based on a representative slab configuration reflecting construction practices in Uganda, demonstrated that the STC slab was capable of withstanding a natural fire scenario for over one hour while maintaining its load-carrying capacity. A 25mm plaster finish at the bottom slab influenced the fire resistance of the hybrid slab, by absorbing a significant amount of heat hence protecting the timber beams, steel beams and concrete. This finding is significant, indicating a robust initial fire performance for this hybrid system.
2. When timber was ignited collapse of plaster and pricking course that were supported by it collapsed after the char layer formed in the nail region. This can be detrimental as it can cause loss of lives or property. On the other hand, collapse of plaster can be useful to extinguish the fire below but cause timber beam members to flame that were in smoldering phase for lack of enough oxygen because they were covered by plaster finish in the slab.
3. Deflections limit of the slab elements was exceeded. Hence failure of the slab in deflection.
4. The numerical simulations, conducted using the finite element software ABAQUS-CAE and incorporating experimentally obtained natural fire temperatures, provided strong corroboration of the experimental results. The close agreement between the numerical predictions and the experimental observations validates the accuracy of the

numerical model in capturing the complex thermal and structural behavior of the STC slab under fire conditions.

5. The numerical simulation based on ECPC, ASTME119 and ISO 834 conducted using ABAQUS CAE showed that the slab elements experience higher temperatures that cause material degradation within less than an hour. Hence according to the above mentioned standards 25mm plaster fails to insulate the slab from degradation by fire within less than 10minutes

The following conclusion were made on the shear connector experiment and numerical models results and deductions: -

- The locally available nails on the Ugandan market can be used as shear connectors since the stiffness can be obtained experimentally and by calculation.
- The average experimental K_{ser} nails slip modulus is 3 times the K_{ser} slip modulus obtain as an average of the Eurocode timber to timber, timber to steel connection for predrill and non-predrilled connection.
- The Expanded Metal lathe (Mesh) model offers high slip modulus values but a weak connection that raptures when load above the tensile force is applied hence a weak shear connector because it lacks rigidity.
- The nails and expanded metal lathe show that they are ductility shear connectors.
- The numerical model shows similar values with the experimental model exhibiting two regions of deformation namely; Elastic and plastic deformation. Therefore, the numerical push out model in ANSYS can be used to study nails and Expanded metal lathe as shear connectors to timber and concrete.

5.2 RECOMMENDATIONS FOR FURTHER RESEARCH

Even though this research has shone light into the fire performance of hybrid steel timber concrete floor system in Uganda, there is much that has not been considered in the timeframe and economic resources available. There are many possible improvements that can be made on the hybrid slab and elements considered. The various structural elements when changed i.e. by varying wood type or plaster additives, it creates a new response to fire hence necessitating further study. The areas to be considered for further research are:

- Modifying the plaster mortar to improve its insulation properties and fire integrity properties to avoid fire spread into other floor system of elements.
- Further studies in Uganda on Timber improvement against ignition need to be carried out since timber is more resistant to loss of structural strength compared to steel at elevated temperatures.
- Further research could explore the fire performance of STC slabs under different loading
- The 3D numerical structural performance of the STC has not been done and this is recommended for further study.

REFERENCES

Aicher, S., Dill-Langer, G. & Klöck, W., 2003. Nails and nailplates as shear connectors for timber-concrete composite constructions. *Otto-Graf,* Volume 14.

Aicher, S., Klöck, ,. & Dill-Langer, G., 2003. NAILS AND NAILPLATES AS SHEAR CONNECTORS FOR TIMBER - CONCRETE COMPOSITE CONSTRUCTIONS. *Otto-Graf-Journal,* Volume 14, pp. 189-210.

American Society for Testing and Materials, 2020. *ASTM E119, Standard Test Methods for Fire Tests of Building Construction and Materials.* West Conshohocken: s.n.

Andreas , M., 2010. *Evaluation of timber-concrete composite floors,* Sweden: s.n.

Anon., n.d. *1. BS 476-20 : 1987 Fire tests on building materials and structures — Part 20: Method for determination of the fire resistance of elements of construction (general principles).* s.l.:s.n.

Burgess, I., 2015. THE INFLUENCE OF CONNECTIONS ON THE ROBUSTNESS OF COMPOSITE STRUCTURES IN FIRE. *ResearchGate.*

Ceccotti, A., 2002. Composite concrete-timber structures. *Progress in Structural Engineering and Materials,* 4(3), pp. 264-275.

Chandrasekaran, S. & Nagavinothini, R., 2020. Behavior of stiffened deck plates under hydrocarbon fire. *Marine Systems & Ocean Technology,* Volume 15, p. 95–109.

Chiara , B. et al., 2018. *Numerical Modelling of Timber Concrete Composite Structures in Fire - Guidance Document,* ETH Zürich Switzerland,: European Cooperation in Science and Technology.

Dias, A., 2005. *"Mechanical behaviour of timber-concrete joints", Ph.D. thesis,.* Delft, Netherlands: Delft Univ. of Technology.

Du, H., Hu, X., Zhang, B. & Minli, Y., 2017. *Numerical simulation on behaviour of timber-concrete composite beams in fire.* Nanjing , IOP Publishing Ltd.

EUROCODE 3, 2005. *EN 1993-1-2 Design of Steel structures – General rules Structural fire design.* s.l.:s.n.

EUROCODE 3, 2005. *EN 1993-1-2 Design of Steel structures – General rules Structural fire design.* s.l.:s.n.

EUROCODE 5, 2004. *EN 1995-1-2 Design of timber structures – General rules Structural fire design.* s.l.:s.n.

Fragiacomo, M. & Lukaszewska, E., 2011. *Development of prefabricated timber–concrete composite floor systems.* s.l., ICE Publishing.

FRANGI , A. & FONTANA , M., n.d. *Thermal expansion of wood and timber-concrete composite members under ISO-fire exposure.* Zurich, Switzerland, Institute of Structural Engineering.

Girhammar, U. A., 2009. A simplified analysis method for composite beams with interlayer slip. *International Journal of Mechanical Sciences,* Volume 51, p. 515–530.

Hao Du, Xiamin, H., Bing, Z. & Yao , M., 2017. *Numerical simulation on behaviour of timber-concrete composite beams in fire.* Nanjing, IOP publishing.

Hong, . K. E. M., 2017. *Structural Performance of Nail-Laminated Timber-Concrete Composite Floors.* s.l.:THE UNIVERSITY OF BRITISH COLUMBIA.

Iman , A., Behrang , S., Alireza , M. & Mohammad , H., 2020. *Evaluating the Dynamic Thermal Properties of Cement Mortar with Different Mix Proportion through Numerical Computation.* Tehran, ISME2020-NC1045.

International Organization for Standardization, 1999. *Fire-resistance tests — Elements of building construction — Part 1: General requirements.* Geneva: s.n.

J, K. & L., 2018. *Structural Fire Engineering.* Virginia: American Society of Civil Engineers.

Kliger, R., 2000. *Mechanical properties of timber products required by end-users.* Whilstler, Canada, s.n.

Kostic , S. M. & Deretic-Stojanovic, B., 2018. Bending Resistance of Composite Sections with Nonductile Shear Connectors and Partial Shear Connection. *Hindawi, Advances in Civil Engineering.*

Lennon, T., 2011. *Structural fire engineering design.* London: ICE Publishing.

Meena, R., Schollmayer, M. & Tannert, T., 2014. Experimental and Numerical Investigations of Fire Resistance of Novel Timber-Concrete-Composite Decks. *Performance of Constructed Facilities.*

NAGAVALLY, . R. R., 2016. *COMPOSITE MATERIALS - HISTORY, TYPES, FABRICATION TECHNIQUES, ADVANTAGES, AND APPLICATIONS.* Bengaluru, India,, ISBN: 978-93-86083-69-2.

National Building Review Board, 2020. *Press Statement on Fire Safety,* Kampala: NBRB.

NBRB, N. B. R. B., 2021. *Consultative Meeting on the viability of the Steel timber composite building method.* Kampala, s.n.

Nora , B., Abdelkrim , M. & Salah , A. E., 2022. STUDY OF THE PHYSICO-MECHANICAL PROPERTIES OF THERMALLY MODIFIED EUCALYPTUS CAMALDULENSIS WOOD: THE CASE OF THE MOROCCAN FOREST. *JP Journal of Heat and Mass Transfer,* Volume 25, pp. 109-125.

O'Neill, J. W., 2009. *The Fire Performance of Timber-Concrete Composite Floors.* Christchurch, New Zealand: s.n.

O, V. et al., 2014. *Eurocode: Baground and Applications Structural Fire Design.* Luxembourg: Publications Office of the European Union.

PROMAT, 2020. *International fire curves – useful tool for designing fire safety.* [Online] Available at: https://www.promat.com/en/construction/news/33637/international-fire-curves-fire-safety/
[Accessed May 2023].

Shafigha, P., Asadi , I. & Akhianic, A., n.d. *Thermal Properties of Cement Mortar with different mix proportions,* Kuala Lumpur: Department of Building Surveying; University of Malaya.

Shafigha, P. et al., 2020. Thermal properties of cement mortar with different mix proportions. *Materiales de ConstruCCión,* July–September .70(339).

Steel & Tube, 2023. *STRUCTURAL STEEL (I-BEAMS AND UPN CHANNELS).* [Online] Available at: https://stil.co.ug/structural-steel/
[Accessed 10 may 2023].

Steel Construction Institute , 2003. *Steel Designers' Manual.* 6th Edition ed. s.l.:Blackwell Plublishing .

Suvranu, D., n.d. *Abaqus Handout: MANE 4240/ CIVL 4240: Introduction to Finite Elements.* s.l.:Rensselaer Polytechnic Institute.

Tom , L., 2011. Structural Fire Engineering Design. In: *Structural Fire Engineering.* s.l.:Institution of Civil Engineers (ICE), pp. 39-74.

UNBS, 2022. *UNBS Tightens Grip On The Quality Of Steel Products.* [Online] Available at: https://www.unbs.go.ug/readmore-slider.php?sl=320&banner
[Accessed may 2023].

Wang, Y., Jia, L. & Li, X., 2018. *Investigation on Behavior of Castellated Composite Beams under Fire.* s.l., EDP Sciences.

Wilf Malcolm Institute of Educational Research, 2009. *What is fire? The Science Learning Hub.* [Online]
Available at: https://www.sciencelearn.org.nz/resources/747-what-is-fire
[Accessed may 2023].

Yeoh , D. & Chuan , E., 2010. *Behaviour and design of timber-concrete composite floor system.* New Zealand : PhD thesis, University of Canterbury.

Zziwa, A., Ziraba, Y. N. & Mwakali, J. A., 2010. Strength properties of selected Uganda Timber. *International Wood Products Journal,* Volume 01, pp. 21-27.

BS 476-20 : 1987 Fire tests on building materials and structures — Part 20: Method for determination of the fire resistance of elements of construction (general principles).

BS 476-21: 1987 Fire tests on building materials and structures — Part 21: Methods for determination of the fire resistance of loadbearing elements of construction.

DD ENV 1994-1-1, Design of composite steel and concrete structures- Part 1.1, EC 4: General rules and rules for building, London: British Standards Institution

APPENDIX

Appendix A: Calculations

Eurocode parametric curve calculation (EPCC)

The parametric approach is well suited to be used in spreadsheets. It provides an estimate of the average time–temperature response for various building compartment parameters. It offers a more realistic fire scenario idealization than nominal curves. The EPCC is phased into an exponential heating curve at a maximum temperature corresponding to a time, t_{max}, followed by a cooling phase which decreases linearly.

The heating phase in BS EN 1991-1-2 is given by:

$$\theta_g = 1325(1 - 0.324e^{-0.2t^*} - 0.204e^{-1.7t^*} - 0.472e^{-19t^*})$$

where

θ_g = temperature in the fire compartment (°C)
$t^* = t.\Gamma$ (h)
t = time (h)
$\Gamma = [O/b]^2/(0.04/1160)^2$ (–)
$b = \sqrt{\rho c \lambda}$ and should lie between 100 and 2200 (J/m^{2}s$^{1/2}$K)
O = opening factor ($A_v\sqrt{h}/A_t$) (m$^{1/2}$)
A_v = area of ventilation openings (m^2)
h = height of ventilation openings (m)
A_t = total area of enclosure (including openings) (m^2)
ρ = density of boundary enclosure (kg/m^3)
c = specific heat of boundary enclosure (J/kgK)
λ = thermal conductivity of boundary (W/mK)

Maximum temperature, t_{max}, "in the heating phase" :

$$t_{max} = \max[(0.2 \times 10^{-3} \times q_{t,d}/O_{lim}); t_{lim}]$$

where

$$q_{t,d} = q_{f,d} \times A_f/A_t$$

t_{lim} = 25 minutes (slow fire growth rate), 20 minutes (medium fire growth rate) and 15 minutes (fast fire growth rate).

Temperature against time equations in cooling zone are given by:

$$\theta_g = \theta_{max} - 625(t^* - t^*_{max}) \text{ for } t^*_{max} \leqslant 0.5(h)$$

$$\theta_g = \theta_{max} - 250(3 - t^*_{max})(t^* - t^*_{max}) \text{ for } 0.5 < t^*_{max} < 2(h)$$

$$\theta_g = \theta_{max} - 250(t^* - t^*_{max}) \text{ for } t^*_{max} \geqslant 2(h)$$

Area of ventilation openings (m2)

$$A_V = 0.6 \times 0.4 + 9 \times 0.2 \times 0.3 = 0.78m^2$$

Compartment floor area

$$A_f = 3 \times 4 = 12m^2$$

Total boundary area

$$A_t = Wallarea\ + floor\ area + roof\ area = 12 \times 2 + 14 = 38m^2$$

Design fire load Annex E BS EN 1991-1-2

$$Fire\ load, q_{fk} = \frac{fuel\ quantity(kg) \times fuel\ calorific\ value\left(\frac{mJ}{kg}\right)}{area\ of\ compartment}$$

$Fire\ load, q_{fk} = 511\ MJ/m^2\ from\ Table\ E4$, BS EN $1991-1-2$ $(office\ space\ \pm 30kg\ of\ fuel\ load)$

$$q_{f,d} = q_{f,k} \cdot m \cdot \delta_{q1} \cdot \delta_{q2} \cdot \delta_n \quad [MJ/m^2] \quad (E.1)$$

where

m is the combustion factor (see E.3)

δ_{q1} is a factor taking into account the fire activation risk due to the size of the compartment (see Table E.1)

δ_{q2} is a factor taking into account the fire activation risk due to the type of occupancy (see Table E.1)

$\delta_n = \prod_{i=1}^{10} \delta_{ni}$ is a factor taking into account the different active fire fighting measures i (sprinkler, detection, automatic alarm transmission, firemen …). These active measures are generally imposed for life safety reason (see Table E.2 and clauses (4) and (5)).

$q_{f,k}$ is the characteristic fire load density per unit floor area [MJ/m²] (see f.i. Table E.4)

Table E.1 — Factors δ_{q1} , δ_{q2}

Compartment floor area A_f [m²]	Danger of Fire Activation δ_{q1}	Danger of Fire Activation δ_{q2}	Examples of Occupancies
25	1,10	0,78	artgallery, museum, swimming pool
250	1,50	1,00	offices,residence, hotel, paper industry
2 500	1,90	1,22	manufactory for machinery & engines
5 000	2,00	1,44	chemical laboratory, painting workshop
10 000	2,13	1,66	manufactory of fireworks or paints

$$q_{fd} = 511 \times 0.8 \times 1.0 \times 1.32 \times 1.0 = 540.5\, MJ/m^2$$

$$q_{t,d} = q_{f,d} \times {A_f}/{A_t} = 154 \times {12}/{38} = 170\, MJ/m^2$$

Thermal inertia of the fire compartment, bricks= 1521J/m^{2}s$^{0.5}$k, Concrete= 2034 J/m^{2}s$^{0.5}$k

$$b = \frac{\sum b_i A_i}{\sum A_i} = \frac{2034 \times 12 + 1521 \times 12 + 1521 \times 12.95}{12 + 12 + 12.95} = 1687.6\text{J/m}^2 s^{0.5}\text{k}$$

Ventilation factor

$$h_{eq} = \frac{\sum b A_{vi} h_i}{\sum A_v} = \frac{1(0.6 + 0.4) \times 6 + 9(0.3 \times 0.3) \times 0.2}{1(0.6 \times 0.4) + 9(0.3 \times 0.3)} = 0.3686\text{J/m}^2 s^{0.5}\text{k}$$

$$O = \frac{A_v \sqrt{h_{eq}}}{A_t} = \frac{1.05\sqrt{0.3686}}{38} = 0.0167 \cong 0.02$$

Maximum temperature occurs at

$$t_{max} = \max\{(0.2 \times 10^{-3} \times q_{t,d}/O_{lim}) : t_{lim}\}$$

$$t_{max} = \max\{(0.2 \times 10^{-3} \times 170/0.02) : {20}/{60}\}$$

$$t_{max} = \max\{1.7hrs : 0.333hrs\}$$

$$\Gamma = {\left[\frac{O}{b}\right]^2}/{\left[\frac{0.04}{1160}\right]^2} = {\left[\frac{0.02}{1688}\right]^2}/{\left[\frac{0.04}{1160}\right]^2} = 0.118 \cong 0.12$$

$$t^*_{max} = t_{max} \times \Gamma = 1.7\text{hrs} \times 0.12 = 0.204\text{hours}$$

Therefore, the values are substituted in the gas equation below

$$\theta_g = 1325\left(1 - 0.324e^{-0.2t^*} - 0.204e^{-1.7t^*} - 0.472e^{-19t^*}\right) + ambient\ temperature$$

$$\theta_{max} = 1325(1 - 0.324e^{-0.2x0.2} - 0.204e^{-1.7x0.2} - 0.472e^{-19x0.2}) + 20 = 726.255^oC$$

Since $t^*_{max} \leq 0.5$ *The cooling curve will be given by*

$$\theta_g = \theta_{max} - 625\{t^* - t^*_{max}.X\}\,; X = 1\ since\ t_{max} > t_{lim}$$

$$\theta_g = 726.225 - 625\{t^* - 0.204\}$$ (cooling curve equation)

To plot the data the equations were programmed in Excel as shown in the table below

Table A.1: parametric gas temperature heating and cooling phase equations excel programming template

	A	B	C	D	E	F	G	H	I	J	K
1											
2	t/minutes	t/hrs	t*	Constant	Constant	$0.324e^{-0.2t^*}$	$0.204e^{-1.7t^*}$	$0.472e^{-19t^*}$	Ambient temperature	θ_g heating phase	Time for plot on x axis
3	Start from 1 to 102 (heating phase	=A3/60	=B3*0.12	=1325	=1	= 0.324*EXP (-0.2*C3)	=0.204*EXP (-1.7*C3)	=0.472*EXP (-19*C3)	=20	= (D3*(E3-F3-G3-H3)) +I3	= A3+80
4											
5	Cooling phase									θ_g cooling phase	
6	Start from 103 to 310 (heating phase	=A6/60	=B6*0.12							=728.81-(625*(C6-0.204))	=A6+80

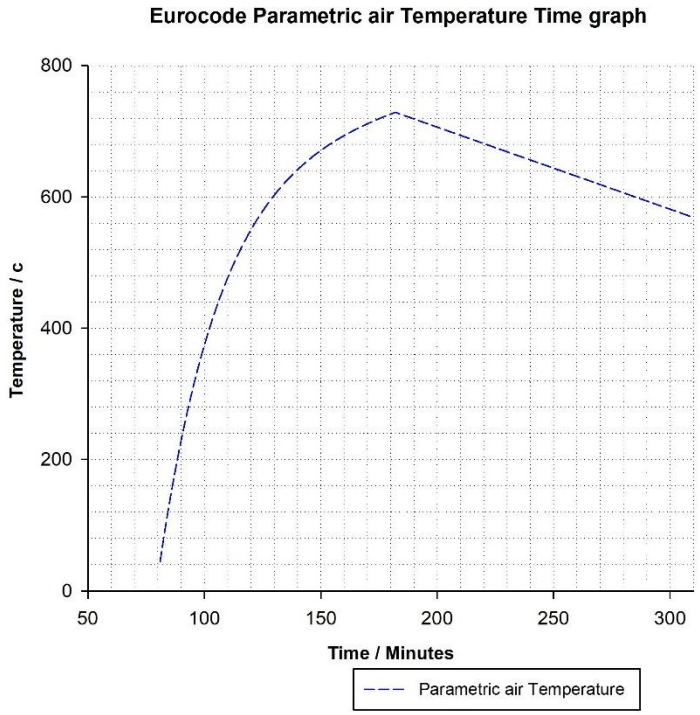

Figure A.1: Eurocode parametric curve, plotted starting at 80minutes when the flashover over begins

Eurocode 5 calculation of slip modulus:

$$K_{ser} = {\rho_k}^{1.5}\frac{d}{20} = 1119.6^{1.5} \times \frac{5.6}{20} = 10.5kN/mm$$

$$K_{ser} = {\rho_k}^{1.5}\frac{d^{0.8}}{25} = 1119.6^{1.5} \times \frac{5.6^{0.8}}{25} = 6.0\ kN/mm$$

Where $\rho_k = \sqrt{\rho_{k1} \cdot \rho_{k2}} = \sqrt{526 \times 2383.4} = 1119.6kg/m^3$

$K_{ser,ave} = 8.25\ kN/mm$

Appendix B: Experimental data Plotted in the test

Table B.2: Experimental temperature time data recorded for gas/air temperature, and concrete temperature

time/ Minutes	Gas Temp	time/ Minutes	Concrete	Concrete	time/ Minutes	Concrete	Concrete
0	27	0	26.7	26.2	0	26.7	25.4
1	112.37	1	26.7	26.2	1	26.7	25.4
3	100.47	3	26.8	26.2	3	26.7	26
4	105.97	4	26.6	26.4	4	27	26.1
5	152	5	26.9	26.4	5	27.3	26
6	129.1	6	27.2	26.4	6	26.7	25.8
7	194.03	7	27.4	26.4	7	26.1	26.1
8	206.3	8	27.7	26.7	8	26.2	25.4
9	260.33	9	26.8	26	9	26.2	25.3
10	260.67	10	26.9	26	10	27	25.1
11	228.43	11	28	26.1	11	26.1	25.1
12	252.97	12	28	26.1	12	26.4	25.4
13	222.57	13	28.1	26.1	13	26.5	25.6
14	285	14	28.1	26.2	14	27.8	25.4
18	264.27	18	29.2	26.3	15	27.9	26
20	207.6	20	29.2	26	16	29.1	27.3
23	235.73	23	30.4	25.8	17	30	27.3
25	253.7	25	30.5	25.9	18	30.5	28.3
28	261.2	28	31.7	26.7	19	31.7	29.4
30	217.2	30	32.9	26.4	20	32.7	31.6
35	153.2	35	34.5	27.6	21	34.5	33.4
40	171.87	40	36	28.2	45	41.4	35
45	201.2	45	36.8	28.6	50	45.7	35.6
50	236.1	50	38.7	29.5	55	49.6	37.7
55	252.73	55	41.6	30.5	60	54.4	38.9
60	198.2	60	43.6	31.6	80	60.8	43.2
81	230.6	81	57.7	38.3	90	69.4	44.1
90	218.27	90	62.7	42.2	105	78.5	55.4
100	361	100	65.8	46.4	125	84.2	61.6
105	344.27	109	73	50.1	127	85.2	64.8
107	352.93	125	77.7	52.1	129	86.9	67.4
125	430.43	127	78.1	53	131	87.9	70.2
127	412	129	78.8	55.6	135	88.8	72.4
128	377.93	131	80.8	57.7	137	89.1	73.1
129	365.1	135	84.6	59.6	143	92.4	76.4
130	380.33	137	86.9	62.6	147	96.1	78.3
147	414.33	143	88.6	64.8	153	99.7	79.5
153	535.3	147	91.5	68.9	158	101.7	80.3
158	502.067	153	96.3	70.5	165	104	83.7

161	625.333	158	99.7	71.7	170	115.4	83.7
165	546.5	161	101.1	77.4	175	157	87.9
170	549.733	165	103.9	79.1	180	187.4	90.5
175	585.533	170	106.3	80.3	185	200.6	92.8
180	733.85	175	107	86.1	190	210	93.9
185	551.3	180	110.1	88.9	195	212.7	97.6
195	477.25	185	113.2	90.1	200	215.6	101.1
200	457.3	195	119.9	93.6	205	218.2	105.6
205	420.85	200	122.2	94.1	210	220	109.3
210	409.95	205	125.6	95.5	215	218.8	113
215	394.65	210	128	96.7	225	214	119.1
225	362.55	215	130.3	97.4	230	206.6	121.6
230	336.3	225	135.1	99.1	235	191.7	126.2
235	275.4	230	138.1	99.4	240	186.8	128
245	262.2	235	140	100.3	245	185.2	128.6
250	262.1	240	140.7	100.6	250	183.7	128.9
255	251.6	250	140.2	100.6	255	178	129.7
260	234	255	140.1	101.3	260	172	130
265	215.55	260	140.2	101.8	270	175.9	129.8
270	209.25	265	140	101.3	275	162.7	128.5
275	191.4	270	139.2	102.3			
		275	138.3	103.2			

Table B.3: Experimental temperature time data recorded for steel I-beam, reinforcement, and external I-beam

time/ Minutes	**Steel top**	**Steel Bot**	**Steel Web**	**time/ Minutes**	**Rebar**	**time/ Minutes**	**Steel external**
0	25.4	26.3	26.3	0	27.2	0	27.1
1	25.4	26.3	26.3	1	27.2	1	27.1
3	26.2	27.8	26.9	3	27.5	3	27.7
4	25.3	28.3	27.2	4	27.2	4	26.9
5	26.4	29.7	27.8	5	27.8	5	27.9
6	26.5	31	28.3	6	27.7	6	28.4
7	26.6	32.2	28.5	7	28.5	7	28.6
8	27.3	32.9	28.7	8	27.8	8	29.9
9	27.5	33.4	29.3	9	27.9	9	30.9
10	28.1	34.5	29.9	10	28.1	10	31.4
11	28.3	35.7	30	11	28.3	11	32.7
12	29.3	37.5	31.2	12	28.4	12	33.9
13	29.5	38.7	31.3	13	28.6	13	35.2
14	30.4	40.6	32.4	14	28.7	14	37.4
18	31.9	45.8	34.7	18	29.2	18	38.4

20	31.3	42.8	31.9	20	28.4	20	41.3
23	28.3	40.9	34.5	23	28.5	23	
25	30.9	44.7	30.3	25	29.9	25	
28	28.5	41.9	32.1	28	28.6	28	
30	31.8	46.8	33.9	30	29.5	30	
35	31.4	48.8	36.9	35	29.7	35	61.5
40	35.9	53	40	40	29.9	40	62.3
45	36.8	54.1	41.8	45	28.9	45	63.2
50	39.1	55.6	41.3	50	30.2	50	63.9
55	37.1	56.9	42.7	55	31.9	55	67.5
60	38.6	50.2	40.9	60	32.8	60	68.7
61	39	57.9	41.9	61	31.8	81	82.3
62	39	57.8	42.8	62	32.9	90	82.4
63	38.9	59.2	43.9	63	30.6	100	101.3
64	39.8	60.8	43.9	64	30.9	105	100.9
65	40.6	62.1	45.9	65	30.7	107	98.1
66	44.1	67.2	50.6	66	31.2	125	119
70	47	69.9	54.3	70	33.4	127	120.4
75	49.7	70.5	57.6	75	35.1	128	121.1
81	52.8	78.7	61.1	81	40.8	129	132.4
85	55.8	82	64.9	85		130	135.1
90	61	86.9	70.3	90	50.8	147	149
95	73.9	98.8	84.9	95	54.3	153	149.4
100	78.6	111.7	88.8	100	56.7	158	149
110	82.6	126.3	98.1	110	58.9	161	149
125	93.8	183.1	119.2	125		165	159.4
127	95.4	196.3	123.4	127		170	159.1
129	97.1	206.4	127.5	129		175	162
130	98.8	218	133.6	130		180	163.2
135	100.8	233.7	136.4	135	70.6	185	162.4
137	101.9	238.5	140.5	137		195	173.1
143	102.7	260.5	150.5	143		200	175
147	105.1	255.5	158.1	147		205	179
153	119.2	272.3	168.9	153		210	177.7
158	136.2	326.3	189.7	158	79.5	215	171.5
161	142.6	336.9	198.3	161	85.3	225	166.4
165	157.5	362.3	214.5	165	87.7	230	174.1
170	165.8	371.5	221.2	170	91	235	162.2
175	184.4	395.2	236.4	175	97.1	245	152.4
180	199	412.2	251.1	180	102.5	250	149.5
185	209.2	421.5	262.8	185	104	255	151
190	220.9	427.7	275.5	190	105.6	260	148
195	231	411.4	290.1	195	103.7	265	146.1
200	240.3	432.4	305.9	200	106.1	270	139.1
205	248.5	429.4	324.3	205	106.8	275	137.2
210	256.4	428	338.5	210	107.7		

215	263.5	428.1	346.5	215	108.4		
225	274.9	414.3	353.8	225	106.9		
230	277.1	410	351.8	230	105.4		
235	281.7	393.4	346.4	235	106.4		
240	283.2	383.7	344.9	240	105.8		
245	283.8	356.2	339.2	245	103.8		
250	285.1	358.9	337.8	250	104.8		
255	283.4	344.7	334.1	255	103.7		
260	282.8	337.7	328.9	260	103.7		
265	281.1	335.6	323.8	265	103.4		
270	277.7	327.1	318.7	270	103.7		
275	273.9	318.1	314.4	275	103.1		

Table B.4: Experimental temperature time data recorded for the plaster and pricking course

time/ Minutes	**Plaster**	**time/ Minutes**	**Plaster**	**time/ Minutes**	**Pricking Coarse**
0	33.9	0	30.9	0	27.5
1	33.9	1	30.9	1	27.5
3	49.1	3	34.8	3	27.8
4	49.2	4	36.9	4	28
5	47.3	5	38.9	5	28.3
6	47	6	41.9	6	29.5
7	46.3	7	44	7	29.7
8	48.4	8	45.1	8	30.9
9	52.1	9	52.2	9	32.2
10	53.7	10	59.3	10	33.4
11	54.7	11	68.6	11	33.5
12	54.1	12	71.3	12	34.7
13	57	13	74.7	13	38.5
14	61	14	77.9	14	38.9
15	60.2	18	87.6	15	40.8
16	74.2	20	85.5	16	42.9
17	72.5	23	90.9	17	43
18	73.7	25	94.2	18	45.1
19	76.5	28	105.6	19	46
20	72.2	30	106.7	20	48.2
21	73.1	35	101.4	21	49.1
45	87.1	40	101.5	45	50.6
50	94.2	45	133.5	50	55.9
55	92.2	50	121.9	55	56.2
60	91.1	55	120	60	57.4
80	96.7	60	125.3	80	62.6
90	100.5	81	141.6	90	59.5
105	173.6	90	139.1	105	79.5
125	509.4	100	178.5	125	95

127	534.6	109	188.2	127	94.4
129	495.3	125	393.2	129	94.2
131	441.1	127	399.2	131	107.9
135	475.3	129	385.3	135	115.9
137	491.2	131	358.5	137	121.1
143	497.1	135	358.9	143	158.4
147	545.9	137	352.9	147	188.5
153	609.8	143	375.7	153	176
180	1150	147	369.3	158	185
		153	403.9	165	914
		158	405.4	170	258.1
		161	482.2	170	269.2
		165	506.3	175	270.6
		170	491.5	180	639.7
		175	496.6	185	607.8
		180	500.5	190	925
		185	501.7	195	505
		195	480.3	200	434.2
		200	466.5	205	413.1
		205	448.5	210	409.2
		210	435.4	215	405.6
		215	422.8	225	365.5
		225	400	230	291.5
		230	367	235	267.5
		235	336	240	240.6
		240	301	245	245.8
		250	294.4	250	246.2
		255	285.1	255	228
		260	277.7	260	201.1
		265	263.3	265	109.5
		270	250.9	270	171.3
		275	238	275	172.8

Table B.5: Experimental force displacement data recorded for the Expanded Metal lathe (Mesh) shear connector samples

EXPANDED METAL LATHE (MESH) SAMPLE 1			**EXPANDED METAL LATHE (MESH) SAMPLE 2**		
TIME/s	**FORCE**	**DISPLACEMENT (mm)**	**TIME/s**	**FORCE**	**DISPLACEMENT (mm)**
23	-	-	7	-	-
78	5.0	-	25	5.0	0.0175
80	6.0	-	26	6.0	0.0525
81	7.0	-	26	7.0	0.0350
82	8.0	-	27	10.0	0.0350
82	9.0	-	28	12.0	0.0350

83	10.0	0.0350	28	13.0	0.0525
83	11.0	0.0525	29	14.0	0.0875
83	12.0	0.0875	29	15.0	0.0875
84	13.0	0.0700	30	16.0	0.1225
84	14.5	0.0875	31	17.0	0.1400
85	15.0	0.1050	32	18.0	0.1750
86	16.0	0.1225	34	19.0	0.2625
88	17.0	0.1925	37	19.0	0.4200
89	17.0	0.2100	39	18.0	0.5075
90	17.0	0.2625	42	17.0	0.6300
93	16.5	0.3500	44	16.0	0.7000
95	16.0	0.3850	46	15.0	0.7525
96	15.5	0.4725	47	14.5	0.7875
98	15.0	0.5250			
102	14.0	0.6475			

Table B.6: Experimental displacement force data recorded for shear connector nail samples

Nail sample 1		Nail sample 4		Nails sample 2		Nails sample 3	
FORCE / kN	DISPLACEMENT / mm	FORCE / kN	DISPLACEMENT/ mm	Force / kN	Displacement/ mm	Force / kN	Displacement/ mm
-	-	-	-	7.50	0.02	7.50	
-	-	-	-	9.00	0.05	9.00	0.01
5.00	0.05	5.00	0.02	18.00	0.12	10.50	0.04
6.00	0.07	6.00	0.04	19.50	0.14	12.00	0.05
7.00	0.12	7.00	0.05	21.00	0.16	13.50	0.06
9.00	0.14	8.00	0.05	22.50	0.18	15.00	0.08
11.00	0.18	9.00	0.07	24.00	0.19	16.50	0.08
14.50	0.23	10.00	0.07	25.50	0.19	18.00	0.09
18.00	0.25	11.00	0.09	27.00	0.21	19.50	0.14
22.00	0.32	12.00	0.11	28.50	0.23	21.00	0.16
25.50	0.33	15.00	0.11	30.00	0.23	22.50	0.20
30.00	0.35	16.00	0.12	31.50	0.25	24.00	0.20
36.00	0.40	17.00	0.14	33.00	0.25	25.50	0.23
40.00	0.42	18.00	0.14	34.50	0.25	27.00	0.27
41.00	0.46	19.00	0.14	34.50	0.26	28.50	0.32
42.00	0.49	20.00	0.16	37.50	0.28	30.00	0.33
48.00	0.53	21.00	0.19	39.00	0.31	32.40	0.40
49.00	0.58	22.00	0.19	40.50	0.34	33.00	0.43
53.00	0.61	23.00	0.19	42.00	0.37	34.50	0.48
54.00	0.63	24.00	0.21	43.50	0.40	36.00	0.54
55.50	0.67	25.00	0.23	45.00	0.46	37.50	0.57
56.00	0.74	26.00	0.23	46.50	0.46	39.00	0.62
57.00	0.75	27.00	0.25	48.00	0.55	40.50	0.68
55.00	0.82	28.00	0.25	49.50	0.61	42.00	0.74

53.00	0.84	29.00	0.25	51.00	0.86	43.50	0.79
52.50	0.93	30.00	0.26	51.80	1.10	45.00	0.85
		31.00	0.28	51.00	1.35	46.50	0.97
		32.00	0.28	49.50	1.62	48.00	1.10
		33.00	0.32	48.00	1.68	49.50	1.21
		34.00	0.32	46.50	1.75	51.00	1.26
		35.00	0.33			52.50	1.38
		36.00	0.37			54.00	1.45
		37.00	0.37			55.50	1.58
		38.00	0.39			57.00	1.61
		39.00	0.42			58.50	1.67
		40.00	0.46			59.70	1.72
		41.00	0.47			58.50	1.72
		42.00	0.54			57.00	1.73
		43.00	0.58			55.50	1.76
		44.00	0.60			54.00	1.76
		45.00	0.60			52.50	1.79
		46.00	0.63			51.00	1.80
		47.00	0.63				
		48.00	0.65				
		50.00	0.72				
		51.00	0.72				
		52.00	0.75				
		53.00	0.81				
		53.50	0.98				
		54.00	1.19				
		55.00	1.23				
		56.00	1.26				
		57.00	1.44				
		55.00	1.52				
		54.00	1.56				
		52.00	1.59				
		51.00	1.63				
		50.00	1.66				
		49.00	1.72				
		48.00	1.77				
		47.00	1.80				
		46.00	1.84				
		45.00	1.89				
		44.00	1.91				
		42.00	1.96				
		39.00	1.98				
		30.00	1.98				

No	Engineer/ Project / Report	Number of structures	Commercial/ Residential	Concrete class	Concrete thickness /mm	Reinforcement	Timber dimensions/ mm	Timber
1	Engineer	5	Residential	C20/25	75	H12	100X75	PINE
2a	Engineer	25	Residential	C20/25	75-100	BRC A142/	100 x 100	Pine / eucalyptus
2b	Engineer	4	Commercial	C20/25	75 -100	H8 & H10	100x100 100x120	Pine / eucalyptus
3a	Engineer	20	Residential	C20/25	75-100	BRC A142/ H8	100 x 100	Pine / eucalyptus
3b	Engineer	3	Commercial	C20/25	75 -100	H8 & H10	100x100 100x120	Pine / eucalyptus
4	Project	1	Commercial	C20/25	75mm	H8	100x100	eucalyptus
5	Project	1	Commercial	C20/25	75mm	H8	100x100	eucalyptus
6	Project	1	Commercial	C20/25	100	H10	100 X 120	eucalyptus
7	Report	50	Residential	C20/25	50-100	BRC A142	100 X 100	Pine / eucalyptus

Table C.7: Timber compression strength test results from the laboratory.

Sample	Dimensions			Failure	Compressive strength (N/mm^2)	Average Compressive strength (N/mm^2)
Code	L(mm)	W(mm)	H(mm)	Load (kN)		
1	101	101	195	300	29.4	26.9
2	101	100	190	290	28.7	
3	103	103	240	240	22.6	

Timber bending Strength EN 408:1995

Table C.8: Timber bending strength results from the laboratory tests.

Section Width, b (mm)	Section depth, h (mm)	W-section modulus, in millimeters to the third power (mm^3)	α – distance between a loading position and the nearest support in a bending test (mm)	F_{max} (N)	Time of failure (s)	Bending strength (N/mm^2)
105	100	175000.0	460	80000	78	105.1
101	101	171716.8	460	79000	76	104.5
102	100	170000.0	460	80500	79	109.6
Average						**106.4**

Deviations from the standard EN 408:1995

Table C.9: Deviations from the standard EN 408:1995

Parameter	EN 408:1995 Provision	Actual set up
Distance between the load points	6h	4.6h

Table C.10: Characteristic Compressive strength value in N/mm2 and density in kg/m3

Sample Code	Date cast	Date tested	Age (days)	Dimensions			Mass (kg)	Density (kg/m3)	Failure load (kN)	Compressive strength (N/mm2)
				L (mm)	W (mm)	H (mm)				
1	04-May-22	01-Jun-22	28	150	155	155	8.740	2,425.3	640	27.53
2	04-May-22	01-Jun-22	28	155	153	151	8.486	2,369.8	620	26.14
3	04-May-22	01-Jun-22	28	153	154	150	8.662	2,450.8	630	26.74
Average								2,415.3		26.80

Appendix D: Pictures

Figure D.2: Setting Universal testing machine (UTM) before testing, the light digital meter was used to measure displacement.

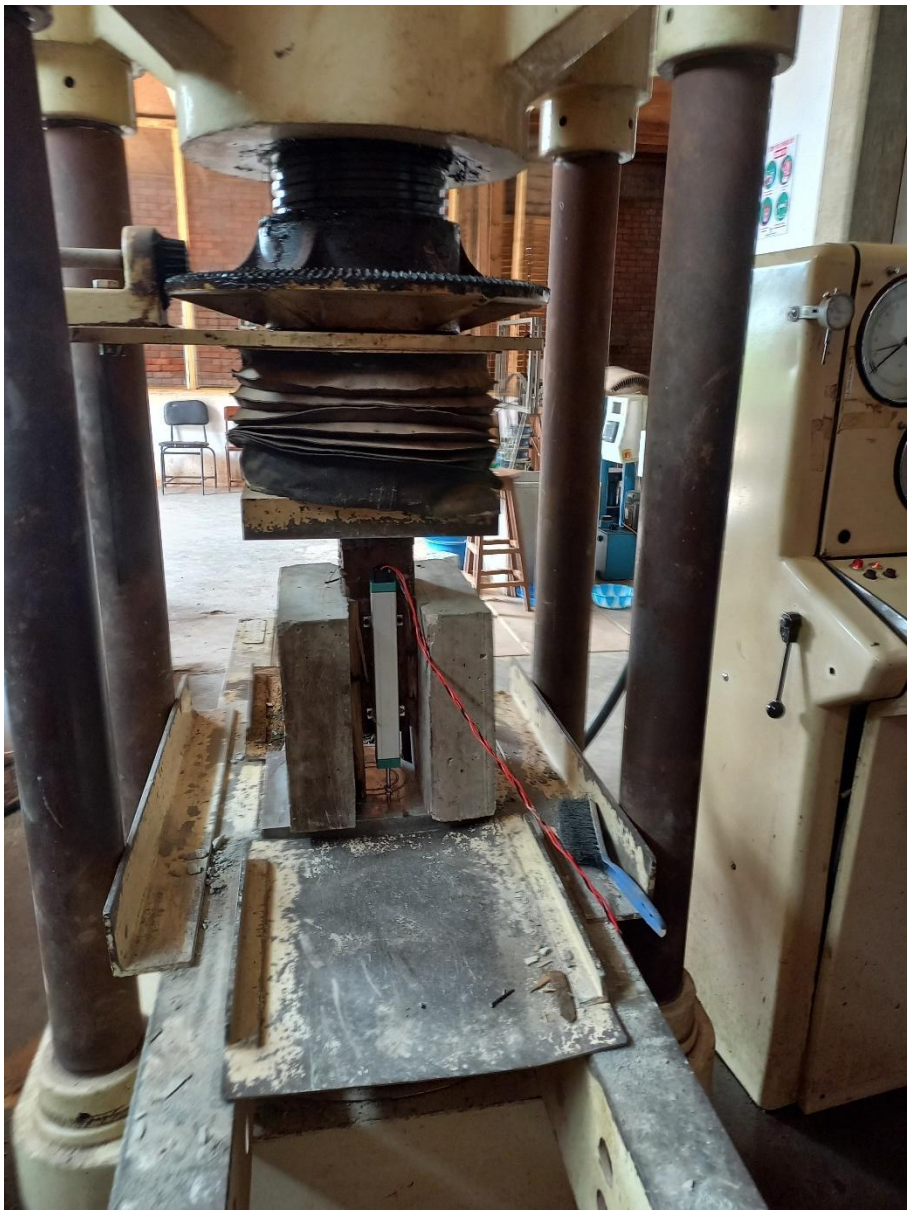

Figure D.3: Setting Universal testing machine (UTM) before testing, loaded with push out sample which was mounted with a Linear variable displacement transformer (LVDT) for measuring slip

Figure D.4: Linear variable displacement transformer (LVDT) mounted on the slab to measure deformation

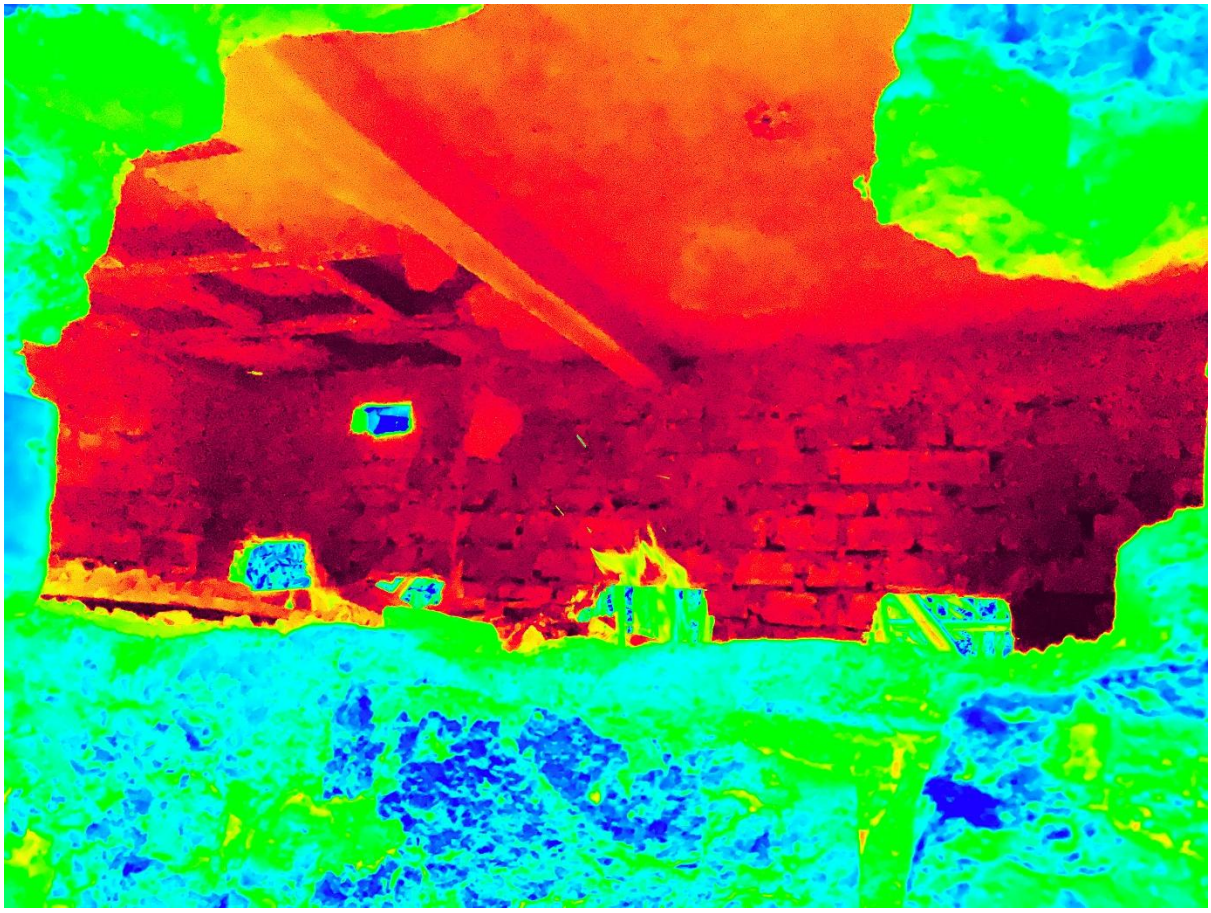

Figure D.5: thermal imaging of the enclosure during burning/ heating

Figure D.6: Char on timber beam after cooling

Figure D.7: Extensive timber section reduction

Figure D.8: Digital thermometer connected to K-thermocouples for taking temperature readings